

TOWARD A GLOBAL MICROSCOPIC THEORY FOR  
NUCLEAR STRUCTURE: MEAN FIELD PLUS  
RANDOM PHASE APPROXIMATION VS. SHELL MODEL

A Dissertation  
Submitted to the Graduate Faculty of the  
Louisiana State University and  
Agricultural and Mechanical College  
in partial fulfillment of the  
requirements for the degree of  
Doctor of Philosophy

in

The Department of Physics and Astronomy

by  
Ionel Stetcu  
B.S., University of Bucharest, 1996  
M.S., University of Bucharest, 1997  
August 2003

*To my parents, for their love and support.*

# Acknowledgments

I was most fortunate that over a period of two decades in my life I met a significant number of great people who helped and guided me; without their support, I would have accomplished much less, if anything at all.

Foremost, I would like to thank Prof. Calvin W. Johnson. He was an ideal adviser, whose door was always open and with whom I spent so many enjoyable hours, discussing so many topics, from physics to literature, often losing track of time. He would never stop encouraging me, always finding a good word when I was down and I thought the whole Universe was against me. Prof. Johnson was not only a great adviser, but also a true friend, and it is most regrettable that, because of his transfer to San Diego State University, the students at LSU will no longer have the opportunity to work with him.

I wish to express my gratitude to Drs. Marilena and Vlad Avriganu, my former advisers in Bucharest, for their continuous support. They taught me that hard work is very rewarding, even if there might be people who would not recognize it: you know you did your best.

Next, I would like to thank Dr. Gabriela Popa, who is responsible for my coming to Baton Rouge. In the spring of 1997, she convinced me to join the Ph.D. program at LSU. After my arrival, she, her husband Dr. Aurel Stan, and my other two close friends Rodica and George Cazacu were always ready to help me and, most importantly, were like a second family far from home. Thank you...

And then, there are my friends from Romania: Oana-Ancuța Dobrescu, Liviu-Cristian Cune (my high school and college buddy), and Ioana Maria Dima (now in Seattle). I'd like to thank them for remaining my faithful friends despite the distances and sometimes my attitude. I know that no matter the circumstances, they will always support me.

Finally, I would like to acknowledge the financial support from Department of Energy Grant No. DE-FG02-96ER40985 and U. S. National Science Foundation Grant No. 0140300, as well as support from Louisiana State University through *Dr. Charles E. Coates Scholar Research Grant*.

# Table of Contents

Acknowledgments . . . . .	iii
List of Tables . . . . .	vii
List of Figures . . . . .	viii
Abstract . . . . .	x
<b>1 Introduction . . . . .</b>	<b>1</b>
<b>2 Motivation for a Global Microscopic Theory . . . . .</b>	<b>6</b>
2.1 Nucleosynthesis . . . . .	6
2.1.1 Short History of a Star . . . . .	6
2.1.2 The $s$ Process Nucleosynthesis . . . . .	8
2.1.3 The Neutrino Process . . . . .	8
2.1.4 The $r$ Process . . . . .	9
2.1.5 The $p$ and $rp$ Processes . . . . .	12
2.2 Parity Violation . . . . .	12
2.3 Survey of Methods for Computing Masses and Radii . . . . .	13
<b>3 Interacting Shell Model . . . . .</b>	<b>18</b>
3.1 General Considerations . . . . .	18
3.2 Basis States in Shell Model . . . . .	19
3.3 Observables . . . . .	21
3.4 Transitions . . . . .	21
3.4.1 Sum Rules . . . . .	22
3.4.2 <i>Lumus Solem</i> for Transitions . . . . .	24
3.5 Shell Model Interaction . . . . .	25
<b>4 Mean-Field Theory and Random Phase Approximation . . . . .</b>	<b>28</b>
4.1 Hartree-Fock Approximation . . . . .	29
4.1.1 Broken Symmetries . . . . .	32

4.1.2	Proton and Neutron Conserving Formalism . . . . .	32
4.1.3	Numerical Algorithm . . . . .	33
4.2	Random Phase Approximation . . . . .	34
4.2.1	Boson Mapping . . . . .	38
4.2.2	Collective Coordinates . . . . .	39
4.2.3	RPA Correlation Energy . . . . .	41
4.2.4	Scalar Observables . . . . .	42
4.2.5	Transitions . . . . .	43
4.2.6	Proton and Neutron Conserving Formalism . . . . .	44
<b>5</b>	<b>Applications of RPA . . . . .</b>	<b>46</b>
5.1	Lipkin Model . . . . .	46
5.1.1	HF Approximation . . . . .	47
5.1.2	RPA . . . . .	49
5.2	Brown-Bolsterli Model . . . . .	51
5.3	Realistic Forces . . . . .	53
<b>6</b>	<b>Results . . . . .</b>	<b>56</b>
6.1	Binding Energies . . . . .	56
6.1.1	Analysis of RPA Accuracy for Binding Energies . . . . .	57
6.1.2	Kinetic Energy of Spurious Modes . . . . .	62
6.2	Scalar Observables . . . . .	63
6.2.1	One-Body Operators . . . . .	63
6.2.2	Two-Body Operators . . . . .	64
6.3	Transitions . . . . .	68
6.3.1	High-Lying Collectivity . . . . .	69
6.3.2	Low-Lying Collectivity . . . . .	73
<b>7</b>	<b>RPA: Myths and Facts . . . . .</b>	<b>76</b>
7.1	Energy-Weighted Sum Rules . . . . .	76
7.2	Symmetry Restoration . . . . .	80
7.2.1	Observables . . . . .	80
7.2.2	Transitions . . . . .	81
<b>8</b>	<b>Conclusions . . . . .</b>	<b>85</b>
	<b>Bibliography . . . . .</b>	<b>88</b>
	<b>Appendix A: Transition Operators . . . . .</b>	<b>96</b>
	<b>Appendix B: Special Eigenvalue Problems . . . . .</b>	<b>98</b>

<b>Appendix C: Letter of Permission . . . . .</b>	<b>100</b>
<b>Vita . . . . .</b>	<b>102</b>

# List of Tables

6.1	Correlation energy ratio vs. geometries of the HF solutions. . . . .	59
6.2	The effect of removing the pairing matrix elements. . . . .	61
6.3	Kinetic energy of RPA zero modes compared with the correlation energy. . .	62
6.4	The number of particles in the $d_{3/2} + s_{1/2}$ orbits. . . . .	64
6.5	Ground-state averages of $S^2$ , $L^2$ , and $J^2$ for nuclei in $sd$ and $pf$ shells. . . .	66
6.6	Ground-state expectation values of $P^\dagger P$ (pairing) and $Q^2$ . . . . .	66
6.7	The effect of removing the single-particle energies from the interaction. . . .	67
6.8	The effect of removing one-body contributions from $J^2$ and $L^2$ . . . . .	67
6.9	Total strength, centroid, and width for isovector $E2$ transition operator. . . .	72
6.10	Same as in Table 6.9 for SF transition operator. . . . .	72
6.11	Same as in Table 6.9 for GT transition operator. . . . .	73
6.12	Same as in Table 6.9 for isoscalar $E2$ transition operator. . . . .	75
7.1	Comparison of the energy-weighted sum rule $S_1$ . . . . .	77
7.2	Comparison of the total strength $S_0$ . . . . .	83

# List of Figures

1.1	Schematic illustration of the interacting SM (left) and HF theory (right). . .	3
1.2	Illustration of the correlated RPA ground-state. . . . .	5
2.1	The half-lives for $N = 82$ isotones calculated in different theoretical models. .	11
2.2	Sn isotopes: various theoretical masses. . . . .	16
4.1	1p-1h configuration from a RPA ground state in a simplified model. . . . .	35
5.1	Exact, HF and HF+RPA ground state energy vs. $\chi$ in the Lipkin model . .	50
5.2	Exact, HF and HF+RPA ground state energy vs. $N$ in the Lipkin model . .	50
5.3	Exact, HF and HF+RPA ground state expectation value of $K_0$ vs. $\chi$ . . . .	51
5.4	Exact, HF and HF+RPA ground state expectation value of $K_0^2$ vs. $\chi$ . . . .	51
5.5	Exact, HF and HF+RPA ground state expectation value of $K_0^2$ vs. $N$ . . . .	52
5.6	Graphical solution to Eq. (5.26). . . . .	53
6.1	Exact and RPA correlation energies for even-even nuclides in the $sd$ shell. . .	57
6.2	Same as in Fig. 6.1 for odd-A nuclides in the $sd$ shell. . . . .	57
6.3	Same as in Fig. 6.1 for odd-odd nuclides in the $sd$ shell. . . . .	58
6.4	Same as in Fig. 6.1 for oxygen isotopes (that is, neutrons only). . . . .	58
6.5	Same as in Fig. 6.1 in the $pf$ -shell. . . . .	58
6.6	$^{28}\text{Si}$ : correlation energy and deformation parameter in a phase transition. . .	60
6.7	The correlation energy ratio $R$ vs. the overlap for select nuclei in $sd$ shell. . .	61

6.8	$n(d_{3/2}) + n(s_{1/2})$ in $^{28}\text{Si}$ as the $d_{5/2}$ single-particle energy is lowered. . . . .	65
6.9	$\langle Q^2 \rangle, \langle P^\dagger P \rangle$ in $^{28}\text{Si}$ as the $d_{5/2}$ single-particle energy is lowered. . . . .	68
6.10	Isovector $E2$ , SF and GT transition strengths for $^{20}\text{Ne}$ in SM and RPA. . . . .	70
6.11	Same as in Fig. 6.10 for $^{21}\text{Ne}$ . . . . .	71
6.12	Same as in Fig. 6.10 for $^{22}\text{Na}$ . . . . .	71
6.13	Isoscalar $E2$ transition strengths for $^{20}\text{Ne}$ in SM and RPA. . . . .	74
6.14	Same as Fig. 6.13 for $^{21}\text{Ne}$ . . . . .	74
6.15	Same as Fig. 6.13 for $^{22}\text{Na}$ . . . . .	74
7.1	$\langle J^2 \rangle$ in $^{28}\text{Si}$ as the $d_{5/2}$ single-particle energy is lowered. . . . .	81
7.2	$^{28}\text{Si}$ : first RPA excited states for both deformed and spherical HF solutions. . . . .	82
7.3	$^{28}\text{Si}$ : Isoscalar $E2$ for deformed and spherical HF state. . . . .	83

# Abstract

Our understanding of nuclear structure is built upon mean-field theories such as Hartree-Fock and time-dependent Hartree-Fock. The small-amplitude limit of the latter is the random phase approximation (RPA), which is widely used to model giant resonances in nuclei. Despite this popularity, RPA has been mostly validated against toy models; tests against complex models are scarce in the literature. We perform a thorough test of the RPA against full  $0\hbar\omega$  shell model (SM) calculations, including in our investigation binding energies, scalar ground-state observables, for which we develop a new method, and transition strengths. We allow deformed Hartree-Fock solutions and compare results for spherical and deformed nuclei. We obtain reasonable agreement between RPA and SM, albeit with some significant failures. Particularly, we find that the low-lying collectivity is poorly described for deformed mean-field solutions, which we interpret as incomplete symmetry restoration in RPA. Results for observables, and in particular for  $J^2$ , also point out toward the same conclusion regarding the symmetries of the ground state. We also prove, both analytically and numerically, that a long-standing theorem regarding RPA is violated in the case of deformation. The worse violation appears for low-lying transitions, such as isoscalar  $E2$ , which we consider as a third argument for an incomplete symmetry restoration.

# 1 Introduction

We have come a long way to understand how the four fundamental forces conspire together to create the nuclei observable today. The secret is hidden in the evolution process of stars [1]. Thus, the abundances of many heavy elements, and even the origin of a large number of isotopes, can be explained by an explosive scenario at the end of the life of massive stars. The *explosive r-process* creates very neutron rich nuclei by rapid ( $r$ ) neutron capture [1–3]. By its nature, it involves nuclei far from stability and with very short life-times, not accessible yet and very challenging to experiment; models of  $r$ -nucleosynthesis must rely entirely upon theoretical predictions for *nuclear binding energies* and *weak transition rates*. Therefore, stellar evolution emphasizes the importance of nuclear theory as one of the main ingredients indispensable to the general understanding of the nature. For this reason, in the first part of Chapter 2 we present briefly the stellar evolution of massive stars, reviewing in some detail the nucleosynthesis of heavy elements.

Theoretical nuclear physics input is essential for a good description of the observed element abundances. Measured binding energies and transition strengths for stable or nearly stable nuclides are valuable tests of nuclear models. But in the absence of direct measurements of binding energies and lifetimes for relevant highly unstable nuclei, how can we test the theoretical models for those nuclei? One very powerful means is the description of neutron radii. Two interesting phenomena related to the neutron radius/density in light nuclei are neutron skins [4–6] and neutron halos [7–9]; the former is related to the isovector forces, while the latter are due to a very weak binding of the outermost neutron, as one expects to happen for nuclei at the neutron dripline. Their quantitative description is a challenge for nuclear models, providing a useful experimental test. In heavy nuclei on the other hand, parity violation could be used in order to determine the neutron radii, providing further stronger constraints for theoretical models. This is the reason in the second part of Chapter 2 we review briefly parity violation.

The large number of nuclides whose description is important in the nucleosynthesis process calls for a global microscopic theory. Its aim is to describe nuclear properties globally, that is from helium to superheavies beyond uranium, and to the driplines relevant to nucleosynthesis. The search started long time ago, and with all the progress along the way, we are not very close yet to a reliable fully microscopic theory. There are three main categories of properties such a theory should describe:

1. binding energies;
2. ground state observables (e.g., nuclear radii, neutron densities);

### 3. transition strengths.

In this work, we consider all of the above in a restricted model, but it is our eventual goal to extend the space and calculate quantities relevant to astrophysical processes. As we will see, the approximate method we use, while good, is not entirely reliable and more work remains to be done before realistic calculations should be considered.

The last part of Chapter 2 reviews the present theoretical advances in describing the nuclear masses and more generally the nuclear properties. From the semiclassical Thomas-Fermi theory to the most advanced large basis shell model calculations, Sec. 2.3 summarize each method, emphasizing their successes and limitations. However, extrapolations of these models to describe properties of unstable nuclei remain unreliable, and sometimes even unjustified.

One of the theoretical methods which can be used in principle in order to describe nuclear properties is the interacting nuclear shell model (SM). It provides solution to the many-body Schrödinger equation including all possible correlations between nucleons in a restricted space. Thus, because the Hilbert space associated with a nucleus is infinite dimensional, one reduces possible configurations by limiting the available single-particle space to just a few orbits, the *valence space*, and by restricting the number of active nucleons to a small number, the *valence particles*. The valence space is usually taken as a major oscillator shell, on top of an inert core, a close shell nucleus such as  $^{16}\text{O}$  or  $^{40}\text{Ca}$ , whose contribution to the nuclear properties is fixed; we illustrate these approximations in Fig. 1.1, left panel. Using a restricted space makes the problem numerically tractable [10, 11]; the consequence is the necessity to use effective *space-dependent* nucleon-nucleon interactions, so that in Chapter 3 we review, besides the interacting shell model, methods to obtain effective shell model Hamiltonians.

The interacting SM is able to provide good description of the low-lying nuclear states, in very good agreement with the experimental data. This includes energy levels and transitions, albeit phenomenological charges have to be used for the latter (due again to the restriction of the space). The SM wave function is obtained by diagonalization of an effective Hamiltonian in the basis of choice; the only required property of the basis states is to be anti-symmetrical under the permutation of two identical nucleons, because these are fermions. This is accomplished by constructing the basis states as Slater determinants. In heavier nuclei ( $A \gtrsim 80$ ), the number of basis states becomes prohibitively large for full space diagonalization, even in a single oscillator shell; therefore, other reductions have to be applied. Note however that for the purposes of the present investigation we will consider only nuclei for which a full space calculation can be performed. Moreover, we assume that the effective shell model Hamiltonian is the exact interaction, and full space shell model calculations provide the exact results.

The main shortcoming of the shell model is an exponential grow with  $A$  of the number of basis states which must be taken into account; this makes full space diagonalization impossible for heavy nuclei. Mean-field theory is an approximation which reduces drastically the computational effort by assuming the ground-state wave-function to be described by just *one* Slater determinant [10]. The “trick” is to assume that the particles, in Hartree-Fock

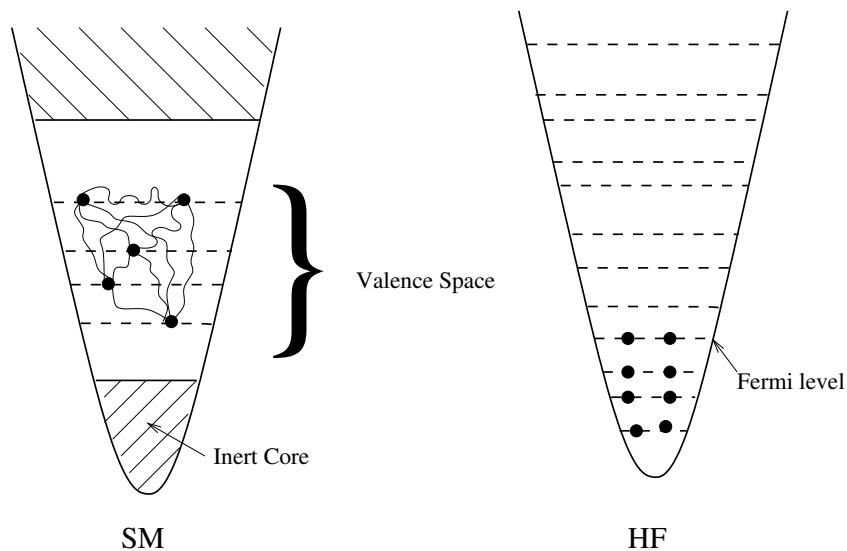


Figure 1.1: Schematic illustration of the interacting SM (left) and HF theory (right); in the SM, particles interact via a two-body force in a restricted space, while in HF the particles interact through an one-body mean-field potential. Diagonalization of the effective Hamiltonian gives in SM the ground-state wave function as a superposition of many Slater determinants; the Slater determinant obtained by filling-out the lowest single-particle levels is the mean-field ground state.

(HF) theory, or quasi-particles, in Hartree-Fock-Bogoliubov (HFB) theory, are completely uncorrelated and that the two-body interaction is absorbed in a mean one-body potential (see Fig. 1.1 right). As a result, instead of solving a many-body problem, one finds the spectrum of a particle moving in a self-consistent one-body potential (for details, see Chapter 4), a considerable simplification of the initial task. However, this model has the disadvantage that leaves out configurations with particles above the Fermi level in the wave function, and, even worse, can break the original symmetries of the Hamiltonian [10–12] such as rotational or translational invariance, or particle number conservation in HFB. Finally, note that while it minimizes the energy and can give reasonable estimates for other observables, the mean-field Slater determinant is *not* an exact eigenfunction of the Hamiltonian.

It is of course disturbing to have a solution which does not incorporate the symmetries of the Hamiltonian, and because the origin of symmetry breaking lies in neglected particle-hole configurations it is natural to introduce such correlations. From the minimization condition, which defines the HF solution, one can show that one-particle, one-hole (1p-1h) configurations (one particle above the Fermi level leaving one hole below it) do not contribute to the ground state. Therefore, the lowest order corrections can come from two-particle, two-hole (2p-2h) configurations. Figure 1.2 shows examples of configurations, aside mean-field solution, which contribute to the ground-state. However, note that if the number of 2p-2h configurations is  $N$ , for an exact diagonalization in this space the dimension of the matrix which has to be diagonalized is of the order of  $N^2$ . Assume that  $N \approx 100$ , so

that one should diagonalize a  $10^4 \times 10^4$  matrix to obtain the nuclear spectra. For nowadays computers, this is almost trivial (although one still uses numerical tricks to obtain just the lowest states), but such a problem was much beyond computational capabilities forty years ago. Therefore theorists made some further assumptions, developing the random-phase approximation [10–12], or RPA, in which the dimension reduces to  $2N$ . This might suggest that RPA is a cleverly truncated version of the SM, which takes into account 2p-2h correlations in the ground state. This is not true, as RPA involves some assumptions which, while reasonable, might not be fulfilled in all cases [10]. In Chapter 4 we present the RPA and all approximations involved.

While it introduces correlations in the mean-field state, RPA is primarily a theory for excited states constructed as 1p-1h configurations from the correlated RPA ground state. Nevertheless, corrections to the mean-field energy can be read off trivially without the construction of the wave function [10]. Furthermore, we have extended the same procedure to calculate corrections to ground-state expectation values of relevant operators [13]. But the main applications of RPA are to evaluate excited state spectra and transition strengths in nuclei. The literature provides numerous references with applications of RPA and in Chapter 5 the interested reader can find a comprehensive, while by no means exhausting, overview.

To summarize, mean-field and RPA provide a model of an improved ground-state and excited states which can be used in principle to determine nuclear properties globally. Recent investigations have proposed mean-field corrected through RPA as good candidate for global binding energy systematics [14, 15], based on test against exact calculation in ‘toy’ models. The main objective of the present work is to test the reliability of mean-field + RPA predictions against exact solution in realistic nuclear models. The investigation will not be limited to the ground state energy, as ground state mean values of observables and transition strengths are also relevant to the  $r$  process. Chapter 6 shows how reliable HF+RPA is, for it presents a thorough test of the mean-field corrected through RPA results against full space shell model calculations for binding energies, ground state observables and transition strengths in several nuclei. While in general correct, HF+RPA occasionally fails to give a good estimate of the exact solution [16]. This is the main result of the present investigation, but not the only one.

Aside from testing the RPA predictions, our investigation provides insight of the RPA features and limitations. Chapter 7 is dedicated to discussing two “myths” in the literature about RPA. First, it is “well-known” that RPA *restores* the symmetries broken by the mean-field solution [10, 17]. This assertion is based again on tests against exact solutions in very simplistic models. In fact, RPA identifies the generators of the broken symmetries as states lying at zero excitation energy, so that it is more appropriate to say that RPA *respects* the symmetries. The results presented in Chapter 6, and especially those concerning ground-state expectation values of the total angular momentum as well as the difference between the RPA description of high and low collectivity, suggest that the restoration of symmetries is only approximate. Second, it is said that RPA respects exactly the energy-weighted sum rule (EWSR), which is an exact relationship between the RPA EWSR and the Hartree-Fock expectation value of a particular double commutator [10, 18]. However, careful manipulation

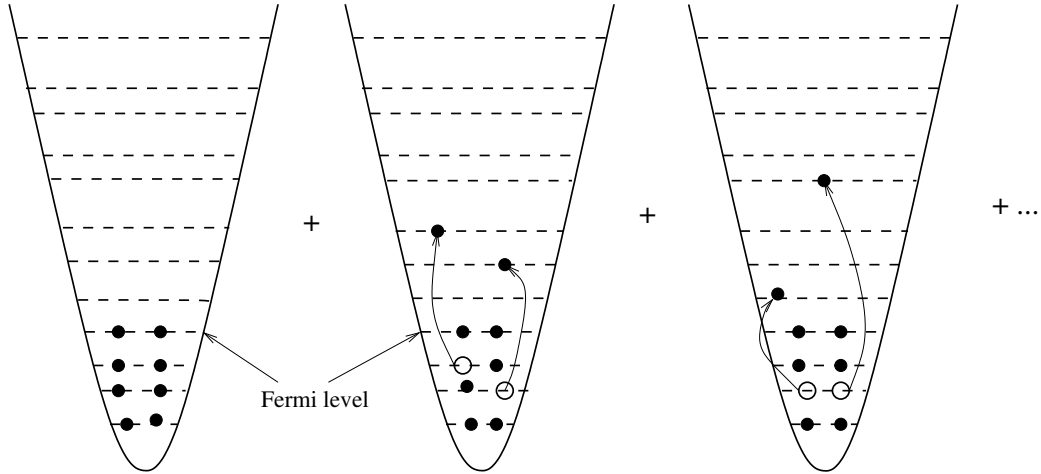


Figure 1.2: Illustration of the correlated RPA ground-state, composed of the mean-field solution (most left) and 2p-2h correlations.

of algebraic formulas proves that the “well-known” equation needs nontrivial corrections if symmetries are broken by the mean-field solution [19].

Chapter 8 could be very well entitled “Period. And start again.” It not only lists the main conclusions of this work, but also makes an overview of the current proposals in the literature for RPA improvement. On one hand, we know now that, despite the good results in ‘toy’ models, RPA cannot be used as it is for a global microscopic nuclear theory. On the other hand, as in the case of unadorned RPA, improved models are usually tested against toy models; their reliability however will be proved only by tests against a complicated and realistic model, much like in the present investigation.

# 2 Motivation for a Global Microscopic Theory

A global microscopic theory of atomic nuclei is one goal not reached yet by nuclear theory. But more than a fundamental theoretical problem, the search for a global microscopic nuclear theory is motivated by its applications to other fields, such as explosive  $r$  nucleosynthesis, search for dark matter and so on. For example, in the dark matter experiments the weakly interacting massive particles, or WIMPs, couple with the target nuclei, and in order to detect them one needs to model the nuclear spin response function; because of the nature of the interaction, the target nuclei must be very heavy even-odd nuclei, difficult to describe in any theoretical model. Finally, near future parity-violating electron scattering experiments are expected to bring new challenges to the existing microscopic theories by imposing new experimental constraints.

This chapter shortly reviews relevant aspects concerning stellar nucleosynthesis and parity violation. The last section is dedicated to presenting methods for nuclear mass and radii systematics, in an attempt to convince the reader about the necessity of a reliable microscopic nuclear theory applicable globally.

## 2.1 Nucleosynthesis

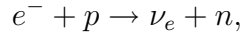
Stars are the main production sites of chemical elements found in nature. According to the big-bang model, only H,  $^3\text{He}$ ,  $^4\text{He}$  and  $^7\text{Li}$  were initially created [2]; the production of all the other elements can be understood as mainly the result of stellar evolution.

### 2.1.1 Short History of a Star

During the evolutionary process, the stars, collections of hydrogen atoms possibly contaminated with small amounts of heavier elements, have to produce energy in order to maintain equilibrium against the gravitational collapse. They burn first hydrogen, producing  $^4\text{He}$  ( $\alpha$  particles) by means of the  $pp$  chain [1]. Then, if the star is massive enough, it will burn He into C, C (and He) into O and Ne, O and Ne into Si, and Si into Fe and Ni. Thus, a very massive star toward the final stage of its evolution contains a core of Fe and Ni, and concentric shells of  $^{28}\text{Si}$ ,  $^{16}\text{O}$  and  $^{20}\text{Ne}$ ,  $^{12}\text{C}$ ,  $^4\text{He}$  and H at exterior. This so called

“onion skin” structure follows actually the star’s history. The other elements and various isotopes up to around Fe and Ni are produced mainly as secondary products of fusion reactions during the *hydrostatic burning*, i.e., production of nuclear energy in hydrostatic equilibrium with the gravitational collapse. Nevertheless, the slow (*s*) process, that is neutron capture followed by  $\beta$ -decay to a stable element, contributes also significantly to the abundances of some isotopes, and its production sites are associated with the helium core burning of the CNO material in massive stars [21], and with helium flashes occurring during shell burning in low-mass stars (asymptotic giant branch or AGB stars).

If the star is very massive, that is the iron core is above Chandrasekhar limit of about  $1.4M_{\odot}$ , the result is a catastrophic event, or supernova. The gravitational collapse continues and with no source of nuclear energy (as  $^{56}\text{Fe}$  is the most tightly bound nucleus and any attempt to burn it into some other elements would require energy) the iron core collapses at about 0.6 of the free fall velocity [20]. This collapse produces heating and compression of the matter, which can release  $\alpha$  particles and nucleons; the electron chemical potential increases, which makes the electron capture on free and bound protons highly favorable



producing neutrinos which escape carrying energy and lepton number. Both the nuclear disassociation and electron capture help the collapse, as they consume energy from the electron gas whose pressure is the only source of star’s support. As a result, the collapse accelerates even further and is accompanied by a neutrino burst. Neutrino induced nucleosynthesis is in that moment possible in outer cooler layers of the star (see Sec. 2.1.3 for a short discussion).

The collapse of the iron core takes place until its central density becomes roughly the density of nuclear matter. At that point, the strong repulsive hard-core component of nuclear potential acts similar to a stiff spring and rebound the core [2, 22]. The rebounding part then encounters the still infalling upper layers, including part of the initial collapsing core, at supersonic relative velocity. This collision was believed to be the mechanism which produces the shock which in turn successfully explodes the star. Some numerical simulations were able to produce explosions [22, 23]; however, they neglected the neutrino emission from behind the shock. When the neutrinos reach lower density regions, they diffuse ahead of the shock and reduce their mean energy by scattering on electrons. This mechanism favors neutrinos’ escape, consuming energy from the shock. (To avoid confusion, note that not the correct, but incomplete treatment of neutrino response is fatal for explosion.) Another means through which the shock loses energy is photodisintegration: the shock heats the nuclei in the infalling layers, breaking them down. The neutrino escape and photodisintegration are therefore the two main means of shock energy dissipation, and models that take them into account fail to end with an explosion [24–26]; it is accepted presently that one needs another source of energy to revitalize the shock and create an explosion.

The scenario accepted today as responsible for providing the necessary energy to the shock is neutrino energy deposition [27, 28]. Basically, it consists in neutrino absorption on free nucleons



Two-dimensional simulations which take into account these processes predict explosions; there are however disagreements concerning other mechanisms involved, such as convective flow, and without any doubt more work remains to be done in this domain.

On its way out, the shock transports a large number of neutrons, on a time scale of about one second. The neutron number densities involved are of the order of  $10^{20} \text{ cm}^{-3}$ , large enough to create neutron-rich isotopes through the  $r$  process. Section 2.1.4 provides some detailed information about the  $r$  nucleosynthesis, such as physical quantities necessary for its description and isotopes produced. The supernovae offer ideal conditions for the  $r$  process, as well as a mechanism, i.e., the explosion, to spread the newly created nuclei. Nonetheless, they are not the only proposed astrophysical sites; other candidates are also discussed in 2.1.4.

### 2.1.2 The $s$ Process Nucleosynthesis

The  $s$  process generates new nuclei by slow capture of neutrons, slow with respect to the beta-decay lifetimes. It involves nuclei close to the line of stability, as the daughter nucleus decays to a stable or long-lived isobar. Being easily accessible experimentally, the  $s$  process is well understood. However, the  $s$  process can synthesize only isotopes up to  $A = 209$  [1]; the most massive stable element is  $^{209}\text{Bi}$  and neutron capture on it produces  $^{210}\text{Bi}$ , which  $\alpha$  decays to  $^{206}\text{Pb}$ , terminating the  $s$  process [29]. Moreover, even for  $A < 209$ , there are stable isotopes observed in nature (e.g., actinides) which cannot be synthesized through the  $s$  process, as the parent nuclei are unstable. In such cases, one should look for another means of production.

Besides contributing to the isotope abundance, the  $s$  process can be used in order to estimate the temperature of the environment, by using the  $\beta$  half-life of a branching point nucleus sensitive to the thermal population of the excited levels. For example, the analysis of the  $^{176}\text{Lu}$   $s$ -process branching yields an environment temperature of about  $T = (2.5 - 3.5) \times 10^8 \text{ K}$  [30].

The  $s$  process is very well understood experimentally, and therefore, by itself, cannot constitute a powerful motivation for a global microscopic theory. Nevertheless, it is important to stress that it cannot be the only mechanism to produce the observed isotope abundances. The other processes summarized below however are very little known experimentally and therefore the theory is very poorly constrained.

### 2.1.3 The Neutrino Process

Neutrinos interact only weakly with the matter, so that their interactions with atomic nuclei have very small cross-sections. Nevertheless, the high flux of neutrino generated at the beginning of the catastrophic collapse of a supernova can produce transmutations of chemical elements in the outer cooler layers [3]. On the other hand, because the neutrino-nucleus interaction rates are so small, such reactions do not affect the abundance of the parent nucleus, but they contribute to the production of the daughter. Neutrino induced excitations

above the threshold for particle emission are the main sources of new isotope synthesis, e.g.,  $^{20}\text{Ne}(\nu_x, \nu'_x p)^{19}\text{F}$ ,  $^{20}\text{Ne}(\nu_x, \nu'_x n)^{19}\text{Ne}(e^+, \nu_e)^{19}\text{F}$ , and  $^4\text{He}(\nu_x, \nu'_x n)^3\text{He}(\alpha, \gamma)^7\text{Be}$ , but knock-out of deuterons or proton neutron pairs is also possible.

The most important contributions come from neutral-current reactions, especially from  $\nu_\mu$  and  $\nu_\tau$  [2, 3], produced through neutrino oscillations (and especially matter-enhanced oscillations). Without neutrino oscillations we would have only electron neutrinos  $\nu_e$  produced by electron capture on free or bound protons in the core collapse. Whereas this phenomenon is beyond the purpose of the present work, it illustrates nicely how another field, neutrino physics, can find application into astrophysics (not for the first time for it was the Solar neutrino problem which actually forced a change in the way we understand neutrinos). What is important from the point of view of the nuclear theory is a good description of the neutrino-nucleus interaction and this investigation tests transitions which in particular can be induced by neutrinos.

### 2.1.4 The $r$ Process

As mentioned in Sec. 2.1.2, there are stable nuclei which cannot be produced through the  $s$  process. For example,  $^{122}\text{Sn}$  is a stable isotope with a measured solar system abundance of 4.8% from the total element abundance. A  $s$ -process production scenario would require that  $^{121}\text{In}$  be stable, so that by neutron capture would produce the unstable  $^{122}\text{In}$ , which in turn would  $\beta$ -decay to  $^{122}\text{Sn}$ . But  $^{121}\text{In}$  is unstable, shielding  $^{122}\text{Sn}$  from the  $s$  process production.  $^{124}\text{Sn}$  (observed abundance 6.1%) and  $^{123}\text{Sb}$  (observed abundance 43%) are just two other examples of nuclei which cannot be produced through the  $s$  process.

The environmental conditions for  $r$ -process nucleosynthesis are temperatures  $T \sim 100$  keV and neutron number densities  $n > 10^{20} \text{ cm}^{-3}$  [31]. Here is a *crude* estimate of the neutron number density, as presented in Ref. [1]. The lifetime of a nucleus against neutron capture is

$$\tau = \frac{1}{\rho_n \langle \sigma v \rangle}, \quad (2.1)$$

where  $\rho_n$  is the neutron number density, and

$$\langle \sigma v \rangle = \int_0^\infty \sigma v \phi(v) dv,$$

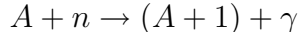
is the thermal average of the product of the neutron capture cross-section  $\sigma$  and velocity  $v$ , with  $\phi(v)$  the neutron flux at velocity  $v$ . Now, a rough estimate gives  $\langle \sigma v \rangle = 3 \times 10^{-17} \text{ cm}^3/\text{sec}$ , so that Eq. (2.1) becomes

$$\tau \approx \frac{10^9}{\rho_n} \text{ years},$$

and inserting the expected time for the  $s$  process of about  $10^4$  years, one obtains the neutron number density of the order of  $10^4 \text{ cm}^{-3}$ , while for the  $r$  process, when one expects characteristic time of one second, the neutron density is of about  $10^{20} \text{ cm}^{-3}$  (for comparison, the thermal neutron density in a reactor is of the order of  $10^7 \text{ cm}^{-3}$ ).

As we saw in Sec. 2.1.1, the shock from a supernova explosion is capable of producing such conditions. However, there are other sites, such as neutron star mergers [32], which provide similar environments; other proposals point out red giant He flashes [33] or inhomogeneous big bangs as possible places for producing isotopes through the  $r$  process [2]. Another very favored scenario at the present time is the neutrino-driven wind just above the surface of a newly born neutron star in a supernova explosion. In this context, the Gamow-Teller and Fermi transitions investigated in this work play an important role in the physics of  $r$  process, as they can be induced by neutrinos.

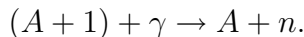
Basically, the  $r$  process nucleosynthesis stands for synthesis of heavy, neutron-rich nuclei through rapid ( $r$ ) neutron capture. Neutrons pile up on the existing nuclei, in good approximation through  $(n, \gamma) \rightleftharpoons (\gamma, n)$  equilibrium reactions. An estimate for



gives for a resonant reaction (which brings the most contribution to the total cross-section) a rate [20]

$$r_{(n,\gamma)} \sim \rho_n \rho_A \left( \frac{2\pi}{\mu kT} \right)^{3/2} \frac{\Gamma_n \Gamma_\gamma}{\Gamma}, \quad (2.2)$$

where  $\rho_A$  stands for the number density of target nuclei  $A$ ,  $\Gamma_n$ ,  $\Gamma_\gamma$  and  $\Gamma$  for the partial and total widths, while  $\mu$  is the reduced mass of the system. Now, let's consider the inverse reaction, that is



In this case, the rate is [20]

$$r_{(\gamma,n)} \sim 2\rho_{A+1} \frac{\Gamma_n \Gamma_\gamma}{\Gamma} \exp\left(-\frac{S_n}{kT}\right), \quad (2.3)$$

with  $S_n = B(Z, N + 1) - B(Z, N)$  the neutron separation energy (i.e., the difference between the binding energies of  $(A + 1)$  and  $A$  isotopes). At equilibrium, the two rates are equal, which gives for the density of neutrons

$$\rho_n \sim 2 \left( \frac{\mu kT}{2\pi} \right)^{3/2} \exp\left(-\frac{S_n}{kT}\right). \quad (2.4)$$

Using in this equation the expected numerical values for neutron number density,  $\rho_n = 10^{20} \text{ cm}^{-3}$ , and  $kT = 100 \text{ keV}$  with a mass  $A = 150$ , one can estimate a separation energy of  $S_n = 2 - 3 \text{ MeV}$ , much smaller than the typical 8 MeV for stable nuclei. Therefore, the  $r$  process path must involve nuclei far from stability and description of various processes, such as neutron capture or neutrino response, has to be extrapolated from the experimentally accessible region of the nuclear chart, to the unexplored one. In this context, Fig. 2.1 emphasizes the role of a reliable nuclear theory, showing differences between predictions for half-lives in different approaches. They can be of orders of magnitude in regions unaccessible experimentally. In Sec. 2.3, we will see similar disagreement between results for the binding

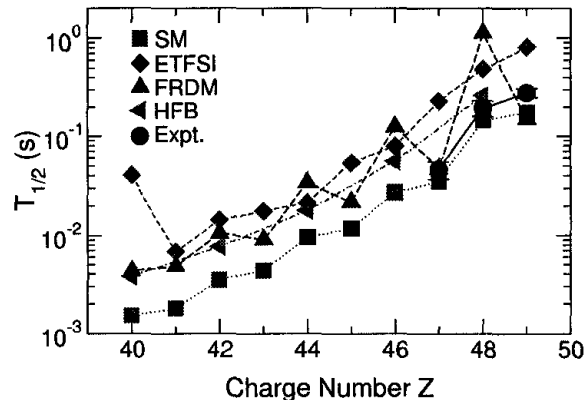


Figure 2.1: The half-lives for  $N = 82$  isotones, calculated in different theoretical models: extended Thomas-Fermi with Strutinsky integral (ETFSI), finite range droplet model (FRDM), Hartree-Fock-Bogoliubov (HFB) approach and SM. For three nuclei, the experimental data is in good agreement with the SM results.<sup>1</sup>

energies predicted by different theories (although there the convergence of the theoretical results to the measured masses is much better for all theoretical models). Successful simulation of the  $r$  process therefore requires good estimate of neutron capture cross-sections, masses [see Eq. (2.3)] and half-lives in a region where the experimental constraints are rare.

In the  $r$  process, the neutrons are captured on nuclei, with a lifetime for capture much smaller than the  $\beta$ -decay time. Therefore, the newly created nuclei can accumulate many neutrons, until the capture is no longer possible due to the absence of bound neutron states in the daughter nucleus. One reaches at that point the neutron dripline. The neutron-rich nuclei will then follow a series of  $\beta$ -decays to stability. Note however that if we still are in a  $r$  process environment, neutron capture is still possible, and is even favored if the  $\beta$ -decaying nucleus was at a magic neutron number. This is because one of the  $\beta$ -decay leaves a hole in the neutron Fermi sea, favoring the neutron capture. The  $r$  process terminates at very heavy nuclei,  $A \sim 270$ . At that point,  $\beta$ -delayed and neutron-induced fission produces two fragments with masses of about  $A_{parent}/2$ , feeding matter back into the process.

Finally, one last comment about the  $r$  process. Besides its relevance for heavy-element nucleosynthesis, the understanding of the  $r$  process can prove helpful for cosmology [36]. Detection of typical  $r$ -process elements Thorium and Uranium in very metal-deficient stars [37], suggests that a correct modeling of the  $r$  process in these first generation stars can be used as a reliable chronometer, a useful test for other measurements.

<sup>1</sup>Reprinted from *Nuclear Physics A* **704**, K. Langanke and G. Martínez-Pinedo, *Applications of the shell model in nuclear astrophysics*, pp. 154c-164c, Copyright (2002), with permission from Elsevier.

### 2.1.5 The $p$ and $rp$ Processes

The proton rich nuclei whose production via  $s$ -process and  $r$ -process is blocked are called  $p$ -process nuclei. While proton capture is possible, the main process which produce  $p$  nuclei is nuclear disintegration in the O/Ne shell heated by the shock wave of the collapsing supernova. This model explains the observed solar abundances for all  $p$  nuclei, except the lightest which are seriously underproduced. However, large part of the theory used is still untested.

The  $rp$ -process is similar to the  $r$ -process, the only difference is that in this case the protons are captured rapidly, extending toward the proton dripline. The evolution to stability is made via  $\beta^+$ -decays, processing material from Ar-Ca up to  $^{56}\text{Ni}$ , the favored site being the surface of an accreting neutron star, in a H rich atmosphere [3, 38].  $N = Z$  even-even nuclei beyond  $^{56}\text{Ni}$  are the main products of this process which terminates at  $^{100}\text{Sn}$ . The experimental information is rich compared to the  $r$ -process. Half-lives up to  $^{80}\text{Zr}$  are measured, and new experiments relevant to the  $rp$ -process, beyond  $A = 80$ , are in progress. The nuclei on the  $rp$ -process path involve strong coupling between  $pf$  orbitals and  $d_{5/2}$  and  $g_{9/2}$ , making theoretical predictions for the life-time unreliable, mainly due to uncertainties in masses [3].

## 2.2 Parity Violation

The weak interaction plays a crucial role in the synthesis of heavy elements, as the  $\beta^\pm$  decays or neutrino reactions are processes driven by the weak force. While the weakest of all, except gravity, it has probably the strongest personality: it is the only fundamental force which breaks parity conservation.

Parity symmetry is mathematically defined as invariance with respect to reflection of the coordinate system (mirror image). Surprisingly, the parity conservation is not required by theory although is respected by strong, electromagnetic and gravitational interactions. Lee and Yang were the first to argue in 1956 a possible parity violation of the weak interaction in  $\beta$ -decays and in hyperons and mesons decays [39]; the same year, the parity violation was confirmed experimentally using the  $\beta$ -decay of polarized  $^{60}\text{Co}$  nuclei [40].

One possible application of parity violating experiments is to constrain theoretical nuclear models. Neutron radii and densities are, as we mentioned in the introduction, quantities that a microscopic model should be able to predict. Parity violating experiments can provide accurate measurements of neutron radii and nuclear matter density. The latter is important to the understanding of neutron stars' structure and is experimentally deduced from the central density of heavy nuclei, e.g.,  $^{208}\text{Pb}$ , applying some corrections for surface tension and Coulomb interaction. There are however large uncertainties because experiments involving non-polarized electron scattering can measure accurately exclusively the proton density. Large uncertainties in the analysis of pion-nucleus experiments do not permit a measurement of neutron densities or radii with an accuracy of 1% [41], which can in turn be achieved through parity violating experiments.

Experimentally one could use polarized electron scattering to measure the parity-violating asymmetry

$$A_{LR} = \frac{\sigma_R - \sigma_L}{\sigma_R + \sigma_L}, \quad (2.5)$$

where  $\sigma_{L(R)}$  is the cross section for scattering left (right) handed electrons. The interaction which describe the process is

$$\mathcal{V}(r) = V(r) + \gamma_5 A(r), \quad (2.6)$$

with  $V(r)$  the usual Coulomb potential, and  $A(r)$  the axial (weak) potential which can be written in terms of protons and neutron densities as [41–43]

$$A(r) = \frac{G_F}{2^{3/2}} [(1 - 4 \sin^2 \theta_W) Z \rho_p(r) - N \rho_N(r)]. \quad (2.7)$$

In the last equation,  $G_F$  stands for the Fermi coupling constant, and  $\theta_W$  for the weak mixing angle.  $A(r)$  is of the order of 1 eV, much smaller than the Coulomb term  $V(r)$  which is of a few MeV. It is therefore difficult to measure its influence by other means than parity violation. Moreover, the value of the mixing angle gives  $\sin^2 \theta_W \sim 0.23$ , so that in the weak interaction sector, the electron couples mostly with neutrons.

In the Born approximation, one obtains for the parity-violating asymmetry, at a momentum transfer  $Q^2$ ,

$$A_{LR} \simeq \frac{G_F Q^2}{4\pi\sqrt{2}} \frac{F_n(Q^2)}{F_p(Q^2)} \quad (2.8)$$

where

$$F_{p(n)}(Q^2) = \frac{1}{4\pi} \int d^3r j_0(qr) \rho_{p(n)}(r) \quad (2.9)$$

is the form factor for protons (neutrons), with  $q = (Q^2)^{1/2}$  and  $j_0$  the zeroth spherical Bessel function. Since the form factor for protons is known from non-polarized electron scattering, one can see that  $A_{LR}$  directly measures the neutron form factor and implicitly the neutron density and radius.

To this moment, there are no parity-violating experiments to measure  $A_{LR}$ , but the thorough analysis in Ref. [41] concludes that they are feasible: (i) there are high quality electron beam facilities able to handle such an experiment and (ii) the corrections to the parity violating asymmetry have small uncertainties which are well understood. Finally, the point relevant to the present investigation is that in the near future new and accurate experimental data will be available for the neutron radii and densities. It is very likely that this will be a serious test of the nuclear microscopic theories with big impact on nuclear physics.

## 2.3 Survey of Methods for Computing Masses and Radii

In this chapter we have reviewed the motivation for a global macroscopic theory. It is time now to discuss the present methods for computing nuclear masses and radii.

One of the oldest and best known mass formula is Bethe-Weizsäcker [44]. It parametrizes the binding energy as a sum of volume, surface, Coulomb, asymmetry and pairing terms, the parameters involved being fitted to obtain the experimental masses. This parametrization gives good description for a large number of medium and heavy nuclei in the stability region, but fails to model correctly binding energies of light nuclei near the driplines. Recently, Samata and Adhikari have proposed corrections [45] to the old formula and they reproduced successfully available experimental data; however, a fundamental basis for the new mass formula is still to be found [45].

The simplest model for radii is to consider the nucleus as a sphere with constant density and sharp surface [10], so that the radius is

$$R = r_0 A^{1/3},$$

with  $r_0 = 1.2$  fm. This is of course an over-simplified model, and one obtains just a rough agreement with the experimental data. Moreover, it does not make any distinction between proton and neutron radii.

Basically, for a global approach, there are two types of methods: macroscopic-microscopic and mean-field approximations. Shell model calculations, while successful and fully microscopic, are limited to light and medium nuclei; furthermore, the effective interaction is space dependent and for different mass regions one has to derive different Hamiltonians.

There are several versions of the macroscopic-microscopic methods, and the most recent ones are finite-range droplet model (FRDM) [46–48] and Thomas-Fermi (TF) [48, 49]. In these models, one writes the binding energy as sum of macroscopic and microscopic contributions [46–48]. The macroscopic part is calculated either from a modified liquid-drop model, as in FRDM, or from an effective nucleon-nucleon interaction, as in TF.

The droplet model is a generalization of the incompressible liquid drop model. In the latter, the proton and neutron densities are considered constant, with a sharp drop at the nuclear surface. The droplet model on the other hand assumes that the densities present a diffuse surface, incorporating a Yukawa plus exponential model for surface tension [46]. The experimental mass data is described with nine parameter determined from direct fit to the ground-state energies of 1654 nuclei and 28 fission-barriers heights, the r.m.s. deviation being 0.669 MeV for the nuclei considered, but only 0.448 MeV for nuclei with  $N > 65$  [46]. Very good agreement with the experimental data has been also obtained for spin and parities of spherical nuclei; notable disagreement however appears (and increases) when going from spherical to deformed nuclei [47]. Gamow-Teller decay rates are calculated in quasi-particle random phase approximation, with the computed nuclear ground-state shapes taken as input quantities [47]; the calculated decay lifetimes can differ however by order of magnitude from the measured ones. But as noted previously, the lifetimes play a crucial role in the description of the  $r$ -process, and such large differences can influence dramatically the predicted abundances.

The TF's basic assumption is that one has two fermions per  $h^3$  of phase space. In order to develop a statistical model of nuclear properties, one combines TF approach with an effective interaction between nucleons, taken to have a Yukawa form and containing seven

parameters adjusted by fit to a comprehensive set of experimental data [49]. The model yields the binding energy of a nucleus as a function of  $N$ ,  $Z$  and the nuclear shape, with an r.m.s. of 0.655 MeV for the data considered. It is very difficult however to predict its reliability for nuclei close to the driplines as it neglects (*i*) nucleon-nucleon correlations, and (*ii*) some quantal effects (higher order terms in  $\hbar^2$  expansion), which should become important in these cases.

Extended Thomas-Fermi model with Strutinski integral (ETFSI) is a hybrid between the HF approximation and the macroscopic-microscopic approach, which uses an expansion of the HF energy in terms of

$$\delta\rho = \rho_{\text{HF}} - \tilde{\rho},$$

where  $\tilde{\rho}$  is a smooth approximation of the one-body HF density  $\rho_{\text{HF}}$ . The binding energy is then given by the Strutinsky theorem [50]

$$E[\rho_{\text{HF}}] \approx E[\tilde{\rho}] + \sum_{i,q} \epsilon_i^q - \text{Tr}(\tilde{h}\tilde{\rho}), \quad (2.10)$$

where  $\tilde{h}$  is the smooth single-particle Hamiltonian,  $\epsilon$  are the its eigenvalues, and  $i$  runs over all occupied states,  $q$  standing for both protons and neutrons. While Eq. (2.10) has the same form as the macroscopic contribution in FRDM, the difference is that in this case its smooth part  $E[\tilde{\rho}]$  is connected with the *microscopic* corrections, as one uses the same smooth density  $\tilde{\rho}$  for both.

For mean-field calculations in ETFSI, one considers a Skyrme (zero range) force whose parameters are obtained through a fit to known nuclear masses. The mean-field density for protons and neutrons has a simple Fermi form [50] with the defining parameters chosen so that one minimizes the smooth contribution of the energy  $E[\tilde{\rho}]$ . Overall, the ETFSI mass formula uses eight parameters, obtaining a r.m.s. error of 0.736 MeV for 1492 nuclei investigated; the charge radius r.m.s. error for 99 nuclides listed in Ref. [51] is remarkably small, of only 0.036 fm. Like for the less sophisticated TF theory though, it is hard to estimate how reliable an extrapolation to nuclei far from stability would be, for similar reasons.

The microscopic method of choice for calculating ground-state properties is the Hartree-Fock-Bogoliubov (HFB) approximation. In most applications, two types of (effective) forces describe the interaction between nucleons: zero range, such as Skyrme interaction [52], and finite range, such as Gaussians [53] or Gogny interactions [54]. A fit to the experimental binding energies over a large range of nuclei provides the adjustable parameters in each case. But due to differences in fitting procedures, such as the actual number of experimental masses used, one obtains different sets of parameters, and therefore different effective interactions. Nevertheless, one fits interactions which in principle could be used to calculate ground-state properties of nuclei throughout the periodic table. Depending upon the interaction used, the r.m.s. deviation for masses is between 2 and 4 MeV for the spherical nuclei considered in Ref. [48], a step back from the macroscopic-microscopic models which as noted before obtain r.m.s. deviations below 1 MeV. Interestingly enough, Bohigas and Leboeuf have

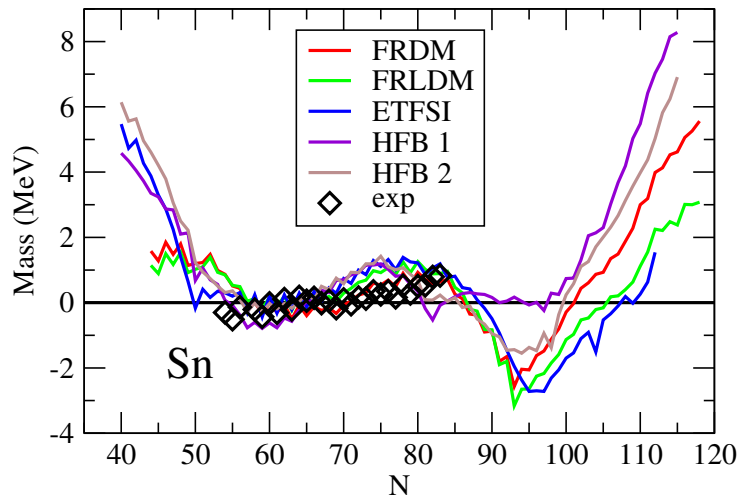


Figure 2.2: Sn isotopes: various theoretical masses relative to the Duflo and Zuker model; diamonds represent experimental values. The two HFB calculations use different sets of parameters.

estimated using chaos theory that the lowest r.m.s. error in mean-field fits should be around 0.5 MeV [55]. Relativistic mean-field calculations come very close to this value obtaining a r.m.s. error of 0.738 MeV [56], reaching basically the level of accuracy of the semiclassical approaches.

Mean-field models however neglect correlations, as discussed extensively in Chapter 4. And although in this approach one obtains in general good agreement with the experimental masses, beyond mean-field correlations become important when describing other properties, such as expectation values or transitions. Another very successful theory which includes all possible correlations in a restricted space is the interacting shell model; within its framework, the r.m.s. for binding energies is under 1 MeV, while other observables are also well described. There are however two major obstacles in adopting the shell model as a global theory. First, the restriction of the available space requires the use of an effective interaction derived so that it takes into account the neglected configurations. Thus, the effective interaction is space dependent, and to be exact one should derive an interaction for each nucleus; fortunately, the  $A$ -dependence can be parametrized as a power law of the two-body matrix elements, and the tedious task of computing an interaction for each nucleus can be avoided. Nevertheless, one derives interactions for nuclei within different major shells, so that shell model diagonalization can be applied only piecewise. Second, for heavy nuclei the number of basis states which should be included even within a major shell becomes too large, and further truncations are necessary. Present state of the art calculations have succeeded full  $0\hbar\omega$  calculations for nuclei in the mid  $pf$  shell; this requires however significant computational effort.

Using general scaling arguments and schematic shell model calculations, Duflo and Zuker have proposed a mass formula which describes the binding energies with r.m.s. error of

375 keV [57]; tests of extrapolation properties were also successful. However this approach involves no less than 28 parameters which must be fitted to known experimental data.

Finally, Fig. 2.2 compares several theoretical models, both semiclassical and microscopic, for tin isotope masses. All models tend to agree in the region where experimental data is available. On the other hand, they widely disagree for isotopes toward proton and neutron driplines, illustrating the need for a reliable nuclear theory.

To summarize this entire chapter, we have argued about the necessity to develop reliable theoretical nuclear models. Explosive  $r$ -nucleosynthesis provides a strong argument, as it requires accurate binding energies, weak transition rates and neutron capture rates for a large number of nuclei far from stability, inaccessible yet experimentally. Theoretical models can be however validated only by successful description of the experimental data; since the latter cannot be obtained for nuclei close or at the driplines, one would like to supplement the experimental binding energies and transition rates for stable nuclei with other tests. Possible candidates are neutron radii and nuclear densities; parity violation reviewed in this chapter provide means to determine both experimentally. Finally, we presented latest nuclear models for masses and radii and saw that for global approaches the most successful are either semiclassical approximations or microscopic mean-field theories. They all have the shortcoming that leave out correlations, important for a good model of nuclear properties. Therefore, none of the successful approaches can claim a reliable extrapolation outside the stability region, so that the search for a reliable microscopic theory is more motivated than ever.

# 3 Interacting Shell Model

In principle, the Hilbert space associated to any nucleus (or quantum system) is infinite dimensional, so one has to truncate the model space to a computationally tractable size. In the shell-model calculations, one starts with a double magic nucleus as an inert core, allowing only a small number of valence nucleons to interact (see Fig. 1.1). The model basis space is consequently defined by the selection of active single nucleon orbits, along with their configurations and couplings. Such a truncated basis requires introduction of a model-space-dependent effective interaction which is a modification of the free-space nucleon-nucleon interaction. This procedure allows taking into account the influence of the eliminated possible configurations.

This chapter outlines main aspects of SM calculation, such as basis states, properties of the solutions and numerical procedures involved.

## 3.1 General Considerations

The solution to the many-body Schrödinger equation

$$\mathcal{H}\Psi(1, 2, \dots, A) = E\Psi(1, 2, \dots, A), \quad (3.1)$$

would constitute the fully microscopic theory of the atomic nucleus. All the nuclear properties, such as energy, spin, parity, magnetic moment, etc., would be computed simply as averages of well defined operators over the wave functions  $\Psi$ .

As already noted, Eq. (3.1) cannot be solved in the full space. It is reasonable to assume that only the nucleons outside a closed shell nucleus determine the properties of the entire system, much like the valence electrons determine the electro-chemical properties in atomic physics [58]. Moreover, the space is reduced to a size allowing a numerical solution by restricting the single particle states to a finite number. The transformation to the restricted model space has to preserve the energy spectra and the structure of the wave-function, so that in the interacting SM Eq. (3.1) becomes

$$H\psi(1, 2, \dots, n) = E\psi(1, 2, \dots, n). \quad (3.2)$$

Here the number of particles has been reduced from  $A$  to  $n$ , valence nucleons only, and  $H$  replaces the original Hamiltonian  $\mathcal{H}$ . Electromagnetic and weak transitions are serious

tests of the ability of the interacting SM to provide correct wave-functions. In principle,  $H$  can contain up to  $A$ -body terms; phenomenologically, one finds that the low-lying spectra and transitions are well described just by using effective two-body interactions. Thus, the Hamiltonian  $H$  can be written

$$H = \sum_i T(i) + \frac{1}{2} \sum_{ij} V(i, j), \quad (3.3)$$

with  $T(i) = -\hbar^2 \nabla_i^2 / (2m)$  the kinetic energy of the nucleon  $i$  and  $V(i, j)$  the two-body interaction term. (From now on  $\hbar = 1$ .)

Determining the Hamiltonian  $H$  in the restricted space is not trivial. In SM one assumes that the two-body part can be absorbed into a central one-body part  $U(i)$ , so that

$$H \simeq \sum_i H_0(i) + \frac{1}{2} \sum_{i,j} H_{12}(i, j), \quad (3.4)$$

with  $H_0(i) = T(i) + U(i)$  and  $H_{12} = V(i, j) - U(i)$ . One chooses  $U(i)$  in such a way that the residual interaction  $H_{12}$  is small enough to be treated in perturbation theory. Usually the assumption is that  $H_0$  is a sum of spherical harmonic oscillator, a spin-orbit ( $l \cdot s$ ) interaction and a term proportional to  $l^2$  [59, 60]. Thus, the first nuclear shell-model calculations were based on just filling the lower orbits according to the Pauli principle [10, 11]; in this simple calculations,  $H_{12}$  is omitted (non-interacting SM). The one-body eigenvalue problem

$$H_0 \phi_m = \varepsilon_m \phi_m \quad (3.5)$$

determines a set of single-particle states. Here  $m$  is a label for the state and includes all the quantum numbers that determine the state (e.g., harmonic oscillator,  $l$ ,  $s$ ,  $j$  and so on). While the number of states is infinite, in the interacting SM one makes available to the valence nucleons just a small number. A  $0\hbar\omega$  is the smallest model space and it includes basis states within a single oscillator shell. In general,  $n\hbar\omega$  means the number of harmonic oscillator quanta excited about the Fermi surface, and full  $n\hbar\omega$  calculation means including all possible configurations within that model space. But the possible use of different model spaces makes the choice of an appropriate two-nucleon interaction a difficult task mainly because this problem does not have a unique answer, the “effective force” depending on the particular model space considered for handling the low-lying states [11].

## 3.2 Basis States in Shell Model

The method for solving any eigenvalue problem is, in principle, simple. One defines a complete basis and transforms from the operator equation, e.g., Eq. (3.2), to a matrix equation. While no matter how one selects the basis, the result is the same, making the right choice can reduce drastically the amount of work required.

How do we choose the basis? First, we have to take into account that the interacting particles are fermions and their wave-function *must* be anti-symmetrical under any two-particle exchange. Thus, starting from a set of single-particle states given by Eq. (3.5), modern SM codes construct the many-body basis states as Slater determinants, represented in the computer as binary words with one for occupied single-particle states and zero for unoccupied ones.

Second, we consider symmetries of the Hamiltonian. For example, the Hamiltonian is rotationally invariant and this translates into the commutation relation

$$[J^2, H] = 0.$$

In such a case, the eigenfunctions of the Hamiltonian will be simultaneously eigenfunctions for  $J^2$ . Consider for example an even-even nucleus. Then,  $J$  can be only integer. So, in order to calculate  $J = 0$  states of  $H$  we would have to include in the basis only multi-nucleon states which have  $J = 0$  and are anti-symmetrical under two nucleon exchange. It turns out though that the  $J^2$  eigenvectors are *superpositions* of Slater determinants, and the manipulation becomes difficult. But we can use a similar commutation relation,

$$[J_z, H] = 0,$$

and construct the basis states to have a fixed total angular momentum projection on  $z$  axis, called  $m$ -scheme states. Shell model codes such as GLASGOW [61], ANTOINE [62], and REDSTICK [63] do build many-body basis states in such a manner. While in this case the basis states do not have good  $J$ , the Hamiltonian wave functions obtained by diagonalization will by simultaneously also eigenvectors for  $J$ . Another possible approach, used in OXBASH [64] shell-model code, is to construct basis states with good spin and isospin from  $m$ -scheme states.

Other symmetries which are sometimes used in modern SM codes in order to reduce the dimensions are charge conjugation ( $N = Z$  nuclei), which allows one to separate out even  $T$  from odd  $T$ , and time reversal (even-even nuclei), which allows one to separate even  $J$  from odd  $J$ .

The main inconvenience in SM calculations is the large number of many-body basis states; to give the reader a feeling about the actual dimensions involved, we consider two nuclei in a particular  $0\hbar\omega$  space. The  $sd$  shell includes the degenerate single particle states having the harmonic oscillator quantum number  $n = 2$  (and therefore the total angular momentum  $j = 1/2, 3/2, 5/2$ ), outside a  $^{16}\text{O}$  inert core. The spin-orbit splitting removes the degeneracy over  $j$ , but not the degeneracy over  $j_z$ . The total number of single-particle states available for one type of particles is 12. Taking for example  $^{24}\text{Mg}$ , i.e., four protons and four neutrons in the valence space, the number of Slater determinants that we can create so that  $J_z = 0$  (for the Slater determinant) is 28503. For  $^{28}\text{Si}$  (six protons and six neutrons in the valence space), 93710. If we use all possible symmetries, one can reduce the number of many-body states to 7326 for  $^{24}\text{Mg}$ , and 23794 for  $^{28}\text{Si}$ . It is obvious that, even when one includes all possible symmetries in the basis, the dimensions involved are too large to consider a diagonalization

which produces all the states. In turn, one uses a numerical trick, the Lanczos algorithm [61] which provides, through an iteration procedure rapidly convergent, the low-lying eigenstates of the Hamiltonian.

In the restricted space, if *all* possible many-body configurations are included, SM provides the exact solution. The wave-functions corresponding to ground and excited states are also eigenstates of the total angular momentum  $J$ , parity and isospin.

### 3.3 Observables

Observables are described in quantum mechanics by operators. Since the diagonalization provides the wave functions in the restricted space as linear superpositions of basis states, it is a simple (while not trivial) exercise to calculate mean-values for operators of interest. Although the space is restricted, some relevant operators such as total angular momentum  $J$  or total spin  $S$ , are complete in the valence space. In such cases, unlike that for the Hamiltonian, one does not have to calculate an effective operator to account for truncation. There is however an important operator,  $Q \cdot Q$  (quadrupole-quadrupole), which is not complete in a  $0\hbar\omega$  space. To keep it within a single oscillator model space, we use an algebraic quadrupole operator introduced by Elliott [65]

$$Q_\mu = \frac{1}{2} \sum_i [r_i^2 Y_{2\mu}(\hat{\mathbf{r}}_i) + b^2 p^2 Y_{2\mu}(\hat{\mathbf{p}}_i)], \quad (3.6)$$

which, for harmonic oscillator single particle states, has the same matrix elements as the physical quadrupole operator

$$Q_\mu^p = \sum_i r_i^2 Y_{2\mu}(\hat{\mathbf{r}}_i). \quad (3.7)$$

In the last two equations,  $Y_{2\mu}$ ,  $\mu = 0, \pm 1, \pm 2$ , are the usual spherical harmonics, and the summation runs over valence particles; in Eq. (3.6)  $p$  stands for momentum operator, while  $b^2 = \hbar/(m\omega)$  is the harmonic oscillator parameter. Using the definition (3.6), one constructs the quadrupole-quadrupole operator  $Q \cdot Q = \sum_\mu (-1)^\mu Q_\mu Q_{-\mu}$ , which is now complete in a  $0\hbar\omega$  space.

One observable which is important to describe is the rms radius. Can we use the SM to calculate this? In principle, yes. But in the process of deriving an effective interaction one removes most of the radial information in the single particle wave function (see Sec. 3.5), so that the result depends at the end upon the choice of the radial form for the single particle wave function (harmonic oscillator, Wood-Saxon, etc.).

### 3.4 Transitions

Transitions offer an ultimate test for the correctness of SM solution to the many-body problem, as they probe into the structure of wave functions. Moreover, experimentalists use gamma transitions in order to assign spin and parities of excited states.

In the long wavelength limit ( $k = \omega/c \ll R$ ,  $R$ =nuclear radius), the transition rate per unit time is [11]

$$T(JT) = \frac{8\pi c e^2}{\hbar c (J+1)} \frac{1}{J[(2J+1)!!]^2} S_{fi}(JT), \quad (3.8)$$

with the transition strength from the initial state ( $i$ ) to the final state ( $f$ )  $S_{fi}$  containing all the information about the nuclear structure

$$S_{fi}(JT) = \sum_{M, T_z, M_f, T_f} |\langle f; J_f T_f | F(JM, TT_z) | i; J_i T_i \rangle|^2. \quad (3.9)$$

Here  $F(JM, TT_z)$  is the transition operator,  $J$  and  $T$  stand for total angular momentum and isospin respectively, while  $M$  and  $T_z$  are the third axis projections of  $J$  and  $T$ . Because the wave functions have good spin and isospin one uses the Wigner-Eckart theorem [67] and writes the strength in Eq. (3.9) in terms of the double reduced matrix element [11]

$$S_{fi} = \frac{1}{(2J_i + 1)} |\langle i; J_i T_i || F_{JT} || f; J_f T_f \rangle|^2. \quad (3.10)$$

Finally, the reduced matrix element can be calculated by using the reduced one-body density and the reduced matrix element of the transition operator in the single particle space, as shown in Appendix A. However, a more efficient procedure involving the Lanczos algorithm is briefly described in Sec. 3.4.2.

The reduction of the available single particle states and active particles presented in this chapter makes the diagonalization numerically tractable. There is a downside though: in order to take into account the restriction of the Hilbert space one has to use modified (effective) operators to describe transitions. In many cases however, a simple phenomenological use of either enhanced or quenched couplings, most famously the former for  $E2$  transitions and the latter for Gamow-Teller transitions, yields good agreement with experiment.

### 3.4.1 Sum Rules

In this section we discuss important quantities which describe transitions and have general applicability. This is the reason in this section we drop the references to total angular momentum or isospin and in turn we consider a complete set of eigenstates of the Hamiltonian  $H$ .

Our investigation focused on transitions from excited to the ground states, as the RPA does not describe excited to excited state transitions. Therefore, similar to Eq. (3.9), the transition strength from an excited to the ground-state is given by the square of the matrix element,

$$S(\nu \rightarrow 0) = |\langle \nu | F | 0 \rangle|^2.$$

The quantity

$$S_k = \sum_{\nu} (E_{\nu} - E_0)^k |\langle \nu | F | 0 \rangle|^2 \quad (3.11)$$

is the (energy weighted) sum rule of order  $k$ . In this equation,  $\nu$  runs over all states, 0 stands for the ground state, and  $F$  is an arbitrary transition operator. Particularly important is  $S_0$ , which is the total transition strength from the ground state to excited states, and which can be rewritten as a ground state expectation value:

$$S_0 \equiv \sum_{\nu} |\langle \nu | F | 0 \rangle|^2 = \langle 0 | F^\dagger F | 0 \rangle. \quad (3.12)$$

In most realistic applications the transition operator is a spherical tensor of rank  $K$ ,  $F_{KM}$ , which has the property  $F_{KM}^\dagger = (-1)^M F_{K-M}$  [67]. Then properly the total strength in Eq. (3.12) should be

$$S_0 = \sum_M (-1)^M \langle 0 | F_{K-M} F_{KM} | 0 \rangle, \quad (3.13)$$

and similarly for the double commutator in the energy-weighted sum rule, etc. To avoid clutter we drop the sum over  $M$  and it should be assumed to be implicit.

In fact one can write all the sum rules of order  $k$  as expectation values, most famously the linear energy-weighted sum rule:

$$S_1 = \sum_{\nu} (E_{\nu} - E_0) |\langle 0 | F | \nu \rangle|^2 = \frac{1}{2} \langle 0 | [F, [H, F]] | 0 \rangle. \quad (3.14)$$

In most applications of interest,  $F$  is an one-body operator for which the double commutator in the last equation is a constant or a simple one-body operator. Consequently, the expectation value in right-hand side of Eq. (3.14) is not very sensitive to the model for ground-state wave function, providing a valuable first test of approximate spectra. Moreover, it can provide answer for relevant quantities, without the need to compute the spectra in detail. For example, the total cross section for dipole absorption ( $\sigma_{tot}$ ) can be written in terms of  $S_1$  associated with the respective transition operator as [10]

$$\sigma_{tot} = \frac{4\pi^2 e^2}{c} S_1. \quad (3.15)$$

A generalization of Eq. (3.14) can be obtained for any starting state  $|\mu\rangle$ :

$$\sum_{\nu} (E_{\nu} - E_{\mu}) |\langle \mu | F | \nu \rangle|^2 = \frac{1}{2} \langle \mu | [F, [H, F]] | \mu \rangle. \quad (3.16)$$

One should emphasize however that  $|\mu\rangle$  has to be an *eigenvector* of the Hamiltonian, although we will find a specific case later when this relation holds for one particular state, which is not an exact eigenstate of the Hamiltonian.

Equation (3.14) is easy to evaluate, especially if one has a transition operator which is just  $r$  dependent, when for *local* interactions one calculates the double commutator with the kinetic energy term only. Moreover, in the particular case of a multipole transition operator,  $F = r^J Y_J$ , Eq. (3.14) becomes [10, 12]

$$S_1 = \frac{1}{2m} A \langle 0 | r^{2J-2} | 0 \rangle. \quad (3.17)$$

For  $J = 1$ , that is electric dipole ( $E1$ ), which more properly should be written with contributions from protons and neutrons [10]

$$D = \frac{NZ}{A} \left( \frac{1}{Z} \sum_{p=1}^Z r_p Y_{10}(\hat{\mathbf{r}}_p) - \frac{1}{N} \sum_{n=1}^N r_n Y_{10}(\hat{\mathbf{r}}_n) \right), \quad (3.18)$$

we obtain the Thomas-Reiche-Kuhn (TRK) sum rule

$$S_1(D) = \frac{NZ}{A} \frac{1}{m}, \quad (3.19)$$

independent upon the model for the ground state. Violation of the TRK sum rule can be interpreted as a measure of the non-locality of the nuclear potential [10].

We will often characterize our results in terms of the centroid,  $\bar{S}$ , and the width,  $\Delta S$ , of the transition strengths, defined in terms of  $S_1$  and  $S_2$

$$\bar{S} = \frac{S_1}{S_0}, \quad \Delta S = \sqrt{\frac{S_2}{S_0} - \bar{S}^2}. \quad (3.20)$$

Both the centroid and the width characterize global properties of collective excitations.

Finally, we have to emphasize that the SM set of states is not complete, as we calculate only the lowest-lying eigenstates. Nevertheless, Eqs. (3.11)–(3.14) remain valid, as in applications of interest the transitions from higher lying states to the ground state are exactly forbidden (that is, for such states,  $\langle \nu | F | 0 \rangle = 0$ ).

### 3.4.2 *Lumus Solem* for Transitions<sup>1</sup>

In principle one can calculate one-body densities and use them to compute reduced matrix elements by means of Eq. (A.3). However, this procedure is not very efficient, so that we have used the Lanczos moment method which is particularly useful when one is interested in the broad distribution of transition strength.

We start with the initial eigenstate  $|\Psi\rangle$  (in our applications the ground state) and apply the transition operator  $F$ , obtaining a new state  $|v_1\rangle$ :

$$|v_1\rangle = F|\Psi\rangle. \quad (3.21)$$

Then, we use  $|v_1\rangle$  as starting vector, or pivot, to construct a system of orthogonal vectors in which the Hamiltonian matrix becomes tridiagonal:

---

<sup>1</sup>*Lumus Solem* in the title of this section is a magical incantation the heroes of *Harry Potter and the Sorcerer's Stone* use to invoke Sun light when they need it; in my case, it express the feeling of almost magic inspired by the “magical” Lanczos algorithm first time I learned about it.

$$\begin{aligned}
H|v_1\rangle &= \alpha_1|v_1\rangle + \beta_1|v_2\rangle \\
H|v_2\rangle &= \beta_1|v_1\rangle + \alpha_2|v_2\rangle + \beta_2|v_3\rangle \\
H|v_3\rangle &= \beta_2|v_2\rangle + \alpha_3|v_3\rangle + \beta_3|v_4\rangle \\
&\vdots \\
H|v_n\rangle &= \beta_{n-1}|v_{n-1}\rangle + \alpha_n|v_n\rangle + \beta_n|v_{n+1}\rangle \\
&\vdots
\end{aligned}$$

The new vectors  $|v_n\rangle$  are obtained by orthogonalizing  $H|v_n\rangle$  with respect to  $|v_n\rangle$  and  $|v_{n-1}\rangle$ . In principle one can construct as many orthogonal vectors as the dimension of the space. But in practice, because the dimensions involved are very large, we stop at a smaller number. Each step is called an iteration, and when the number of iterations is large enough, the extreme eigenvalues converge to the exact ones (like magic). The tridiagonal matrix is the Jacobi matrix associated with the moments

$$\mu_n = \langle v_1|H^n|v_1\rangle, \quad (3.22)$$

and for  $N$  iterations, it provides the first  $(2N - 1)$  moments exactly [68]. It is a simple exercise to obtain the energy-weighted sum rules from the moments (3.22), so that one can immediately see that this procedure provides exactly the first  $(2N - 1)$  sum rules. The size of the pivot vector is the total transition strength  $S_0$ , and the overlap of the pivot with the final eigenstate, which it turns out can be read off trivially, is the transition amplitude. The interested reader is referred to Ref. [69] for further details.

### 3.5 Shell Model Interaction

As already mentioned, obtaining the effective SM Hamiltonian is a non-trivial task. One way is to start from the bare nucleon-nucleon interaction and use a well defined procedure to project all the operators, including the Hamiltonian, in the valence space [70]. In the following we sketch the formalism.

Consider two interacting particles and let  $|\tau\rangle$  be the wave function; the Schrödinger equation is

$$(H_0 + V)|\tau\rangle = E_\tau|\tau\rangle, \quad (3.23)$$

where  $V$  can be, in principle, the bare nucleon-nucleon interaction. The last equation transforms into two equations if we multiply on the left by  $P$  and  $Q$ , the projectors inside and outside the valence space respectively:

$$(-E_\tau + H_0 + PVP)P|\tau\rangle = -PVQ|\tau\rangle, \quad (3.24)$$

$$(-E_\tau + H_0 + QVQ)Q|\tau\rangle = -QVP|\tau\rangle. \quad (3.25)$$

Solving the latter for the wave function outside the model space  $Q|\tau\rangle$ , and plugging into the former, one obtains a Schrödinger equation inside the valence space [10]:

$$(H_0 + PV_{eff}^{E_\tau}P)P|\tau\rangle = E_\tau P|\tau\rangle, \quad (3.26)$$

with the effective nucleon-nucleon interaction in the valence space given by

$$V_{eff}^{E_\tau} = V + VQ \frac{1}{E_\tau - H_0 - QVQ} QV. \quad (3.27)$$

This can be rewritten as an integral equation for  $V_{eff}^{E_\tau}$  [10]; furthermore, in the particular case when the  $Q$  operator corresponds to the two-particle excited states outside the model space (which brings the largest contribution), one can show that the equation for  $V_{eff}$  is similar to the equation for Brückner  $G$ -matrix [71]. Therefore, computation of effective interaction reduces to calculation of the  $G$ -matrix.

The effective interaction obtained through the procedure outlined above does not provide good description of the low-lying states. Therefore, one further adjusts the two-body interaction using a fitting procedure so that one obtains a correct description of ground and excited states for a large number of nuclei. Thus, as we saw in Sec. 3.1, one chooses the two-body part so that it is small enough to consider it as perturbation. Hence, we can solve the single-particle eigenvalue problem for  $H_0$ , and obtain a set of single-particle states. Using the determined single-particle wave functions, the integral

$$\langle \alpha'_1 \alpha'_2 | H_{12} | \alpha_1 \alpha_2 \rangle = \int d\mathbf{r}_1 d\mathbf{r}_2 \phi_{\alpha'_1}^*(\mathbf{r}_1) \phi_{\alpha'_2}^*(\mathbf{r}_2) H_{12}(\mathbf{r}_1, \mathbf{r}_2) \phi_{\alpha_1}(\mathbf{r}_1) \phi_{\alpha_2}(\mathbf{r}_2) \quad (3.28)$$

yields the (non-symmetrized) two-body matrix element (TBME), where each  $\alpha$  is a label for the single-particle quantum numbers.

Note that the integral in (3.28) is a *number*, so that one possible approach is to completely ignore the analytical form of the nucleon-nucleon interaction potential  $H_{12}(\mathbf{r}_i, \mathbf{r}_j)$ . The effective TBME approximation consists in assuming that each matrix element, normally given by (3.28) with the appropriate anti-symmetrization, is a parameter which can be adjusted in order to obtain the experimental spectra of nuclei, and the  $G$ -matrix is usually the first step of the iteration. Because it is analytically convenient, one usually chooses single-particle states corresponding to the harmonic oscillator. This has no relevance for diagonalization, but it becomes important for calculating transition strengths when one has to evaluate matrix elements of different operators, as the reduced matrix elements of the corresponding operator depend upon the radial structure of the single-particle wave function. In most cases, one limits to a single major shell ( $0\hbar\omega$ ). Extension to multiple shells, essential for description of transitions which involve parity change (e.g.,  $E1$ ), is difficult because, aside from increase in the dimensionality of the space, one has to separate the center of mass motion.

In the full  $sd$  space the parameters are the three single-particle energies (the spin-orbit interaction removes the degeneracy)  $\varepsilon_{1s_{1/2}}$ ,  $\varepsilon_{0d_{3/2}}$  and  $\varepsilon_{0d_{5/2}}$  plus 63 TBME. One way to determine the parameters is to use an iterative least-square fit to experimental data. Since

a direct fit of all the parameters is computationally very expensive, the linear combination method can be applied. The Hamiltonian parameters and experimental energies form a set of equations; rather than solving it directly, the matrix can be diagonalized, the eigenvectors being combinations of the Hamiltonian parameters which are uncorrelated one from another with respect to the data set. The Wildenthal “USD” interaction [72] is fitted to reproduce 447 ground and excited states of  $sd$  shell nuclei ( $A = 17 - 40$ ). Of the total of 66 parameters, 47 linear combinations of parameters were varied in the last iteration [66].

We also use in our investigation the monopole-modified Kuo-Brown “KB3” interaction [73]; this was derived starting from the  $G$ -matrix as first approximation, and then fitting the matrix elements to describe experimental data. The valence space is the  $pf$  shell, that is nucleons limited to  $1p_{1/2} - 1p_{3/2} - 0f_{5/2} - 0f_{7/2}$  single particle states outside a  $^{40}\text{Ca}$  inert core. However, the number of exact calculations in full  $0\hbar\omega$  space that our computer code can handle is small, as the dimensions increase very rapidly in this valence space.

Finally, while not directly related with our investigation, we should mention in this context the no-core interacting shell model (NCSM). Within its framework, *all* the nucleons are allowed to interact, and for this reason it was successful in describing the nuclear spectra in very light nuclei ( $A \leq 12$ ) only. One limits however the number of available single-particle states, and this requires an effective interaction from the bare nucleon-nucleon interaction. Unlike that for phenomenological interactions described above, one does not fit any longer the two-body effective nucleon-nucleon interaction to experimental data. The solution is to increase available single-particle space until one obtains convergence of the solution [74, 75]; three-body effective forces have been shown to increase the convergence rate [76]. Furthermore, *realistic* three-body interaction has been shown to be essential for the correct description of the ground state in  $^{10}\text{B}$  [77] and the low-lying spectrum of  $^{12}\text{C}$  [78]. Despite the exciting results, the NCSM is still in an incipient phase; for example, the low-lying spectra has to be supplemented with calculations of transition distributions, which will truly confirm the correctness of theoretical wave functions. However, a detailed discussion about the NCSM is well beyond the purpose of the present work.

# 4 Mean-Field Theory and Random Phase Approximation

In the interacting SM, a complete basis will provide a fully microscopic description of the many-body system, the ground and excited states being linear superpositions of Slater determinants. Mean-field theory on the other hand aims to describe the ground state of interacting fermions with just *one* Slater determinant. And it does a reasonable good job, while not extraordinary: mean-field theory provides a good *first* approximation to the exact solution, but leaves out correlations and can break symmetries.

This chapter presents one particular type of mean-field theory, that is the Hartree-Fock (HF) approximation. In HF theory, only rotational and translational symmetries can be broken. Other approaches involve proton and neutron number breaking (instead of protons and neutrons, one uses the isospin quantum number and constructs “deformed” single-particle orbits as superpositions of both proton and neutron states), or particle number breaking, i.e., Hartree-Fock-Bogoliubov method.

The basis of mean-field theory is a variational principle with the trial wave function a Slater determinant. This allows derivation of a mean one-body potential from the two-body interaction. Thus, the mean-field solution preserves the simplicity of the non-interacting shell-model, as the Slater determinant is built by considering the particles uncorrelated and filling up the lowest single-particle orbits determined by the *mean* one-body Hamiltonian; such a procedure ensures therefore a first order treatment of the two-body interaction. Moreover, because the mean field is derived from a variational principle, we know that the mean-field energy is *above* the exact energy.

Nevertheless, in order to obtain a better wave function as well as a more correct treatment of the two-body interaction, one introduces correlations on top of the mean-field solution. One way, investigated in this work, is the random phase approximation (RPA), which treats the energy surface around the mean-field minimum as a multi-dimensional harmonic oscillator whose excitations approximate the excited states of the many-body system. The zero motion energy of the harmonic oscillator is the correction to the mean-field energy. We should mention at this point that most of the material covered in this chapter can be found in any nuclear physics textbook, in a form or another. We draw however the reader’s attention to Sec. 4.2.4, where we present an original extension to the RPA formula for correlation energy, which allows us to compute RPA corrections to mean-field expectation values of general scalar observables.

Depending on the mean-field theory used and the symmetries broken, one can also have more types of correlations. For example, quasi-particle RPA builds quasi-particle correlations on top of the HFB solution and breaks particle-number conservation. Since as already mentioned, our mean-field solution is the HF state, we consider only the particle-number conserving RPA, although we have plans to test other RPA versions in the near future.

## 4.1 Hartree-Fock Approximation

Consider a general one- plus two-body Hamiltonian, e.g., the shell model effective interaction. For the time being, we will assume just one type of particles, as the generalization to protons and neutrons is straightforward. Using a complete set of *single-particle* states denoted by Greek letters and referred to below as *fundamental*, the general form of the Hamiltonian  $H$  in the second quantization is [10, 11]

$$H = \sum_{\alpha\beta} t_{\alpha\beta} a_{\alpha}^{\dagger} a_{\beta} + \frac{1}{4} \sum_{\alpha\beta\gamma\delta} V_{\alpha\beta;\gamma\delta} a_{\alpha}^{\dagger} a_{\beta}^{\dagger} a_{\delta} a_{\gamma}, \quad (4.1)$$

where  $V$  is the anti-symmetrized two-body matrix element,

$$V_{\alpha\beta;\gamma\delta} = -V_{\alpha\beta;\delta\gamma} = -V_{\beta\alpha;\gamma\delta},$$

with  $a_{\alpha}^{\dagger}$  ( $a_{\beta}$ ) the creation (annihilation) operator of one fermion on the state  $\alpha$  ( $\beta$ ) fulfilling the usual anti-commutation relations:

$$\{a_{\beta}, a_{\alpha}^{\dagger}\} = a_{\beta} a_{\alpha}^{\dagger} + a_{\alpha}^{\dagger} a_{\beta} = \delta_{\alpha\beta}, \quad \{a_{\beta}, a_{\alpha}\} = 0, \quad \{a_{\beta}^{\dagger}, a_{\alpha}^{\dagger}\} = 0. \quad (4.2)$$

(To avoid confusion, note that in the last equation  $\delta_{\alpha\beta}$  stands for the Kronecker symbol which is equal to one if  $\alpha = \beta$ , that is the same state, and zero otherwise.)

Any Slater determinant can be written as

$$|\psi\rangle = \prod_{i=1}^N c_i^{\dagger} |0\rangle, \quad (4.3)$$

where  $N$  is the number of particles,  $|0\rangle$  is the vacuum state defined by the condition  $c_{\alpha}|0\rangle = 0$ , and  $c_i^{\dagger}$  is the creation operator for the occupied states. A unitary transformation connects the fundamental and the new (deformed) basis states so that one preserves the commutation relations (4.2). (In other words, we assume that each particle does not occupy in general one of the fundamental basis states, but a superposition of such states.) In the HF approximation we use Slater determinants given by Eq. (4.3) as trial wave functions; the variational principle is equivalent with finding the unitary transformation which minimize the expectation value of the Hamiltonian on the trial wave function,  $\langle\psi|H|\psi\rangle$ .

In the deformed basis, the occupation numbers are zero for particle states (one can only create particles there), and one for hole states (one can only create holes by removing particles

from those states); we will refer to this basis as the *particle-hole* or ph basis. In the process of deriving the HF equations we will have to distinguish between occupied and unoccupied states. Therefore, we will follow the usual convention of further denoting occupied (hole) states by  $i, j$  and unoccupied (particle) states by  $m, n$ ; in case we do not distinguish between them, we use  $a, b$ . Mathematically, the ph basis corresponding to  $|\psi\rangle$  is defined by the conditions  $c_m|\psi\rangle = 0$ ,  $\langle\psi|c_i = 0$ , and their hermitian conjugates. Another way to state this into equations is by means of the single-particle density matrix defined in the fundamental basis as:

$$\rho_{\beta\alpha} = \langle\psi|a_\alpha^\dagger a_\beta|\psi\rangle. \quad (4.4)$$

This becomes diagonal in the ph basis with  $\rho_{ii} = 1$  and  $\rho_{mm} = 0$ .

In this context, we have to point out that *each* Slater determinant defines a ph basis; in other words, such a basis is not characteristic only to deformed bases, or to the HF approximation. Take for example the *sd* shell, considering just two particles. One can create the anti-symmetrical many-body state with one particle in the state ( $j = 1/2, j_z = 1/2$ ), and the other in the state ( $j = 5/2, j_z = -3/2$ ). These two single-particle states are the hole states, while all the other (deformed or not) available states are particle states, thus defining a ph basis for the Slater determinant in our example. Whether or not this wave function minimizes the Hamiltonian (4.1) is a completely different question, independent of the definition for the ph basis.

In order to obtain the HF equations, we have to consider fluctuations from the trial Slater determinant  $|\psi\rangle$ . For this, let us consider a very specific Thouless transformation. Define the Thouless particle-hole creation operator,

$$\hat{Z}^\dagger = \sum_{mi} Z_{mi}^* c_m^\dagger c_i, \quad (4.5)$$

and a new state by

$$|\psi'\rangle = \exp(\hat{Z}^\dagger - \hat{Z})|\psi\rangle. \quad (4.6)$$

According to the Thouless theorem [79],  $|\psi'\rangle$  is also a Slater determinant, not orthogonal to  $|\psi\rangle$ . The fact that in Eq. (4.6) we use  $\hat{Z}^\dagger - \hat{Z}$  in the exponent ensures the unitarity of the transformation, so that if  $\langle\psi|\psi\rangle = 1$ , then also  $\langle\psi'|\psi'\rangle = 1$  (norm conservation). Just for convenience, we will always use normalized wave functions.

An expansion of the energy functional to second order in  $\hat{Z}$  gives

$$\begin{aligned} E(\hat{Z}) = \langle\psi'|H|\psi'\rangle &= \langle\psi|H|\psi\rangle + \left\langle\psi\left|[H, \hat{Z}^\dagger] - [H, \hat{Z}]\right|\psi\right\rangle \\ &+ \frac{1}{2} \left\langle\psi\left|[\hat{Z}^\dagger, [H, \hat{Z}]] + [\hat{Z}, [H, \hat{Z}^\dagger]] - [\hat{Z}, [H, \hat{Z}]] - [\hat{Z}^\dagger, [H, \hat{Z}^\dagger]]\right|\psi\right\rangle. \end{aligned} \quad (4.7)$$

Considering now  $\{Z_{mi}\}$  as a multidimensional vector  $\vec{z}$  ( $\{mi\}$  is treated as a single index) instead of a matrix, and same for  $h$ , we can transform Eq. (4.7) to an equivalent form

$$E(\vec{z}) = E_0 + (\vec{h}^*, \vec{h}) \cdot \begin{pmatrix} \vec{z} \\ \vec{z}^* \end{pmatrix} + \frac{1}{2} (\vec{z}^*, \vec{z}) \cdot \begin{pmatrix} \mathbf{A}, & \mathbf{B} \\ \mathbf{B}^*, & \mathbf{A}^* \end{pmatrix} \cdot \begin{pmatrix} \vec{z} \\ \vec{z}^* \end{pmatrix} \quad (4.8)$$

where  $E_0 = \langle \psi | H | \psi \rangle$ , and

$$h_{mi} \equiv \langle \psi | [H, c_m^\dagger c_i] | \psi \rangle, \quad (4.9)$$

$$A_{nj,mi} \equiv \langle \psi | [c_j^\dagger c_n, [H, c_m^\dagger c_i]] | \psi \rangle, \quad (4.10)$$

$$B_{nj,mi} \equiv \langle \psi | [[H, c_n^\dagger c_j], c_m^\dagger c_i] | \psi \rangle. \quad (4.11)$$

Note that, although in Eqs. (4.7) and (4.8) we used  $H$ , one can make the same expansions for the expectation value of any arbitrary operator, not only for the Hamiltonian. This is how we will derive corrections to HF expectation values in the RPA.

Suppose the trial Slater determinant is the HF state, that is  $E_0 = E_{\text{HF}} = \min$ . The extremum condition, that is vanishing gradient, translates into the HF equations

$$h_{mi} = 0 \quad (4.12)$$

and its hermitian conjugate. The minimum also requires that the curvature (i.e., the stability matrix) be positive definite; we leave for a separate section a more thorough discussion regarding the stability matrix and symmetries.

Using the general Hamiltonian (4.1) and Eq. (4.9), we define in the ph basis

$$h_{ab} = T_{ab} + \sum_i V_{ai;bi},$$

which is the mean-field one-body potential (for  $h$ , we return shortly to the matrix form which is more appropriate for the present discussion). The HF conditions (4.12) can be therefore restated through the requirement that the matrix  $h$  does not mix particle and hole states. This ensures that, at the HF minimum,  $h$  commutes with the density matrix  $\rho$ , so that they are both simultaneously diagonal in the ph basis (but not necessarily in the fundamental basis):  $h_{ab} = \delta_{ab} \epsilon_a$ , with the eigenvalues  $\epsilon$  interpreted as single-particle energies. Note that the eigenvalue problem for  $h$  is not linear, as  $h$  depends on the density  $\rho$ ; this also means that we transformed the two-body problem into an one-body problem with a *self-consistent* potential, for the one-body single particle density in turn depends upon the wave functions of  $h$ .

Finally, we can compute now the HF energy as the expectation value of the Hamiltonian over the HF wave function [10]

$$E_{\text{HF}} = \sum_{i=1}^A \epsilon_i - \frac{1}{2} \sum_{i,j=1}^A V_{ij;ij}. \quad (4.13)$$

The HF energy therefore is not simply the sum of single particle energies, as the two-body interaction also contributes to the binding energy of the system.

### 4.1.1 Broken Symmetries

The HF solution is not an exact eigenstate of the many-body Hamiltonian  $H$ , but to its one-body component  $h$ ; for this reason, symmetries can be broken. Thus, while  $H = h + V_{res}$  ( $V_{res}$  being the residual interaction), one cannot assume that a commutation relation which holds for  $H$  is going to hold separately for  $h$  and  $V_{res}$ .

Broken symmetries show up in the properties of the stability matrix. To illustrate this, we return to the second condition necessary for a minimum, that is the positivity of the stability matrix. In general one can allow all the coefficient to be complex, so that one can rewrite Eq. (4.8) in terms of real numbers only

$$E(\vec{z}) = E_0 + 2(\operatorname{Re} \vec{h}, \operatorname{Im} \vec{h}) \cdot \begin{pmatrix} \operatorname{Re} \vec{z} \\ \operatorname{Im} \vec{z} \end{pmatrix} \quad (4.14)$$

$$+ (\operatorname{Re} \vec{z}, \operatorname{Im} \vec{z}) \cdot \begin{pmatrix} \operatorname{Re}(\mathbf{A} + \mathbf{B}), & -\operatorname{Im}(\mathbf{A} - \mathbf{B}) \\ \operatorname{Im}(\mathbf{A} - \mathbf{B}), & \operatorname{Re}(\mathbf{A} - \mathbf{B}) \end{pmatrix} \cdot \begin{pmatrix} \operatorname{Re} \vec{z} \\ \operatorname{Im} \vec{z} \end{pmatrix}.$$

More compactly, the latter becomes

$$E(\vec{z}') = E_0 + \vec{h}' \cdot \vec{z}' + \frac{1}{2} \vec{z}' \cdot \mathbf{S} \cdot \vec{z}', \quad (4.15)$$

where the primes remind us we have gone from complex variables to purely real numbers.

In many cases  $\mathbf{S}$  may be not positive-definite, but semi-positive-definite. Zero eigenvalues correspond to spurious (or Goldstone) modes, such as translations or rotations. They signal a flat energy surface in that direction, therefore an *invariance* with respect to certain transformations. For example, suppose the HF state is deformed; the HF energy will not change as the orientation is rotated, and this is reflected in an invariance of  $E(\vec{z})$ . Similar arguments hold for any symmetry of the system.

To simplify numerical calculations, we use only real numbers. In this case, the curvatures for  $\operatorname{Re} \vec{z}$  are eigenvalues of  $(\mathbf{A} + \mathbf{B})$  and for  $\operatorname{Im} \vec{z}$  are eigenvalues of  $(\mathbf{A} - \mathbf{B})$ . Consider again rotations, which are of the form  $\exp(i\hat{J}_i\theta_i)$ , where  $i = x, y, z$ . Because the matrices for  $\hat{J}_{x,z}$  are real, the corresponding Thouless matrices are imaginary and the zeros ought to be found in  $(\mathbf{A} - \mathbf{B})$ . Rotations about the  $y$ -axis ought to be found in the real sector, that is, zeros of  $(\mathbf{A} + \mathbf{B})$ . This is a very useful test: we can identify in our calculations whether we break the symmetries with respect to the  $y$  axis by computing the HF expectation value of  $\hat{J}_y^2$ . Using the above deduction, we see that we should obtain no zero eigenvalues for  $(\mathbf{A} + \mathbf{B})$  if the rotational symmetry with respect  $y$  axis is not broken. Also, if only the rotational symmetry can be broken in the model, we expect at the most three zero modes for the stability matrix: one for  $(\mathbf{A} + \mathbf{B})$ , and two for  $(\mathbf{A} - \mathbf{B})$ .

### 4.1.2 Proton and Neutron Conserving Formalism

Up to now we considered just one type of particles, while we know very well that in the nuclei there are both protons and neutrons. There are several approaches to include

both kinds of particles. We have opted for a formalism which conserves the proton and neutron numbers. In this approach, the trial functions are direct product of proton and neutron Slater determinants and Thouless transformations allow the proton and neutron single particle states to mix separately.

For a Hamiltonian which include both proton and neutron terms (one-body, proton-proton, neutron-neutron, and proton-neutron), Eq. (4.1) becomes

$$\begin{aligned}
H = & \sum_{\alpha\beta} t_{\alpha\beta}^p \pi_{\alpha}^{\dagger} \pi_{\beta} + \frac{1}{4} \sum_{\alpha\beta\gamma\delta} V_{\alpha\beta;\gamma\delta}^{pp} \pi_{\alpha}^{\dagger} \pi_{\beta}^{\dagger} \pi_{\delta} \pi_{\gamma} \\
& + \sum_{\alpha\beta} t_{\alpha\beta}^n \nu_{\alpha}^{\dagger} \nu_{\beta} + \frac{1}{4} \sum_{\alpha\beta\gamma\delta} V_{\alpha\beta;\gamma\delta}^{nn} \nu_{\alpha}^{\dagger} \nu_{\beta}^{\dagger} \nu_{\delta} \nu_{\gamma} + \sum_{\alpha\beta\gamma\delta} V_{\alpha\beta;\gamma\delta}^{pn} \pi_{\alpha}^{\dagger} \pi_{\beta} \nu_{\gamma}^{\dagger} \nu_{\delta}, \quad (4.16)
\end{aligned}$$

where  $\pi^{\dagger}$  ( $\nu^{\dagger}$ ) stands for proton (neutron) creation operators; as before, the Greek letters stand for the fundamental basis, but this time we have to distinguish between proton and neutron single particle state labels. With this, we can obtain the single-particle Hamiltonian  $h$  in the ph bases:

$$h_{ab}^p = t_{ab}^p + \sum_{i(\text{protons})} V_{ai;bi}^{pp} + \sum_{i(\text{neutrons})} V_{ab;ii}^{pn}, \quad (4.17)$$

$$h_{ab}^n = t_{ab}^n + \sum_{i(\text{neutrons})} V_{ai;bi}^{nn} + \sum_{i(\text{protons})} V_{ii;ab}^{pn}. \quad (4.18)$$

Other possible approach would be a formalism which does not conserve the proton and neutron numbers. The isospin becomes an additional quantum number and one uses one single Slater determinant for both protons and neutrons. However, the minimization becomes subject to a condition: on average, the solution must have the same number of protons and neutrons as the initial system. (A similar condition is imposed in HFB, where one breaks the number of particles.)

### 4.1.3 Numerical Algorithm

In this section we briefly discuss the numerical algorithm adopted for finding the HF minimum. In principle, one can use the iterative diagonalization method where one follows the following steps:

1. generate random Slater determinants for protons and neutrons;
2. calculate the single particle densities  $\rho^p$  and  $\rho^n$ ;
3. compute the proton and neutron single particle Hamiltonian using Eqs. (4.17)-(4.18);
4. solve the eigenvalue problems for  $h^p$  and  $h^n$ ;
5. define new Slater determinants by filling up the lowest levels.
6. if the new single particle densities differ from the ones calculated at 2, go back to 3 and repeat the process until it converges.

However, this procedure is not efficient, and in realistic situations the solution may oscillate back and forth, without converging [10]. We have encountered such situations mainly for even-odd and odd-odd nuclei, as sometimes the time-reversed state for the last particle has a lower single particle energy, so that the particle jumps between time-conjugate states.

The best way to find the minimum is to use *gradient descent* method. In such a case one starts with Eq. (4.15) or the equivalent ones. If one is near a minimum and  $\mathbf{S}$  is positive-definite, one can solve directly:

$$\vec{z} = -\lambda \mathbf{S}^{-1} \cdot \vec{h}, \quad (4.19)$$

where  $\lambda$  is a small positive parameter which limits the step. (Note that if the curvature is semi-positive definite, one has to use *singular matrix decomposition*, or SVD, in order to invert  $\mathbf{S}$ .) Then, using the Thouless transformation (4.6) with the parameters  $\vec{z}$  calculated in (4.19), one obtains a new Slater determinant guaranteed to have lower energy than the previous one. The new Slater determinant can be used then to calculate the gradient  $\vec{h}$  and the curvature, and the procedure continues until the minimum is obtained, i.e.,  $h_{mi} \equiv 0$ . The path followed in this algorithm can be completely different from the diagonalization method, and jumping back and forth between solutions is excluded. Depending on the method one uses for computing  $\exp(\hat{Z}^\dagger - \hat{Z})$ , the path is also different even for the gradient method. Thus, we found that the fastest convergence is obtained when we used the Padé approximation [80]; we have developed a method to calculate the exponential exactly, but this method has a much slower convergence rate. Finally one has to note that in numerical calculations we use the gradient descent in a slightly modified way. We follow the Davidson-Fletcher-Powell algorithm [80], in which the inverse of the curvature is calculated following a procedure which avoids the inversion of a large and possibly singular matrix; our algorithm, although much improved with respect the diagonalization method, still has sometimes troubles converging for odd- $A$  and odd-odd nuclei.

## 4.2 Random Phase Approximation

The HF model ignores correlations in the ground state and the residual interaction; the result is, as we saw in Sec. 4.1.1, that it can break the symmetries of the Hamiltonian.

One way to correct the mean field is to allow for oscillations about the mean-field solution, by means of the time-dependent HF (TDHF) theory [10, 12]. RPA is the small amplitude oscillation limit of TDHF theory, taking into account the residual interaction introducing small 2p-2h correlations on top of the mean-field state. One might ask why not 1p-1h correlations? After all, in the fully correlated SM ground states we might find contributions from these states. This is because the HF solution cannot talk with 1p-1h states through the Hamiltonian  $H$ ; in other words the space spanned by the 1p-1h configurations is completely decoupled from the HF state by means of the minimization condition (4.12).

The assumption of small 2p-2h correlations in the ground state is supplemented with another one, which will reduce the dimensions with respect to a direct diagonalization in

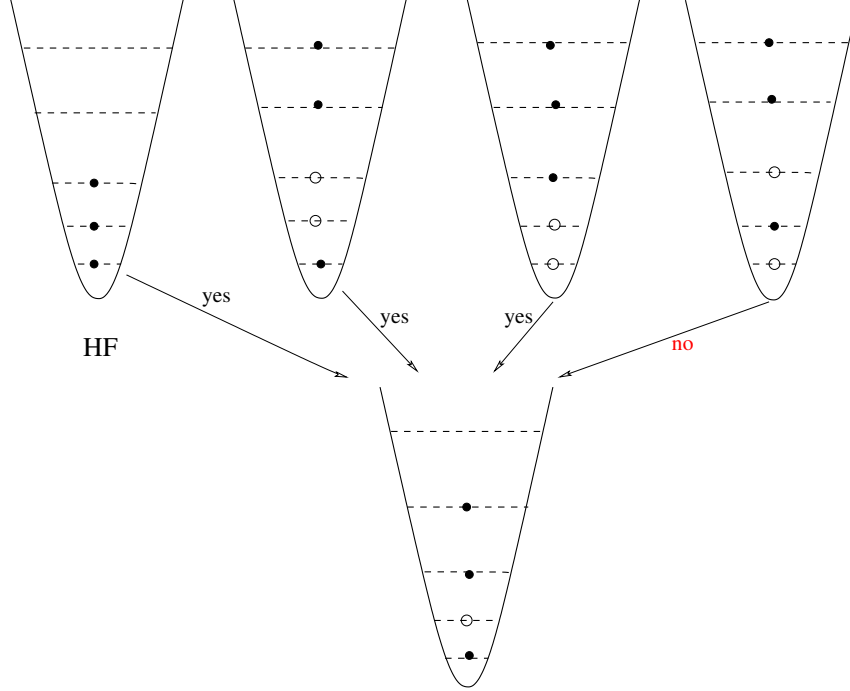


Figure 4.1: 1p-1h configuration from a RPA correlated ground state in a simplified model.

full 2p-2h space. This extra approximation is that the excited states are combinations of just 1p-1h configurations, constructed subject to constraints. For example, Fig. 4.1 shows in a very restricted model (three particles in five non-degenerate single particle levels) how a certain 1p-1h is constructed from the ground state. The upper part presents all possible configurations which contribute to the ground state in this model, while in the lower part we chose for exemplification a certain 1p-1h configuration. In RPA only the first three configurations in the ground state (HF, most left, and two other 2p-2h configurations) can generate the 1p-1h configuration in the lower part. Mathematically, this is translated by writing the excited state creation operators  $\beta_\nu^\dagger$  ( $\beta_\nu^\dagger|RPA\rangle = |\nu\rangle$ ) for the excited state  $\nu$  as [10, 11]

$$\beta_\nu^\dagger = \sum_{mi} \left( X_{mi}^\nu c_m^\dagger c_i - Y_{mi}^\nu c_i^\dagger c_m \right), \quad (4.20)$$

where  $X$  and  $Y$  are particle-hole and hole particle amplitudes respectively. Note that while the first terms describe particle-hole correlations on top of the HF state, the terms  $Y_{mi}^\nu c_i^\dagger c_m$  describe correlations coming from 2p-2h configurations in the ground state. Using the annihilation operators associated with  $\beta_\nu^\dagger$ , one defines the RPA ground state  $|RPA\rangle$  so that

$$\beta_\nu |RPA\rangle = 0. \quad (4.21)$$

In order to derive the RPA equations, we follow next the *equation of motion* method [10, 81]. Thus, we rewrite the eigenvalue problem for the Hamiltonian in Eq. (4.1), as

$$[H, \beta_\nu^\dagger]|0\rangle = (E_\nu - E_0)\beta_\nu^\dagger|0\rangle, \quad (4.22)$$

where here 0 stands for the grounds state, while  $\nu$  for any excited state. Note that no approximation is necessary to obtain the last equation. Next, we multiply Eq. (4.22) by the variation  $\langle 0|\delta\beta$ , so that we obtain

$$\langle 0|[\delta\beta, [H, \beta_\nu^\dagger]]|0\rangle = (E_\nu - E_0)\langle 0|[\delta\beta, \beta_\nu^\dagger]|0\rangle, \quad (4.23)$$

equation which is again exact since the variation chosen exhausts the whole Hilbert space.

Now we start taking into account the RPA assumptions. Thus, we plug the definition of the excited state operators (4.20) in Eq. (4.23) obtaining

$$\begin{aligned} & \sum_{mi} \sum_{nj} \delta X_{nj}^* \left( \langle \text{RPA} | [c_j^\dagger c_n, [H, c_m^\dagger c_i]] | \text{RPA} \rangle X_{mi}^\nu - \langle \text{RPA} | [c_j^\dagger c_n, [H, c_i^\dagger c_m]] | \text{RPA} \rangle Y_{mi}^\nu \right) \\ & - \sum_{mi} \sum_{nj} \delta Y_{nj}^* \left( \langle \text{RPA} | [c_n^\dagger c_j, [H, c_m^\dagger c_i]] | \text{RPA} \rangle X_{mi}^\nu - \langle \text{RPA} | [c_n^\dagger c_j, [H, c_i^\dagger c_m]] | \text{RPA} \rangle Y_{mi}^\nu \right) \\ & = \sum_{mi} \sum_{nj} \delta X_{mi}^* \left( \langle \text{RPA} | [c_j^\dagger c_n, c_m^\dagger c_i] | \text{RPA} \rangle X_{mi}^\nu - \langle \text{RPA} | [c_j^\dagger c_n, c_i^\dagger c_m] | \text{RPA} \rangle Y_{mi}^\nu \right) \\ & - \sum_{mi} \sum_{nj} \delta Y_{mi}^* \left( \langle \text{RPA} | [c_n^\dagger c_j, c_m^\dagger c_i] | \text{RPA} \rangle X_{mi}^\nu - \langle \text{RPA} | [c_n^\dagger c_j, c_i^\dagger c_m] | \text{RPA} \rangle Y_{mi}^\nu \right). \end{aligned} \quad (4.24)$$

Next, we try to make some sense out of this long equation. From the properties of the fermion operators  $c$ ,

$$[c_j^\dagger c_n, c_i^\dagger c_m] = [c_n^\dagger c_j, c_m^\dagger c_i] = 0, \quad (4.25)$$

$$[c_j^\dagger c_n, c_m^\dagger c_i] = \delta_{ij} \delta_{mn} - \delta_{mn} c_i c_j^\dagger - \delta_{ij} c_m^\dagger c_n. \quad (4.26)$$

This simplifies very little Eq. (4.24). We do not know yet the RPA wave function  $|\text{RPA}\rangle$ , as we did not determine the annihilation operators  $\beta$  which define it. But in order to obtain the particle-hole amplitudes, we do have to calculate some averages over the correlated wave function. It looks like we are in a situation with no way out. The solution is to use another RPA assumption, that is that the 2p-2h correlations in the ground state are small, so that the ground state can be still approximated by the HF solution, that is

$$|\text{RPA}\rangle \approx |\text{HF}\rangle. \quad (4.27)$$

With this further assumption, we obtain

$$\langle \text{RPA} | [c_j^\dagger c_n, c_m^\dagger c_i] | \text{RPA} \rangle \approx \langle \text{HF} | [c_j^\dagger c_n, c_m^\dagger c_i] | \text{HF} \rangle = \delta_{ij} \delta_{mn}, \quad (4.28)$$

which is called *quasi-boson* approximation. This would be exact if the operators obeyed the commutation relations for boson operators. However, we neglected the additional terms in Eq. (4.26), and this violates the Pauli principle [10].

In order to have indeed small corrections to the HF solution, the amplitudes  $Y_{mi}$ , which describe ground state correlations, have to be much smaller than the coefficients  $X_{mi}$ . Otherwise the replacement of the correlated state by the HF Slater determinant, and implicitly the quasi-boson approximation (4.28), is not valid anymore.

With the approximation (4.27), we can rewrite Eq. (4.24) in the well-known matrix form [10]

$$\begin{pmatrix} \mathbf{A} & \mathbf{B} \\ -\mathbf{B}^* & -\mathbf{A}^* \end{pmatrix} \begin{pmatrix} X \\ Y \end{pmatrix} = \Omega \begin{pmatrix} X \\ Y \end{pmatrix}, \quad (4.29)$$

where  $\Omega$  is the excitation energy which we can now determine. Matrices  $\mathbf{A}$  and  $\mathbf{B}$  are defined by Eqs. (4.10) and (4.11), implying

$$A_{mi;nj} = (\epsilon_m - \epsilon_i)\delta_{ij} - V_{mi,nj}, \quad (4.30)$$

$$B_{mi;nj} = V_{mn,ij}. \quad (4.31)$$

(The two-body matrix elements  $V$  are now written in the ph basis.) We can prove simply that  $\mathbf{A}$  is Hermitian, and  $\mathbf{B}$  is symmetric.

The eigenvalue equation (4.29) involves a non-hermitian matrix and the eigenvectors cannot be orthonormalized in the usual sense. In order to derive the orthogonality relations, we consider again Eq. (4.27) and write

$$\begin{aligned} \delta_{\nu\mu} &= \langle \nu | \mu \rangle \\ &= \langle \text{RPA} | \beta_\nu \beta_\mu^\dagger | \text{RPA} \rangle = \langle \text{RPA} | [\beta_\nu, \beta_\mu^\dagger] | \text{RPA} \rangle \\ &\approx \langle \text{HF} | [\beta_\nu, \beta_\mu^\dagger] | \text{HF} \rangle, \end{aligned} \quad (4.32)$$

which becomes

$$\delta_{\nu\mu} = \sum_{mi} (X_{mi,\nu}^* X_{nj,\mu} - Y_{mi,\nu}^* Y_{nj\mu}). \quad (4.33)$$

Note that the RPA eigenvalue equation (4.29) has also the property that if  $(\vec{X}_\nu, \vec{Y}_\nu)$  is an eigenvector corresponding to eigenvalue  $\Omega_\nu$ , then  $(\vec{Y}_\nu^*, X_\nu^*)$  will be eigenvector corresponding to  $-\Omega_\nu$ ; therefore, the eigenvectors of (4.29) come in pairs, and from Eq. (4.33) we see that the norms of the eigenvectors corresponding  $\Omega_\nu$  and  $-\Omega_\nu$  have the same absolute value, but differ in sign.

Thouless showed [18] that if the HF solution corresponds to a minimum in energy surface, the corresponding RPA equation (4.29) has only real frequencies. In addition, if the Hartree-Fock state is invariant under some particle-hole transformation, such as rotation about an axis, this corresponds to a zero frequency RPA mode. Thus, the generators of symmetries broken by a mean-field solution are eigenvectors of Eq. (4.29) lying at at zero excitation energy. This is frequently interpreted as ‘‘approximate restoration of broken symmetries’’ [10]; in fact, it is more accurate to say that the RPA *respects* symmetries by separating out exactly spurious motion. As we will see in Chapter 7, our results suggest that broken symmetries are only partially restored by the RPA. We turn to the problem of spurious states which requires more careful treatment in Sec. 4.2.2 where we define generalized collective coordinates.

## 4.2.1 Boson Mapping

We considered previously the equation of motion method to derive the matrix formulation of RPA; in the derivation, we introduced the quasi-boson approximation (4.28). Let us define

$$b_{mi}^\dagger = c_m^\dagger c_i, \quad b_{mi} = c_i^\dagger c_m, \quad (4.34)$$

and reconsider now Eqs. (4.25)–(4.26), which are exact; these are nearly, but not quite, commutation relations for boson operators. If we neglect however the last two terms in the right hand side of Eq. (4.26), we obtain the commutation relations for boson fields

$$[b_{mi}, b_{nj}] = [b_{mi}^\dagger, b_{nj}^\dagger] = 0, \quad [b_{mi}, b_{nj}^\dagger] = \delta_{mn}\delta_{ij}, \quad (4.35)$$

so that the operators  $b$ ,  $b^\dagger$  are the approximative boson images of the fermion operators. Therefore we map the fermion Hamiltonian onto the boson image [10]

$$H_B = E_{HF} + \vec{h} \cdot (\vec{b}^\dagger + \vec{b}) + \vec{b}^\dagger \mathbf{A} \vec{b} + \frac{1}{2}(\vec{b}^\dagger \cdot \mathbf{B} \cdot \vec{b}^\dagger + \vec{b} \cdot \mathbf{B} \cdot \vec{b}), \quad (4.36)$$

which has the parallel result

$$h_{mi} \equiv \langle \text{RPA} | [H_B, b_{mi}^\dagger] | \text{RPA} \rangle, \quad (4.37)$$

$$A_{nj,mi} \equiv \langle \text{RPA} | [b_{jn}, [H_B, b_{mi}^\dagger]] | \text{RPA} \rangle, \quad (4.38)$$

$$B_{nj,mi} \equiv \langle \text{RPA} | [[H_B, b_{nj}^\dagger], b_{mi}^\dagger] | \text{RPA} \rangle. \quad (4.39)$$

Because this has the same commutation relations as the fermion Hamiltonian, we say this is the boson image to RPA order. (For now we keep the linear part even though it disappears for the Hamiltonian at the HF minimum; nevertheless, we use the same procedure to obtain the boson image of an arbitrary operator, and in this case the linear terms do not vanish.)

We can rewrite now Eq. (4.36) into matrix form, which induces an addition constant term:

$$\hat{H}_B = E_{HF} - \frac{1}{2} \text{Tr} \mathbf{A} + \vec{h} \cdot (\vec{b} + \vec{b}^\dagger) + \frac{1}{2} \begin{pmatrix} \vec{b}^\dagger & \vec{b} \end{pmatrix} \cdot \begin{pmatrix} \mathbf{A} & \mathbf{B} \\ \mathbf{B} & \mathbf{A} \end{pmatrix} \cdot \begin{pmatrix} \vec{b} \\ \vec{b}^\dagger \end{pmatrix}. \quad (4.40)$$

The last equation is similar to (4.8), with the fluctuations  $\vec{z}$  replaced by the boson operators  $b$ . Thus, Eq. (4.40) is equivalent with a bosonization of the quadratic energy surface (4.8).

We turn our attention now to the collective boson operators  $\beta^\dagger$  defined in Eq. (4.20). In terms of boson operators  $b$  they become

$$\beta_\nu^\dagger = \sum_{mi} \left( X_{mi,\nu} b_{mi}^\dagger - Y_{mi,\nu} b_{mi} \right) \quad (4.41)$$

(and similarly for  $\beta$ ). Consequently, they fulfill now exactly the commutation relations for boson operators

$$[\beta_\mu, \beta_\nu] = [\beta_\mu^\dagger, \beta_\nu^\dagger] = 0, \quad (4.42)$$

$$[\beta_\mu, \beta_\nu^\dagger] = \delta_{\mu\nu}, \quad (4.43)$$

so that we see immediately that the RPA ground state is *vacuum* for the set of collective boson operators  $\beta$ . Moreover, plugging Eq. (4.41) into (4.43) we regain the orthogonality relation (4.33). In order to obtain the completeness relations, we have to invert Eq. (4.41); however, the system of operators is not complete when there are zero modes, as for such cases one cannot define a boson operator. Therefore, we postpone the derivation of the completeness relations for the next section where we can treat correctly the vanishing RPA modes.

In our calculations we have used real Slater determinants, so that the matrices  $\mathbf{A}$  and  $\mathbf{B}$  are real and one can assume that the particle hole-amplitudes are real as well. For simplicity therefore, we drop any reference to complex conjugation.

## 4.2.2 Collective Coordinates

In this section we introduce generalized collective coordinates  $\hat{Q}_\lambda$  and their conjugate momenta  $\hat{P}_\lambda$  [10, 17], with the usual commutation relations,

$$[\hat{Q}_\lambda, \hat{Q}_\mu] = [\hat{P}_\lambda, \hat{P}_\mu] = 0, \quad [\hat{Q}_\lambda, \hat{P}_\mu] = i\delta_{\lambda\mu}, \quad (4.44)$$

as well as the equations of motion

$$[H_B, \hat{P}_\lambda] = i\Omega_\lambda^2 M_\lambda \hat{Q}_\lambda, \quad [H_B, \hat{Q}_\lambda] = -\frac{i}{M_\lambda} \hat{P}_\lambda. \quad (4.45)$$

Here  $M_\lambda$  is a real constant, interpretable as mass or moment of inertia whose value will be determined later from a normalization condition. For nonzero modes we can write down the relation between the collective boson creation and annihilation operators and the collective coordinates using the same transformations as for a harmonic oscillator

$$\beta_\lambda^\dagger = \sqrt{\frac{M_\lambda \Omega_\lambda}{2}} \hat{Q}_\lambda + i\sqrt{\frac{1}{2M_\lambda \Omega_\lambda}} \hat{P}_\lambda, \quad (4.46)$$

$$\beta_\lambda = \sqrt{\frac{M_\lambda \Omega_\lambda}{2}} \hat{Q}_\lambda - i\sqrt{\frac{1}{2M_\lambda \Omega_\lambda}} \hat{P}_\lambda. \quad (4.47)$$

Because for nonzero eigenvalues normalizable eigenvectors  $(X, Y)$  exist, we will continue to treat them as before. However, the eigenvectors corresponding to zero eigenvalues cannot be normalized, so that we are forced to go to collective coordinates.

The collective coordinates and momenta are hermitian operators, and consequently they can be represented in terms of boson operators as

$$\hat{Q}_\lambda = \sum_{mi} \left( Q_{mi,\lambda} b_{mi}^\dagger + Q_{mi,\lambda}^* b_{mi} \right), \quad (4.48)$$

$$\hat{P}_\lambda = \sum_{mi} \left( P_{mi,\lambda} b_{mi}^\dagger + P_{mi,\lambda}^* b_{mi} \right). \quad (4.49)$$

Direct substitution of the latest two equations in the equations of motion (4.45) gives a set of coupled equations for determining  $\vec{P}$  and  $\vec{Q}$ :

$$\mathbf{A}\vec{P}_\mu - \mathbf{B}\vec{P}_\mu^* = 0, \quad (4.50)$$

$$\mathbf{A}\vec{Q}_\mu - \mathbf{B}\vec{Q}_\mu^* = -\frac{i}{M_\lambda}\vec{P}_\lambda. \quad (4.51)$$

Also, from the commutation relations (4.44) one immediately obtains

$$\sum_{mi} (Q_{mi,\lambda}^* P_{mi,\mu} - Q_{mi,\lambda} P_{mi,\mu}^*) = i\delta_{\lambda,\mu} \quad (4.52)$$

We mentioned the reasons why we can choose the particle-hole amplitudes to be real; nevertheless, for zero modes, this assumption does not hold any more as we can see by inspection of the last equation. (Actually we can choose them in a special way: one real and one imaginary.)

From Eqs. (4.50) and (4.51), we can identify the zero modes with the zero eigenvalues of the stability matrix as we did previously. Assume  $\vec{P}_\lambda$  is purely real. Then it is a zero of  $\mathbf{A} - \mathbf{B}$ , which, as we discussed earlier, can be found for  $\text{Im } \vec{z}$ , such as rotations about the  $x$ - or  $z$ - axis. In this case  $\vec{Q}_\lambda$  is purely imaginary,  $\vec{Q}_\lambda = -i\vec{q}_\lambda$  and  $(\mathbf{A} + \mathbf{B})\vec{q}_\lambda = M_\lambda^{-1}\vec{P}_\lambda$ .

Conversely, if  $\vec{P}_\lambda = i\vec{p}_\lambda$  is purely imaginary, it is a zero of  $(\mathbf{A} + \mathbf{B})$  and  $(\mathbf{A} - \mathbf{B})\vec{Q}_\lambda = M_\lambda^{-1}\vec{p}_\lambda$ . Note that both  $\mathbf{A} \pm \mathbf{B}$  in principle can have zero modes, and therefore strictly speaking they are singular, but in order to obtain  $Q$  one has to invert one or the other. We do this numerically by using the SVD decomposition [80]. One can then find  $P$ ,  $Q$ , subject to the normalization condition

$$2\vec{q}_\lambda \cdot \vec{p}_\lambda = 1, \quad (4.53)$$

which helps to define  $M_\lambda$ . In the normalization condition (4.53),  $p$  and  $q$  are either the real or imaginary part of  $P$  and  $Q$  respectively, depending upon their nature.

Having defined the generalized coordinates and momenta for zero modes, we can invert now Eq. (4.41), obtaining

$$b_{mi} = \sum_{\lambda(\Omega_\lambda > 0)} (X_{mi,\lambda}\beta_\lambda + Y_{mi,\lambda}\beta_\lambda^\dagger) - i \sum_{\mu(\Omega_\mu = 0)} (P_{mi,\mu}\hat{Q}_\mu + Q_{mi,\mu}\hat{P}_\mu) \quad (4.54)$$

and its hermitian conjugate, so that we can derive now from Eqs. (4.42)–(4.44) the completeness relations

$$\sum_{\lambda(\Omega_\lambda > 0)} (X_{mi,\lambda}Y_{nj,\lambda} - Y_{mi,\lambda}X_{nj,\lambda}) - i \sum_{\mu(\Omega_\mu = 0)} (P_{mi,\mu}Q_{nj,\mu} - Q_{mi,\mu}P_{nj,\mu}) = 0, \quad (4.55)$$

$$\sum_{\lambda(\Omega_\lambda > 0)} (X_{mi,\lambda}X_{nj,\lambda} - Y_{mi,\lambda}Y_{nj,\lambda}) - i \sum_{\mu(\Omega_\mu = 0)} (Q_{mi,\mu}P_{nj,\mu}^* - P_{mi,\mu}Q_{nj,\mu}^*) = \delta_{mn}\delta_{ij}. \quad (4.56)$$

Finally, the generalized Bogoliubov transformation (4.54) allows us to obtain a representation for the particle-hole matrices  $\mathbf{A}$  and  $\mathbf{B}$ , a generalization of the Eq. (8.94) in Ref. [10] which includes zero modes:

$$A_{mi,nj} = \sum_{\lambda(\Omega_\lambda>0)} \Omega_\lambda (X_{mi,\lambda}X_{nj,\lambda} + Y_{mi,\lambda}Y_{nj,\lambda}) + \sum_{\mu(\Omega_\mu=0)} \frac{1}{M_\mu} P_{mi,\mu} P_{nj,\mu}^*, \quad (4.57)$$

$$-B_{mi,nj} = \sum_{\lambda(\Omega_\lambda>0)} \Omega_\lambda (X_{mi,\lambda}Y_{nj,\lambda} + Y_{mi,\lambda}X_{nj,\lambda}) + \sum_{\mu(\Omega_\mu=0)} \frac{1}{M_\mu} P_{mi,\mu} P_{nj,\mu}. \quad (4.58)$$

The last terms in Eqs. (4.57) and (4.58) are very important, not only for computing the expectation values of scalar observables including the Hamiltonian, but also for deriving Thouless's energy-weighted sum rule theorem [18]. Their contribution has been systematically neglected for the latter since it was proved for the first time. In Chapter 7 we revisit the derivation, showing explicitly that the well known formula needs non trivial corrections for broken mean-field symmetries.

Before concluding this section, we have to point out that the RPA does not respect the quantization rules for angular momentum. Let us take for example a system with a HF solution which breaks the symmetries with respect to two axes; we can rotate the system until  $x$  and  $z$  are the axes with respect to which the symmetries are broken, and therefore the two conjugate momenta associated with two zero modes will be  $J_x$  and  $J_z$ . From Eq. (4.44) one obtains immediately

$$[J_x, J_z] = 0, \quad (4.59)$$

which proves indeed that the quantization rules for angular momentum are not respected.

Summarizing, we have first derived the RPA equation using the equation of motion method. Then, because for zero modes (associated with broken symmetries) one cannot apply the normalization condition (4.33), we have supplemented the collective boson operators for excited states with generalized coordinates and momenta corresponding to zero modes. Now we are ready to transform the RPA order expansion of the Hamiltonian in Eq. (4.36) to a simpler form in order to obtain corrections to the HF energy. Also, we will generalize the Hamiltonian expansion to general scalar operators, obtaining RPA corrections to their mean-field expectation values.

### 4.2.3 RPA Correlation Energy

One might expect that in order to calculate the RPA ground state energy one should first obtain the correlated wave function. It is possible nevertheless to obtain the ground state energy without explicitly constructing the wave function. Thus, using the generalized Bogoliubov transformation (4.54) derived earlier, we can rewrite Eq. (4.36) in a diagonal form

$$H_B = E_{\text{HF}} - \frac{1}{2} \text{Tr} \mathbf{A} + \frac{1}{2} \text{Tr} \mathbf{\Omega} + \sum_{\lambda(\Omega_\lambda>0)} \Omega_\lambda \beta_\lambda^\dagger \beta_\lambda + \sum_{\mu(\Omega_\mu=0)} \frac{\hat{\mathcal{P}}_\mu^2}{2M_\mu}. \quad (4.60)$$

(Note that at the HF minimum  $\vec{h} = 0$ , so that we left out the linear terms in  $b$ .) Since the RPA ground state is vacuum for the set of collective quasi-bosons  $\vec{\beta}$  and by construction  $\hat{P}_\mu|\text{RPA}\rangle = 0$  [10, 17], the correlated ground state energy can be read off trivially:

$$E_{\text{RPA}} = E_{\text{HF}} - \frac{1}{2}\text{Tr } \mathbf{A} + \frac{1}{2}\text{Tr } \mathbf{\Omega}. \quad (4.61)$$

And if in the latest equation we use the representation of matrix  $\mathbf{A}$  (4.57), we obtain an equivalent formula for the RPA ground state energy [10, 17]

$$E_{\text{RPA}} = E_{\text{HF}} - \sum_{\lambda} \sum_{mi} \Omega_{\lambda} Y_{mi,\lambda}^2 - \sum_{\mu} \sum_{mi} \frac{P_{mi,\mu}^2}{2M_{\mu}}, \quad (4.62)$$

which explicitly segregates the contribution from the kinetic energy of zero modes, that is, from broken symmetries [10, 14, 15, 17, 81]. We will be able to express the correction term to the energy-weighted sum rule coming from zero modes in terms of a similar kinetic energy contribution. Finally, note that another way to compute the correlation energy is within the response-function formulation of RPA [82].

#### 4.2.4 Scalar Observables

We can follow a similar procedure in order to derive the RPA ground-state expectation value of a general operator. Thus, defining

$$\mathcal{O}_{\text{HF}} \equiv \langle \text{HF} | \mathcal{O} | \text{HF} \rangle, \quad (4.63)$$

$$o_{mi} \equiv \langle \text{HF} | [\mathcal{O}, c_m^\dagger c_i] | \text{HF} \rangle, \quad (4.64)$$

$$\tilde{A}_{nj,mi} \equiv \langle \text{HF} | [c_j^\dagger c_n, [\mathcal{O}, c_m^\dagger c_i]] | \text{HF} \rangle, \quad (4.65)$$

$$\tilde{B}_{nj,mi} \equiv \langle \text{HF} | [[\mathcal{O}, c_n^\dagger c_j], c_m^\dagger c_i] | \text{HF} \rangle, \quad (4.66)$$

for a general operator  $\mathcal{O}$ , the boson image is similar to Eq. (4.36), i.e.,

$$\mathcal{O}_B = \mathcal{O}_{\text{HF}} - \frac{1}{2}\text{Tr } \tilde{\mathbf{A}} + (\vec{\sigma}^*, \vec{\sigma}) \cdot \begin{pmatrix} \vec{b} \\ \vec{b}^\dagger \end{pmatrix} + \frac{1}{2}(\vec{b}^\dagger, \vec{b}) \cdot \begin{pmatrix} \tilde{\mathbf{A}} & \tilde{\mathbf{B}} \\ \tilde{\mathbf{B}} & \tilde{\mathbf{A}} \end{pmatrix} \cdot \begin{pmatrix} \vec{b} \\ \vec{b}^\dagger \end{pmatrix}. \quad (4.67)$$

By transforming to the collective quasi-bosons (4.54), we again can trivially read off the quasi-boson vacuum expectation value, which is the RPA ground-state expectation value, without explicit construction of a wave function [13]:

$$\mathcal{O}_{\text{RPA}} = \mathcal{O}_{\text{HF}} - \frac{1}{2}\text{Tr } \tilde{\mathbf{A}} + \frac{1}{2}\text{Tr } \mathbf{\Theta}, \quad (4.68)$$

where

$$\mathbf{\Theta} = \mathbf{X}^T \tilde{\mathbf{A}} \mathbf{X} + \mathbf{Y}^T \tilde{\mathbf{A}} \mathbf{Y} + \mathbf{X}^T \tilde{\mathbf{B}} \mathbf{Y} + \mathbf{Y}^T \tilde{\mathbf{B}} \mathbf{X}. \quad (4.69)$$

Substitution of Eq. (4.29) with  $A, B$  derived from the Hamiltonian immediately regains the RPA binding energy (4.61). It is important to emphasize here that the  $X, Y$  used here are those calculated from Eq. (4.29) using the *original*  $A, B$  matrices (from the Hamiltonian); one does *not* compute  $X, Y$  using  $\tilde{A}, \tilde{B}$ .

Finally, as before we can rewrite (4.68) into an expression with explicit segregation of the zero modes:

$$\begin{aligned} \mathcal{O}_{\text{RPA}} = \mathcal{O}_{\text{HF}} + & \sum_{\lambda(\Omega_\lambda > 0)} \sum_{mi, nj} (\tilde{A}_{mi, nj} Y_{mi, \lambda} Y_{nj, \lambda} + \tilde{B}_{mi, nj} Y_{mi, \lambda} X_{nj, \lambda}) \\ & - \frac{1}{2} i \sum_{\mu(\Omega_\mu = 0)} \sum_{mi, nj} \tilde{A}_{mi, nj} (P_{mi, \mu}^* Q_{nj, \mu} - Q_{mi, \mu}^* P_{nj, \mu}). \end{aligned} \quad (4.70)$$

We have confirmed numerically that (4.70) yields the same values as (4.68).

## 4.2.5 Transitions

The RPA provides a model for excited states, and to calculate the transition probability from any non-spurious state to the ground state one needs the transition matrix element  $\langle \nu | F | \text{RPA} \rangle$ . In the RPA, the latter can be written in terms of particle-hole amplitudes  $X^\nu$  and  $Y^\nu$ , namely, if one has a one-body transition operator (and a spherical tensor of rank  $K$ ),  $F_{KM}$ , which can be written as

$$F_{KM} = \sum_{mi} \left[ f_{mi}^M c_m^\dagger c_i + (-1)^M f_{mi}^{-M} c_i^\dagger c_m \right], \quad (4.71)$$

where  $f_{mi}^M = \langle m | F_{KM} | i \rangle$ , then [10]

$$\langle \nu | F_{KM} | \text{RPA} \rangle = \sum_{mi} [f_{mi}^M X_{mi, \nu} + (-1)^M f_{mi}^{-M} Y_{mi, \nu}] \equiv f^M \cdot X_\nu + (-1)^M f^M \cdot Y_\nu. \quad (4.72)$$

With the transition matrix element (4.72), it is possible to calculate in the RPA any moment of the distribution strength, and therefore the total strength, the centroid and the width. We will compare the RPA results for these quantities against the interacting SM predictions in Chapter 6.

One important feature, essential in realistic applications, is that RPA satisfies the energy sum rule (3.14) as follows [10, 12, 18]:

$$\sum_{\nu} \Omega_{\nu} |\langle \nu | F | \text{RPA} \rangle|^2 = \frac{1}{2} \langle \text{HF} | [F, [H, F]] | \text{HF} \rangle. \quad (4.73)$$

That is, in the left-hand side we use the RPA excitation energies and transition strengths, and in the right-hand side we replace the RPA ground state wave function by the mean field solution. Note the similarity with Eq. (3.16) as well as the fact that for RPA, the exact eigenstate  $|\mu\rangle$  is replaced by the HF solution, which is not an eigenstate of the Hamiltonian.

We revisit the derivation of Eq. (4.73) in Chapter 7, and find that if the HF state breaks symmetries, Eq. (4.73) is violated.

While we can test symmetries by calculating the RPA expectation values of relevant scalar operators, e.g.,  $J^2$ , transition strengths can be also very sensitive to the so called symmetry restoration in RPA. The Brown-Bolsterli schematic model [10–12, 83] provides insight into giant collective resonances. We discuss it in some detail in Chapter 5, so we only summarize here. It assumes the model Hamiltonian to be single-particle energies plus a separable residual interaction. In the RPA, all of the Brown-Bolsterli transition strength is to a single state, the collective state, which is a model for giant resonances. If the residual interaction is repulsive, then the collective state will be at high energy. If the interaction is attractive, then the collective state will be low in energy. In more realistic models, of course, the residual interaction includes more complicated two-body forces, causing the giant resonance to spread over many states. The important lesson of the Brown-Bolsterli model, however, is that an attractive interaction, such as isoscalar quadrupole-quadrupole, leads to large collective transitions low in the spectrum, while repulsive interactions, such as  $\sigma \cdot \sigma$ , produce collective transitions lying higher in the spectrum.

Breaking of symmetries can result in low-lying collectivity being subsumed into the ground state. For example, the strongly attractive isoscalar quadrupole-quadrupole interaction leads to a quadrupole deformation in the HF state. While the RPA identifies broken symmetries, those symmetries are not fully restored by RPA, and in Chapter 6 we bring evidence that significant strength is missing for low-lying transitions.

## 4.2.6 Proton and Neutron Conserving Formalism

In the case of a nucleus with two types of nucleons described by the Hamiltonian in Eq. (4.16), the creation operator for excited states (4.20) properly becomes:

$$\begin{aligned} \beta^\dagger = & \sum_{mi} \left( X_{mi}(pp) \pi_m^\dagger \pi_i - Y_{mi}(pp) \pi_i^\dagger \pi_m \right) + \sum_{mi} \left( X_{mi}(nn) \nu_m^\dagger \nu_i - Y_{mi}(nn) \nu_i^\dagger \nu_m \right) \\ & + \sum_{mi} \left( X_{mi}(pn) \pi_m^\dagger \nu_i - Y_{mi}(pn) \nu_i^\dagger \pi_m \right) + \sum_{mi} \left( X_{mi}(np) \nu_m^\dagger \pi_i - Y_{mi}(np) \pi_i^\dagger \nu_m \right). \end{aligned} \quad (4.74)$$

In our approach however, we did not consider terms which annihilate one type of particles and create the other type, as these would mix excited states from neighboring nuclei. In the future, we plan to include them, and hopefully obtain a better treatment of the proton-neutron correlations.

Consequently, the matrices **A** and **B** in Eqs. (4.30) and (4.31) will have a proton-proton block, that is

$$A_{mi,nj}^{pp} = (\epsilon_m^p - \epsilon_i^p) \delta_{ij} - V_{mi;nj}^{pp}, \quad (4.75)$$

$$B_{mi,nj}^{pp} = V_{mn;ij}^{pp}, \quad (4.76)$$

and similarly a neutron-neutron block. In addition, the proton-neutron interaction induces a proton-neutron block:

$$A_{nj,mi}^{pn} = \langle \text{HF} | [\pi_j^\dagger \pi_n, [H, \nu_m^\dagger \nu_i]] | \text{HF} \rangle = V_{nj,im}^{pn}, \quad (4.77)$$

$$B_{nj,mi}^{pn} = \langle \text{HF} | [[H, \pi_n^\dagger \pi_j], \nu_m^\dagger \nu_i] | \text{HF} \rangle = -V_{jn,im}^{pn}. \quad (4.78)$$

Note that in the last two equations  $n, j$  stand for proton ph states, while  $m, i$  for neutron ones. Similar formulas can be derived for matrices  $\tilde{\mathbf{A}}$  and  $\tilde{\mathbf{B}}$  necessary to obtain corrections to scalar observables, although the term which replaces the single-particle energies in Eq. (4.75) is slightly more complicated.

# 5 Applications of RPA

In the previous chapter we have derived RPA corrections to the binding energy and ground state observables. Moreover, RPA provided a way to describe transitions from excited states to the ground state. In this chapter, we apply the HF + RPA to calculate approximate ground state expectation values for a system of identical particles interacting by means of a very simple Hamiltonian, and we test the results against the exact values obtained through exact diagonalization. In addition, we review a simple model which offers insight into the features of collective states.

RPA is successful in describing the experimental position of giant resonances, and for this reason, in the second part of this chapter, we overview its application in realistic systems. While a good agreement with experiment might suggest that the present investigation becomes somehow unnecessary, there are two points to emphasize: (i) RPA is not always successful, and (ii) even if it would describe correctly the experiment in all cases, the question if RPA is indeed a good approximation to an exact microscopic model, allowing later reliable extrapolations for nuclei non-accessible experimentally, is still unanswered by tests in complicated and realistic models.

## 5.1 Lipkin Model

In the following, we use for illustration a pedagogical model introduced by Lipkin, Meshkov and Glick [84], Lipkin model for short. One considers  $N$  particles in two single particle states, each  $N$  fold degenerate, the system being described by the Hamiltonian

$$H = \varepsilon K_0 - \frac{V}{2} (K_+ K_+ + K_- K_-), \quad (5.1)$$

where

$$K_0 = \frac{1}{2} \sum_{i=1}^N (a_{i\uparrow}^\dagger a_{i\uparrow} - a_{i\downarrow}^\dagger a_{i\downarrow}), \quad (5.2)$$

$$K_+ = \sum_{i=1}^N a_{i\uparrow}^\dagger a_{i\downarrow}, \quad K_- = (K_+)^\dagger, \quad (5.3)$$

with  $a_{i\uparrow}^\dagger$  ( $a_{i\downarrow}^\dagger$ ) the creation operator for the state  $i$  having the single particle energy  $\varepsilon/2$  ( $-\varepsilon/2$ ). (Note that here  $i$  runs over all the states in the fundamental basis, and does not

denote an occupied state as before; it will become important to distinguish again between occupied and unoccupied states only later.) The operators  $K$  satisfy the usual commutation relations for angular momentum

$$[K_+, K_-] = 2K_0, \quad [K_0, K_\pm] = \pm K_\pm. \quad (5.4)$$

As in the case of usual angular momentum operator, one can define  $K^2$ :

$$K^2 = K_0^2 + K_x^2 + K_y^2 = K_0^2 + \frac{1}{2}(K_+K_- + K_-K_+), \quad (5.5)$$

and since it satisfies the usual  $SU(2)$  commutation relations, one often refers to  $K$  as quasi-spin. Because  $H$  commute with  $K^2$  (but not with  $K_0$ ), the exact solution will be simultaneously eigenvector for both operators, so that we can choose the basis states as eigenvectors for  $K^2$  and  $K_0$

$$K^2|km\rangle = k(k+1)|km\rangle, \quad K_0|km\rangle = m|km\rangle, \quad (5.6)$$

the Hamiltonian matrix is

$$\begin{aligned} \langle k'm'|H|km\rangle &= m\varepsilon\delta_{k'k}\delta_{m'm} \\ &- \frac{1}{2}V [(k(k+1) - m(m+1))(k(k+1) - (m+1)(m+2))]^{1/2} \delta_{k'k}\delta_{m',m+2} \\ &- \frac{1}{2}V [(k(k+1) - m(m-1))(k(k+1) - (m-1)(m-2))]^{1/2} \delta_{k'k}\delta_{m',m-2}. \end{aligned} \quad (5.7)$$

Diagonalization of this matrix provides the exact solution to the Lipkin Hamiltonian. Note however that  $|km\rangle$  should be anti-symmetrical many-body states and their expansion into Slater determinants is not trivial (but unnecessary).

### 5.1.1 HF Approximation

In order to calculate the mean-field solution to the Lipkin Hamiltonian, we assume that the ground state is approximated by a Slater determinant which minimizes the energy, as described in Chapter 4. We consider therefore a quasi-spin transformation from the fundamental basis to the new single-particle basis

$$\Phi_{i-}^\dagger = u_i a_{i\uparrow}^\dagger + v_i a_{i\downarrow}^\dagger, \quad (5.8)$$

$$\Phi_{i+}^\dagger = -v_i^* a_{i\uparrow}^\dagger + u_i^* a_{i\downarrow}^\dagger, \quad (5.9)$$

and hermitian conjugate, the occupied states denoted by minus, and the non-occupied ones by plus.  $u_i$  and  $v_i$  are the elements of a unitary transformation which has to be determined from the minimum condition; in principle, one should consider a different transformation for each initial state, but because of the simplicity of the model, we can use a uniform transformation [10] having the general form

$$u_i = \cos \theta, \quad v_i = \sin \theta e^{i\varphi}. \quad (5.10)$$

The trial Slater determinant is

$$|\psi\rangle = \prod_{i=1}^N \Phi_{i-}^\dagger |0\rangle, \quad (5.11)$$

where 0 stands here for the vacuum state. We determine the parameters  $\theta$  and  $\varphi$  through the requirement that  $|\psi\rangle$  minimize the energy, that is the equivalent of Eq. (4.12),

$$\langle \psi | [H, \Phi_{i+}^\dagger \Phi_{i-}] | \psi \rangle = 0. \quad (5.12)$$

This translates into two equations, one for the real part and one for the imaginary part, as

$$\varepsilon N \sin 2\theta (1 - \chi \cos 2\theta \cdot \cos 2\varphi) = 0, \quad (5.13)$$

$$\frac{1}{2} \varepsilon N \sin 2\theta \cdot \sin 2\varphi = 0, \quad (5.14)$$

where  $\chi = (N-1)V/\varepsilon$  is the strength parameter. One can find two solutions satisfying these equations:

$$\varphi_{\text{HF}} = 0, \quad \theta_{\text{HF}} = 0, \quad \text{if } \chi < 1, \quad (5.15)$$

$$\varphi_{\text{HF}} = 0, \quad \cos 2\theta_{\text{HF}} = 1/\chi, \quad \text{if } \chi > 1. \quad (5.16)$$

Note that even for  $\chi > 1$ ,  $(\varphi = 0, \theta = 0)$  is still a solution of Eqs. (5.13) and (5.14); however, the mean field energy

$$E_{\text{HF}} = -N \frac{\varepsilon}{2} \left( \cos 2\theta + \frac{1}{2} \chi \sin^2 2\theta \cdot \cos 2\varphi \right) \quad (5.17)$$

is lower for (5.16), while the trivial solution becomes a local maximum. One usually calls the regime with  $\chi < 1$  “spherical”, and  $\chi > 1$ , “deformed” [10]; however, we have to point out that there are no broken symmetries in the mean-field solution, even for the “deformed” regime. Thus, taking the HF solution (5.11) with the parameters determined in Eqs. (5.15) or (5.16) one can easily show that the mean-field state is an eigenvector for  $K^2$ . This feature of the Lipkin model makes it even less realistic. One generalization is the three-level Lipkin model [14], which allows for broken symmetries in the mean-field solution; for some values of parameters, this model mimics quadrupole motion in nuclei. But because it involves essentially an one-parameter Hamiltonian, the three-level Lipkin is still too simple with respect to realistic interactions in nuclei.

### 5.1.2 RPA

We introduce now correlations in the mean-field solution by means of the RPA. The particle (unoccupied) states are denoted by plus and the hole (occupied) states are denoted by minus; therefore, we can easily calculate now the RPA  $A$  and  $B$  matrices defined in Eqs. (4.10) and (4.11) respectively and obtain

$$A_{ij} = \left\langle \psi \left| \left[ \phi_{i-}^\dagger - \phi_{i+}, \left[ H, \phi_{j+}^\dagger + \phi_{j-} \right] \right] \right| \psi \right\rangle = a + \Delta_a \delta_{ij} \quad (5.18)$$

$$B_{ij} = - \left\langle \psi \left| \left[ \phi_{i-}^\dagger - \phi_{i+}, \left[ H, \phi_{j-}^\dagger - \phi_{j+} \right] \right] \right| \psi \right\rangle = b + \Delta_b \delta_{ij}, \quad (5.19)$$

where

$$a = 1 - \frac{1}{2} \sin^2 2\theta, \quad \Delta_a = \varepsilon \cos 2\theta + V \left[ (N-1) \sin^2 2\theta - \frac{1}{2} (1 + \cos^2 2\theta) \right], \quad (5.20)$$

$$b = -\frac{1}{2} V (1 + \cos^2 2\theta), \quad \Delta_b = -b. \quad (5.21)$$

The special form of  $\mathbf{A}$  and  $\mathbf{B}$  allows us to obtain an analytical solution to the RPA equation (4.29). As shown in Appendix B, there is one RPA eigenvalue associated to a collective excitation

$$\Omega_c = \sqrt{(Na + \Delta_a)^2 - (N-1)^2 b^2}, \quad (5.22)$$

and  $N-1$  corresponding to non-collective excitations

$$\Omega_{nc} = \sqrt{a^2 - b^2}, \quad (5.23)$$

so that the RPA ground-state energy (4.61) for the Lipkin model becomes

$$E_{\text{RPA}} = E_{\text{HF}} - \frac{1}{2} N (a + \Delta_a) + \frac{1}{2} [\Omega_c + (N-1)\Omega_{nc}]. \quad (5.24)$$

Figures 5.1 and 5.2 present the ground state energy calculated by exact diagonalization, in the HF approximation (5.17) and HF+RPA, i.e., Eq. (5.24), in two distinct situations. Thus, in Fig. 5.1 we keep the number of particle constant,  $N = 15$ , varying the strength parameter  $\chi$ , while in Fig. 5.2 we vary the number of particles holding  $\chi = 3$  constant (for a better comparison, in the latter we plot the ground-state energy normalized at the number of particles). Especially for large  $\chi$  or large  $N$ , one obtains a very good agreement between the RPA and exact ground-state energies.

In Fig. 5.3 we plot the expectation value of  $K_0$  vs. the strength parameter  $\chi$ , for fixed  $N = 15$ . Here we obtain an RPA improvement over the HF values for small strength, while in all the other case HF+RPA expectation values performs worse, or about the same as in the mean-field approach. Similar results, although slightly better RPA values for large strength parameters, are shown in Fig. 5.4 for the ground-state mean value of  $K_0^2$ ; RPA on the other hand approximates  $\langle K_0^2 \rangle$  well the exact result in the limit of large number of particles for fixed parameter strength  $\chi = 3$  in Fig. 5.5.

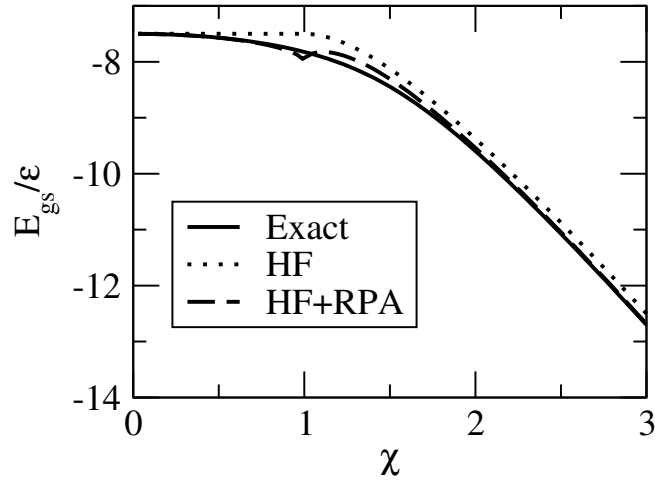


Figure 5.1: Exact, HF and HF+RPA ground state energy vs.  $\chi$  in the Lipkin model, for a fixed number of particles  $N = 15$ .

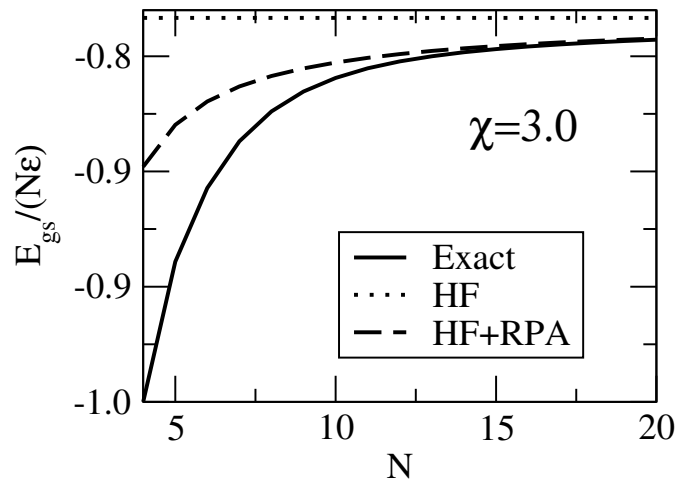


Figure 5.2: Exact, HF and HF+RPA ground state energy vs.  $N$  in the Lipkin model for a fixed strength parameter  $\chi = 3$ .

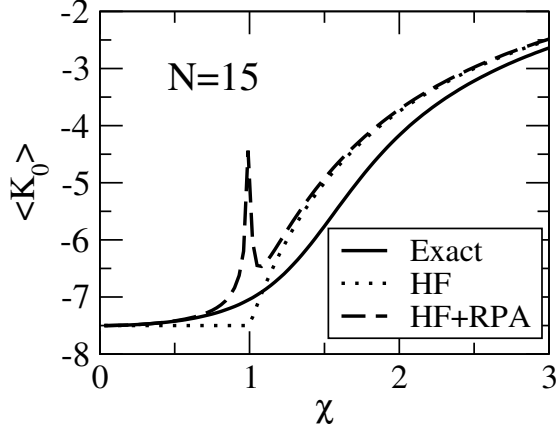


Figure 5.3: Exact, HF and HF+RPA ground state expectation value of  $K_0$  vs.  $\chi$  for fixed number of particles  $N = 15$ .

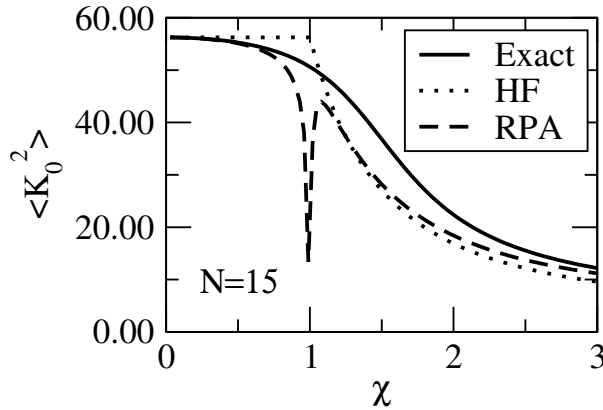


Figure 5.4: Exact, HF and HF+RPA ground state expectation value of  $K_0^2$  vs.  $\chi$  for fixed number of particles  $N = 15$ .

To summarize, in a very simple model, HF+RPA is a very good approximation of the exact results for the ground state energy, even in the neighborhood of a “phase transition.” Similar results have been obtained by Hagino and Bertsch using the three-level Lipkin model [14] which allows symmetry breaking in the mean-field solution. Less satisfactory in general are the results for ground state expectation values of other observables, although good values are obtained for  $\langle K_0^2 \rangle$  in the limit of large number of particles.

## 5.2 Brown-Bolsterli Model

Separable particle-hole interactions provide qualitative understanding of the position of collective states, as in the Brown-Bolsterli model [10, 12, 83] reviewed in this section. Suppose we have computed the HF state for a system of interacting fermions, that is we have

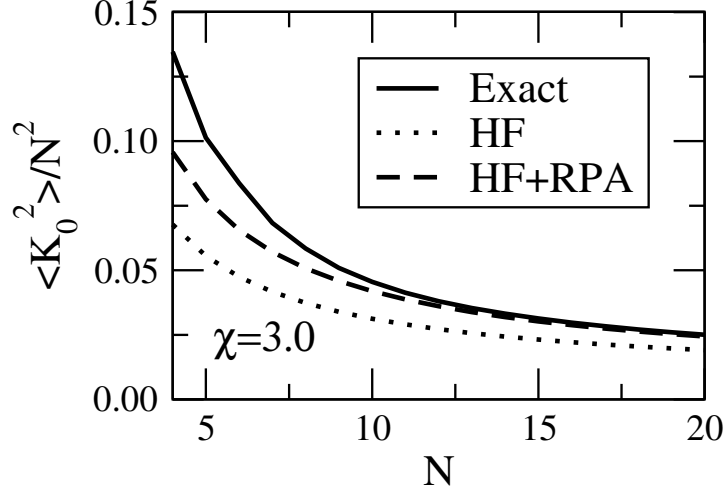


Figure 5.5: Exact, HF and HF+RPA ground state expectation value of  $K_0^2$  vs.  $N$  for fixed strength parameter  $\chi = 3$ .

determined the single particle states/energies; in this basis we assume that the residual particle-hole interaction is

$$V_{mi,jn} = -\lambda Q_{mi} Q_{nj}^*. \quad (5.25)$$

Here  $\lambda$  is a strength parameter, and the interaction is attractive if  $\lambda > 0$ , and repulsive if  $\lambda < 0$ . Simple algebra reduces the RPA eigenvalue equation (4.29) to a dispersion equation for excitation energies  $\Omega$ :

$$\frac{1}{\lambda} = 2 \sum_{mi} \frac{|Q_{mi}|^2 \epsilon_{mi}}{\epsilon_{mi}^2 - \Omega^2}, \quad (5.26)$$

where  $\epsilon_{mi} = \epsilon_m - \epsilon_i$  is the difference between particle and hole single particle energies. Equation (5.26) has no analytical solution, but qualitative features of the solution can be obtained from a graphical representation. We plot in Fig. 5.6 the right-hand side (RHS) which has asymptotes at  $\epsilon_{mi}$ ; the blue lines represent the left-hand side, that is  $1/\lambda$ . In the trivial limit  $\lambda = 0$  the excitation energies are, as expected for non-interacting systems, the difference between particle and hole single particle energies. For interacting systems however, RPA brings corrections to the trivial solution. Moreover, if we calculate transitions induced by the operators  $Q$ , all strength goes into a single, collective state represented in our figure by a circle. Using Fig. 5.6, we can finally understand the assertions made in Sec. 4.2.5 about the position of the collective strength: if the interaction is attractive ( $\lambda > 0$ ), the collectivity lies at low energies, while if the interaction is repulsive ( $\lambda < 0$ ), the collective state is high in energy. In realistic cases, when the interaction has a more complicated form, the collective strength is spread out over more states; however, the position of collective states is influenced in the same manner by the attractive or repulsive character of the residual interaction.

We finalize our discussion about this very simple model with a couple of comments. First, note that we obtain symmetric RPA eigenvalues, as predicted from general considerations

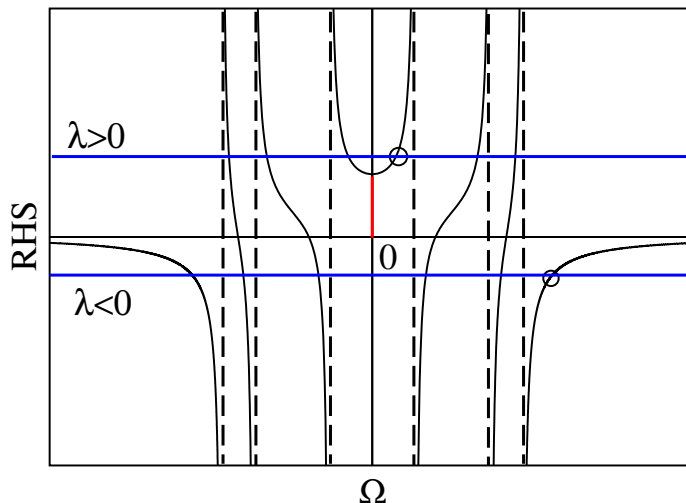


Figure 5.6: Graphical solution to Eq. (5.26).

of the RPA equation. Of course, we have to eliminate the negative excitation energies as unphysical. Second, for values of  $1/\lambda$  in a certain interval, represented with red color in Fig. 5.6, we are short of the collective solution. Actually, the solution is imaginary and the reason is that the HF solution becomes unstable. But this is a simple model, where we decoupled completely the HF solution from the residual interaction; if we would have solved self-consistently RPA, another HF state would have been the correct stable mean-field solution. The main result is a general insight into the features of collective states, and these remain qualitatively correct even in more sophisticated models.

### 5.3 Realistic Forces

RPA is the simplest many-body theory that allows for simple expressions for odd-moment sum rules, which become exact in the limit of small correlations. This fundamental feature made it suitable for the description of giant resonances [85]. Note that in Chapter 7 we revisit the derivation of the RPA linear energy-weighted sum rule and find that non-trivial correction terms were neglected in some specific cases; despite this new result, RPA was in general successful for the description of giant resonances. In this section we review some of the many applications to realistic forces.

We have to point out at the beginning that, for numerical convenience, in realistic applications the RPA equations are usually not solved self-consistently [86, 87]. Thus, one frequently determines a mean-field solution from a phenomenological force, e.g., Skyrme, and then uses a (separable) phenomenological particle-hole interaction, such as Landau-Migdal [88]. Because of this inconsistency, one usually mixes spurious modes with true excitations, and their removal is extremely cumbersome. On the other hand, in calculations where one uses correctly single particle energies and particle-hole configurations derived from

the same underlying force, the agreement with experimental data is not as good as in the other cases [89].

Another point recognized in literature [90] is that one should use different effective forces fitted to describe ground-state properties. This depends upon whether one does HF or HF+RPA calculations, as the latter introduce correlations on top of the mean-field solution. And yet, in realistic applications, one seldom makes this point clear; furthermore, effective forces derived to describe properties in mean-field theory are used very often in RPA calculations. Our plan was to apply RPA globally, and therefore we would have eventually needed an effective force, fitted so that RPA described correctly the available experimental data.

Very schematic, zero-range forces, such as surface delta interaction [91], reduce the amount of numerical effort necessary to diagonalize the non-symmetrical RPA matrices. For this reason, they are very popular in realistic calculations [92, 93]. Even simpler than zero-range forces are separable interactions, such as pairing plus quadrupole-quadrupole [65] or Gamow-Teller ( $\vec{\sigma}\vec{\tau} \cdot \vec{\sigma}\vec{\tau}$ ). The former have been used for the description of quadrupole giant resonances [94–96], while the latter for Gamow-Teller resonances [97] or  $\beta$ -decays [98].

Pairing correlations are very important in nuclear physics, explaining the low-lying structure of the nuclear spectra. (In this context, it is worth mentioning that recently it was argued that this type of spectra is not specific only to pairing, but to two-body interactions in general [99].) The onset of pairing is non-perturbative and the HFB approach, which introduces pairing correlations into the mean-field solution, is considered superior to the HF theory. This is the reason why in almost all investigations reviewed here one uses HFB+QRPA.

RPA is the approach of choice when it comes to estimating negative parity states [100–107], and low-lying spectra in general [108–110] in closed shell nuclei. While in principle most calculations concentrate on  $^{16}\text{O}$  or  $^{208}\text{Pb}$ , the main difference being the interaction used and/or the model space, they all tend to give a good description of the experimental spectra. For example, Ref. [100] uses for the description of  $^{16}\text{O}$  spectra the free nucleon-nucleon interaction in a space allowing one hole in the  $p$  shell, and one particle in the  $sd$  shell; on the other hand, Gillet and Vin Mau used an effective force fitted to the spectra of neighboring nuclei, in a larger model space [101]. Nevertheless, both found reasonable good agreement with the experimental negative parity spectra, although large discrepancies have been reported for  $2^-$  and  $0^-$  states [100].

Successful RPA applications are not restricted to closed shell nuclei. Thus, while the main purpose of Ref. [93] was to study the surface delta interaction, the calculations obtained good description of several excited states ( $2^+$   $\gamma$  vibrational,  $1^-$   $K = 0$  octupole states) for a large number of medium and heavy nuclei. Good results have been obtained also for  $^{12}\text{C}$  [100, 111, 112], but there are features of the experimental spectrum which cannot be accounted for quantitatively within the RPA framework.

One has to point out again that a good description of the observed nuclear spectra has to be supplemented by a good description of transition strength distributions, as the latter probe the theoretical wave functions. This is why in the following we investigate RPA's ability to describe correctly experimental transition strengths in realistic applications.

**Isoscalar monopole giant resonance.** Phenomenological Skyrme forces, adjusted to predict incompressibilities in the 200 – 250 MeV range, have been used successfully in RPA calculations in order to describe the experimental isoscalar giant monopole resonance in  $^{208}\text{Pb}$  [113]. This case is not singular. Thus, starting from a mean-field constructed by superposition of Wood-Saxon single-particle states, and using phenomenological Landau-Migdal particle-hole interaction, reasonable agreement between theory and experiment was also obtained in an extended continuum-RPA for  $^{90}\text{Zr}$ ,  $^{124}\text{Sn}$ , and  $^{208}\text{Pb}$  [114]. However, the centroids were found to be systematically lower in energy than the experimental values, consistent with our results in Chapter 6.

**Dipole response.** A significant fraction of RPA's applications is to the description of experimental giant dipole resonances [89, 102, 108, 110–112, 115–123]. Despite the difference in the model spaces and interactions used, the RPA results were overall very close to the experimental values. However, there are cases when RPA fails to describe the isoscalar dipole resonance; for example, Ref. [119], an unexpected failure in a model space that was successful previously in describing the isoscalar giant monopole resonance in  $^{208}\text{Pb}$  [113]. In another calculation [102], the centroid was found 2 MeV lower than the experimental value.

**Higher order multipole response.** Extensive work [89, 108] tested several multipole transition RPA distributions in  $^{16}\text{O}$ ,  $^{40}\text{Ca}$ ,  $^{90}\text{Zr}$  and  $^{208}\text{Pb}$  against experimental data. The results, fairly insensitive to the interaction used [108], showed again reasonable agreement, as for example the centroids were within 12% of the measured values, while the experimental sum rules were exhausted within 13% [89]. The agreement is far from being perfect, as the low-lying transitions, especially isoscalar  $E2$ , were very badly described [108, 110]. We show similar results for low-lying collectivity in Chapter 6.

**Gamow-Teller response.** QRPA provides an overall good description of the observed Gamow-Teller strength [124–129]. For example, the Gamow-Teller distribution strength for  $^{70}\text{Ge}(n, p)^{70}\text{Ga}$  reaction was well reproduced in QRPA calculations, although the total theoretical strength was found to be a factor of two lower than the experimental value [125]. Studies of several unstable proton rich isotopes in the  $A \sim 70$  mass region have shown also that QRPA predicts rather well experimental half-lives, as well as main features of the distribution [129]; moreover, a better agreement with the experiment has been observed in higher energy domain.

In summary, RPA is generally successful in describing the low-lying nuclear spectra, and produces reasonable approximations for wave functions. In some calculations described here one uses the RPA in occupation space [93, 100, 101, 119, 121] as in our approach, while the others solve the RPA equations in the coordinate space [89, 108, 110, 116–118]. The latter, usually cast in the Green's function response formulation, can more properly describe giant resonances, as they implicitly include contributions from other oscillator shells. However, occasionally it fails to describe some experimental low-lying states, and misses an important fraction of the observed total strength; often, the distribution centroids are lower than the measured ones. In the next chapter we present tests of RPA estimates against exact diagonalization, finding similar features; we bring evidence suggesting that the problem lies within incomplete restoration of symmetries broken in the mean-field solution.

# 6 Results

In this chapter, we present the main results of our investigation. We compare the HF+RPA results for ground-state energy, scalar observables and transition strengths against the exact values provided by full  $0\hbar\omega$  shell model calculations.

We remind the reader that for the Hamiltonian we use the Wildenthal “USD” effective interaction in the  $sd$  shell, while in the  $pf$  shell, we use monopole modified Kuo-Brown “KB3”; these *realistic* interactions provide very good description of the experimental data. In our calculations, we solve the RPA equations self-consistently, as we compute the particle-hole interaction from the starting Hamiltonian.

## 6.1 Binding Energies

We start presenting our results with the ground state energy. For an easier comparison, we define the correlation energy in RPA as [16]

$$E_{\text{RPA}}^{\text{corr}} = E_{\text{HF}} - E_{\text{RPA}} = \frac{1}{2}\text{Tr}(A) - \frac{1}{2}\sum_i \Omega_i. \quad (6.1)$$

Ideally one would hope for a good agreement between  $E_{\text{RPA}}^{\text{corr}}$  and the shell model correlation energy

$$E_{\text{SM}}^{\text{corr}} = E_{\text{HF}} - E_{\text{SM}}, \quad (6.2)$$

which we consider to be exact.

Figures 6.1–6.5 compare the exact and RPA correlation energies for nuclides in the  $sd$ - and  $pf$ -shells respectively [16]. All the nuclei in the  $sd$ -shell are numerically tractable for a full diagonalization; to ease comparison, we grouped into even-even (Fig. 6.1), even-odd (Fig. 6.2), odd-odd (Fig. 6.3) and oxygen isotopes, that is, only neutrons active (Fig. 6.4). In the  $pf$ -shell the dimension of the SM basis rapidly increases with increasing the number of particles in the valence shell, limiting the number of exact cases we can hand; in Fig. 6.5(a) we present nuclides with both protons and neutrons in the active  $pf$  space, while Fig. 6.5(b) contains calcium isotopes (neutrons only).

The general trend is a good agreement between  $E_{\text{SM}}^{\text{corr}}$  and  $E_{\text{RPA}}^{\text{corr}}$ ; in each group, except for oxygen, there is only one or two nuclides where RPA significantly overestimates or underestimates the correlation energy. In the  $sd$ -shell, if one excludes the oxygen results, the

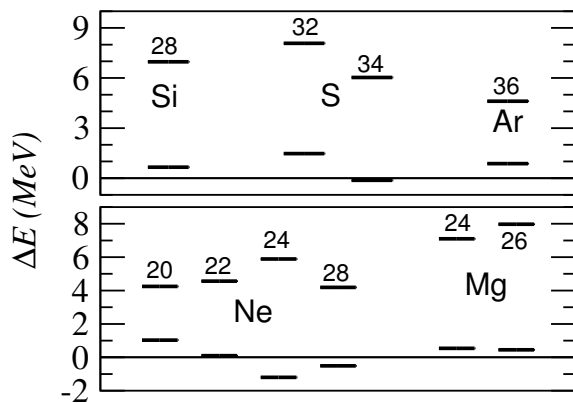


Figure 6.1: Exact and RPA correlation energies for even-even nuclides in the *sd* shell. The upper bars are the HF energy and the lower bars the HF+RPA energy.

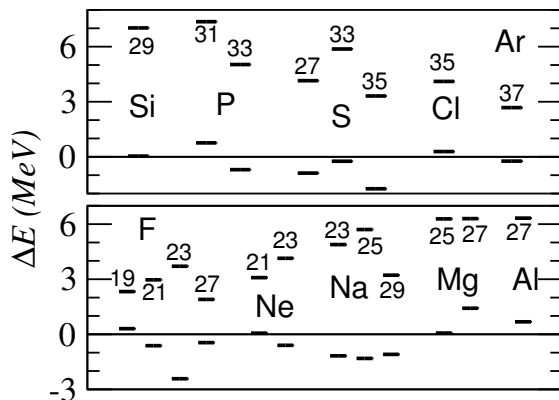


Figure 6.2: Same as in Fig. 6.1 for odd-A nuclides in the *sd* shell.

rms deviation for 41 nuclides is 870 keV; in the lower *pf*-shell, excluding calcium, the rms deviation is 480 keV for 11 nuclides. There was not a significant difference between even-even, odd-odd, and odd-even/even-odd nuclides. The single-species results were significantly worse, however: 1800 keV for 6 oxygen isotopes and 730 keV for 7 calcium isotopes [16]. We searched for potential explanations for this difference, as described in Sec. 6.1.1 below, but found none.

### 6.1.1 Analysis of RPA Accuracy for Binding Energies

Despite our overall good agreement, RPA sometimes fails to accurately reproduce the exact correlation energy. In this section we search for measures that correlate with the success or failure of RPA, which may in turn point toward possible solutions. For example, if RPA fails to describe pairing correlations, one may turn to HFB+ QRPA. For another example, one might expect RPA, which implicitly assumes only small 2p-2h correlations, to be more accurate when the original HF state has a large overlap with the exact ground

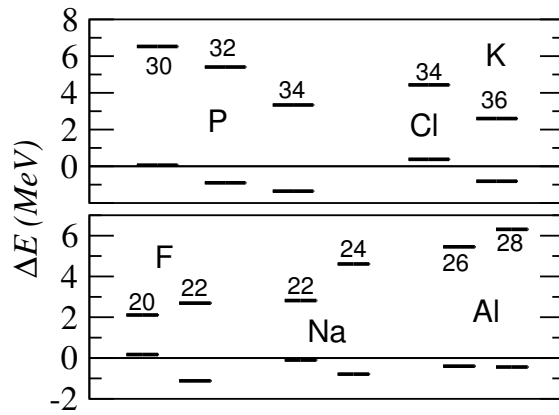


Figure 6.3: Same as in Fig. 6.1 for odd-odd nuclides in the  $sd$  shell.

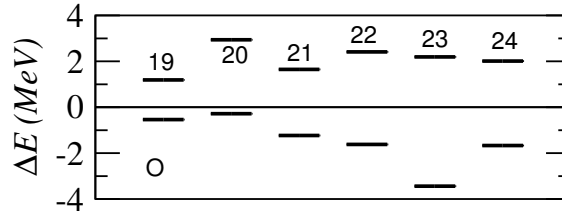


Figure 6.4: Same as in Fig. 6.1 for oxygen isotopes (that is, neutrons only).

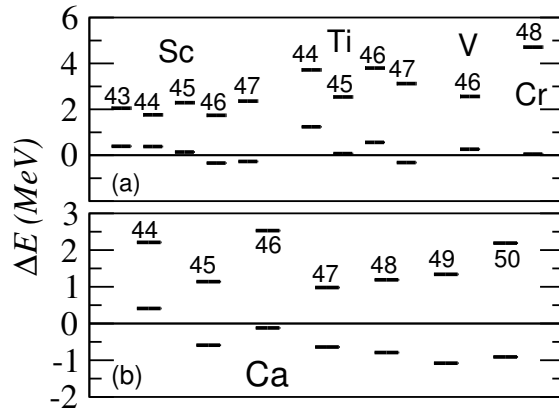


Figure 6.5: Same as in Fig. 6.1 in the  $pf$ -shell for (a) nuclides with both protons and neutrons in the valence space and (b) calcium isotopes (neutrons only).

state wave function. If this were the case, one might correct through some self-consistent or renormalized RPA scheme.

To quantify our search we use the ratio

$$R = \frac{E_{\text{RPA}}^{\text{corr}}}{E_{\text{SM}}^{\text{corr}}}. \quad (6.3)$$

$R = 1$  when HF+RPA agrees with the exact shell-model binding energy.

We begin by considering how well RPA works with different geometries of the mean-field solution. In particular, how well does the RPA correlation energy account for (“restore”) broken symmetries? Table 6.1 lists the deformation geometry (spherical, prolate, oblate, triaxial) for various nuclides [19]; we compute  $\beta$ ,  $\gamma$  by diagonalizing the mass quadrupole tensor of valence nucleons for the HF state [130].  $R$  is close to one for a wide range of deformation parameters. In fact, if anything RPA is *less* reliable for a spherical mean-field geometry, overestimating the correlation energy by as much as a factor of two. This result is surprising. In exact shell-model calculations, the excited states for these “spherical” nuclei are dominated by 1p-1h configurations, so one might expect RPA to be more successful than for “deformed” nuclei.

Table 6.1: Correlation energy ratio vs. geometries of the HF solutions for select nuclides in *sd* and *pf* shells.

Nucleus	$\beta$	$\gamma$ (degrees)	$R$
<sup>22</sup> O	0	–	1.67
<sup>24</sup> O	0	–	1.83
<sup>20</sup> Ne	0.46	0	0.75
<sup>22</sup> Ne	0.33	0	0.97
<sup>23</sup> F	0.11	60	1.65
<sup>24</sup> Na	0.24	13	1.17
<sup>24</sup> Mg	0.29	14	0.92
<sup>26</sup> Al	0.20	33	1.07
<sup>28</sup> Si	0.20	60	0.90
<sup>31</sup> P	0.14	40	0.81
<sup>32</sup> S	0.13	32	0.82
<sup>34</sup> S	0.09	48	1.02
<sup>34</sup> Cl	0.10	42	0.91
<sup>36</sup> Ar	0.09	60	0.81
<sup>43</sup> Sc	0.28	60	0.80
<sup>44</sup> Ti	0.44	0	0.66
<sup>45</sup> Ti	0.38	0	0.97
<sup>46</sup> Ti	0.35	0	0.85
<sup>46</sup> Ca	0.12	0	1.04
<sup>48</sup> Ca	0	–	1.66

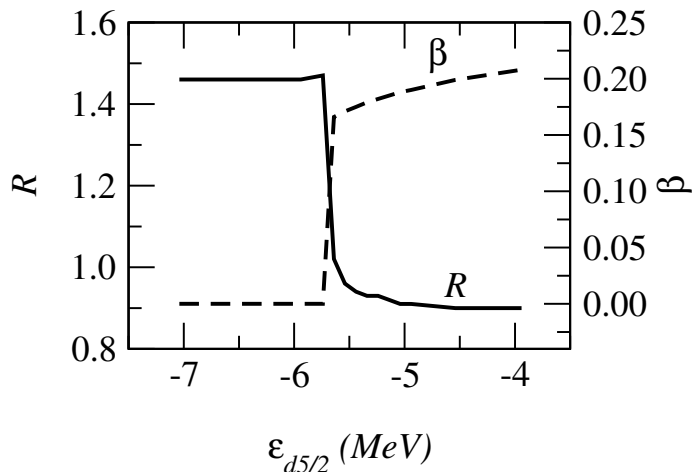


Figure 6.6:  $^{28}\text{Si}$ : correlation energy and deformation parameter in a phase transition obtained by lowering the  $d_{5/2}$  single-particle energy relative to the other single-particle energies. The solid line is  $R$ , the ratio of correlation energies, while the dashed line is the deformation  $\beta$ .

All of the spherical nuclei we found in the  $sd$ -shell were oxygen isotopes (valence neutrons only); this is not surprising as the proton-neutron interaction is well-known to induce deformation. To pursue this issue further, we took  $^{28}\text{Si}$ , which normally has an oblate mean-field solution, and lowered the  $0d_{5/2}$  single-particle energy, until the mean-field solution became spherical (filled  $d_{5/2}$  for both protons and neutrons). In Fig. 6.6 we plot  $R$  as function of the  $d_{5/2}$  single particle energy. Once again  $R$  is closer to 1 for the deformed regime than for the spherical, or closed-shell, regime [16].

Now, as mentioned at the beginning of this section, one possible explanation for the poor results for spherical nuclides is inadequate treatment of pairing. Because the onset of pairing is non-perturbative one might not expect RPA to describe pairing correlations well. In order to test this idea, we made two tests. First, we set all the “pairing” ( $J = 0$ ) two-body matrix elements to zero and redid our calculations for several even-even nuclides. One can see indeed from Table 6.2, the ratio of the correlation energies  $R$  is about the same, but for single-species (oxygen) isotopes  $R$  has even larger deviations from 1.

Second, we computed the expectation value of the pairing Hamiltonian in both the exact shell model calculation and in HF+RPA. (The results are presented in Sec. 6.2, dedicated to ground-state mean-values of scalar observables.) We found, surprisingly, *better* agreement for oxygen and calcium nuclides and considerably poorer results for nuclides with more deformation and better RPA correlations energies. From these two experiments, we cannot conclude that poor treatment of pairing is the culprit.

Another place RPA may stumble is in its implicit assumption that the admixture of 2p-2h correlations in the ground state is small. This shows up in two places, in the bosonization of the energy surface about the Hartree-Fock minimum, which does not enforce the Pauli principle, and, in the computation of the RPA  $\mathbf{A}$  and  $\mathbf{B}$  matrices, the replacement of the RPA wave function by the HF state, i.e., Eq. (4.27). To test this possibility, we calculate the

Table 6.2: The effect of removing the pairing matrix elements: correlation energy ratio  $R$  for several nuclides for the Wildenthal interaction with and without the  $J = 0$  two-body matrix elements.

Nucleus	Wildenthal	Mod. Wildenthal (TBME=0 for $J = 0$ )
$^{20}\text{Ne}$	0.76	0.70
$^{24}\text{Mg}$	0.92	0.97
$^{28}\text{Si}$	0.91	0.91
$^{32}\text{S}$	0.82	1.08
$^{36}\text{Ar}$	0.81	0.83
$^{20}\text{O}$	1.09	1.23
$^{22}\text{O}$	1.67	1.95
$^{24}\text{O}$	1.83	2.24

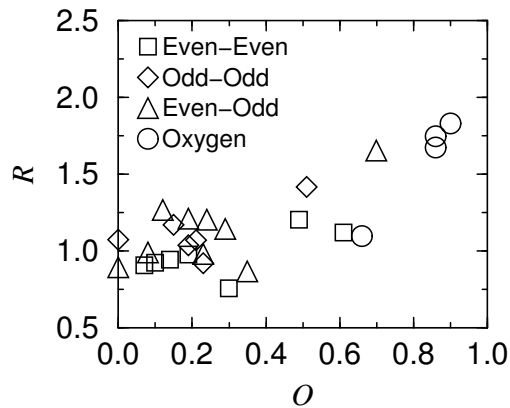


Figure 6.7: The correlation energy ratio  $R$  vs. the overlap  $O$  for select nuclei in  $sd$  shell.

overlap between the HF state and the exact wave function. This cannot be done by simply taking the projection

$$\mathcal{O} = \langle \text{HF} | \text{SM} \rangle. \quad (6.4)$$

In our SM calculations, we took the basis states to have  $J_z = 0$  for  $A$  even and  $J_z = 1/2$  for  $A$  odd; the HF state is a superposition of states with good  $J_z$  which are not restricted to the SM values. Therefore, any rotation of the Slater determinant can change the weight of  $J_z$  components so that  $\mathcal{O}$  is not invariant, although both  $E_{RPA}^{corr}$  and  $E_{SM}^{corr}$  are. We therefore define the overlap as [16]

$$O = \text{Max}(\langle \text{HF} | \text{SM} \rangle), \quad (6.5)$$

where the maximum is taken when rotating about the  $y$  axis. Note that when the exact ground state has  $J = 0$ ,  $\mathcal{O}$  is independent of orientation.

Figure 6.7 shows  $R$  as function of the overlap  $O$  [16]; here we have included only nuclides in the  $sd$ -shell, but the results for  $pf$  are similar.  $O$  varies from close to zero to close to one, but no compelling correlation with  $R$  appears. That is to say, the accuracy of the RPA

Table 6.3: Kinetic energy of RPA zero modes compared with the correlation energy obtained after projection of the HF state on good  $J$ .

Nucleus	$E_{proj}^{corr}$ (MeV)	$KE_0$ (MeV)	$E_{SM}^{corr}$ (MeV)
$^{20}\text{Ne}$	3.29	2.55	4.25
$^{22}\text{Ne}$	1.86	2.29	4.56
$^{28}\text{Si}$	2.67	3.85	6.97
$^{24}\text{Mg}$	5.34	4.65	7.10
$^{32}\text{S}$	2.35	4.20	8.08
$^{44}\text{Ti}$	1.18	1.60	3.72
$^{46}\text{Ti}$	1.82	1.33	3.24

correlation energy does not seem predicated on how well the HF state approximates the exact ground state wave function.

A similar measure would be the amount of correlations in the RPA wave function, that is,  $N_{ph}^{\text{RPA}} = \sum_{\nu} \sum_i |Y_{mi}^{\nu}|^2$ . In principle, RPA is more accurate when  $N_{ph}^{\text{RPA}}$  is small, but, as in Fig. 6.7, we find no correlation between  $N_{ph}^{\text{RPA}}$  and  $R$ . Because of this, it is not obvious that any renormalized, self-consistent, extended, etc., RPA scheme would in practice yield substantial improvements.

### 6.1.2 Kinetic Energy of Spurious Modes

One of the features that makes RPA appealing for correcting the mean-field results is its capacity to identify and separate out, as zero excitation energy, the modes associated with conserved quantities. Consequently, one can identify in Eq. (4.62) a term in the correlation energy corresponding to the kinetic energy of the spurious solution

$$KE_0 = \sum_{\mu(\Omega_{\mu}=0)} \frac{\langle \mathcal{P}_{\mu}^2 \rangle}{2M_{\mu}}. \quad (6.6)$$

On the other hand, the simplest way to correct the broken symmetries in the mean-field solution is to project it onto good quantum numbers. Table II presents the correlation energy obtained by projection of the HF Slater determinants onto good  $J$ ,  $E_{proj}^{corr}$ , and the kinetic energy of the spurious modes given by Eq. (6.6); for comparison we have also included the exact correlation energy missing from the mean-field state. We conclude that  $KE_0$  cannot be identified with the correlation energy obtained by direct restoration of symmetries obtained by projecting the HF state onto good quantum numbers. This may have relevance when if one goes to a multi- $\hbar\omega$  space and wants to remove contamination by spurious center-of-mass motion.

## 6.2 Scalar Observables

In Sec. 4.2.4 we have derived RPA corrections to scalar observables. However, having a formula is not enough. Does it produce useful and reliable results? After all, RPA is an approximation, and because it violates the Pauli exclusion principle RPA is not even variational. In this section, we compare the expectation values of scalar observables in HF+RPA against the exact shell model ground-state averages.

As noted in the introduction, one of the relevant quantities one would like to compute is the rms radius,  $\langle R^2 \rangle$ . Unfortunately in  $0\hbar\omega$  harmonic oscillator model spaces,  $\langle R^2 \rangle$  is trivial: the operator  $R^2$  has two pieces, a one-body piece  $r^2$ , with a constant expectation value in a single major harmonic oscillator shell, and a two-body piece  $r(1) \cdot r(2)$ ; but because  $r$  is an odd-parity operator, the two-body piece is non-zero only across major shells. Therefore in this investigation we instead compute and compare the expectation values of a one-body operator: the number of particles outside the  $0d_{5/2}$  orbit. We will also show in the next section that Eq. (4.68) reduces to the expression derived by Rowe for one-particle densities in spherical nuclei [12,131]. In addition, we test several two-body operators:  $J^2$  (total angular momentum),  $S^2$  (total spin),  $L^2$  (orbital angular momentum),  $Q^2$  (quadrupole-quadrupole), and the pairing Hamiltonian  $H_{\text{pair}} = P^\dagger P$ .

### 6.2.1 One-Body Operators

Using the quasi-boson approximation, Rowe derived the RPA one-particle densities for spherical nuclei [12,131]; related formulas have been used to compute the isotope shift in calcium [132], ignoring the two-body contribution. Let  $\rho_M = \langle c_M^\dagger c_M \rangle$  be the number of particles excited above the Fermi surface into the particle state  $M$ . ( $M$  is not a magnetic quantum number.) Here  $\tilde{A}_{mi,nj} = \delta_{ij}\delta_{mM}\delta_{nM}$  and from (4.68)

$$\rho_M = \sum_{\lambda} \sum_i |Y_{Mi,\lambda}|^2, \quad (6.7)$$

which is Rowe's result for *spherical* Hartree-Fock states. If the HF state is deformed, however, one has to take into account zero modes. The second term in (4.68) can be simplified if one sums over all particle states  $M$ , that is, the total number of particles excited above the Fermi surface; in that case one can use Eq. (4.44) and find [13]

$$\sum_M \rho_M = \sum_{\lambda} \sum_{Mi} |Y_{Mi,\lambda}|^2 - \frac{1}{2} N_{\text{zero}} \quad (6.8)$$

where  $N_{\text{zero}}$  is the number of zero modes,  $N_{\text{zero}} = 2$  for an axisymmetric Hartree-Fock state, such as for  $^{20}\text{Ne}$ , and  $=3$  for a triaxial state, found for  $^{24}\text{Mg}$ . We find Eq. (6.8) often leads to negative occupation numbers! Note, however, that  $\sum \rho_M$  is not an angular momentum scalar, nor even a spherical tensor of fixed rank, for deformed states.

Instead we considered the only scalar one-body operators in our system, the occupation numbers of a  $j$ -shell. Table 6.4 tabulates the HF, RPA, and exact SM values of  $n(d_{3/2}) +$

Table 6.4: The number of particles in the  $d_{3/2} + s_{1/2}$  orbits ( $\dagger = f_{7/2}$  orbit for  $^{48}\text{Ca}$ ). An asterisk denotes nuclides with spherical HF states.

Nucleus	HF	RPA	SM
$^{20}\text{Ne}$	1.60	1.75	1.60
$^{22}\text{Ne}$	1.49	1.64	1.47
$^{24}\text{Mg}$	2.13	1.85	2.31
$^{28}\text{Si}$	3.87	3.77	3.15
$^{20}\text{O}$	0.24	0.46	0.54
$^{21}\text{O}$	0.06	0.53	0.38
$^{22}\text{O}^*$	0.00	0.67	0.54
$^{24}\text{O}^*$	2.00	2.50	2.25
$^{48}\text{Ca}^{*\dagger}$	8.00	7.73	7.78
$^{22}\text{Na}$	1.51	1.69	1.52
$^{26}\text{Al}$	2.29	2.51	2.18
$^{19}\text{F}$	1.02	1.10	1.52
$^{21}\text{F}$	0.84	0.56	0.87
$^{25}\text{Mg}$	2.21	3.09	1.96

$n(s_{1/2})$ . The results are rather poor [13], except for three cases with spherical HF states,  $^{22}\text{O}$ ,  $^{24}\text{O}$ , and  $^{48}\text{Ca}$  [for which we instead tabulate  $n(f_{7/2})$ ].  $^{21}\text{O}$  is weakly deformed and also shows a reasonable, albeit imperfect, improvement as one goes from the HF value to the RPA value.

To explore this issue further, we induced again a “phase transition” in  $^{28}\text{Si}$ , as in Sec. 6.1.1 and plot the average number of particles in  $0d_{3/2}$  and  $1s_{1/2}$  single particles in Fig. 6.8. Again we see reasonable agreement for the spherical region, but poor agreement in the deformed regime [13].

To summarize our results for one-body operators: we regain, for spherical Hartree-Fock states, Rowe’s one-particle occupation numbers and get improved values over the Hartree-Fock occupation numbers. For deformed nuclides, however, the RPA value is generally worse than the HF value. The fault does not appear to lie in the corrections due to zero modes; in the next section, we will find that the RPA expectation value of  $J^2$  is more accurate in the deformed regime than in the spherical regime [13].

## 6.2.2 Two-Body Operators

We now turn to two-body operators, or more properly operators with both one- and two-body pieces. Moreover, we investigate below the pure two-body pieces by removing the one-body part from several operators; the results in such cases were not better or worse than for the general two-body operators.

Table 6.5 shows results for  $S^2$  (total spin),  $L^2$  (total orbital angular momentum), and  $J^2$  (total angular momentum). The RPA expectation value is generally a significant improve-

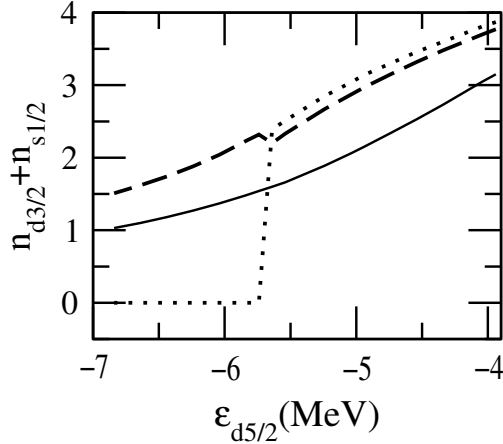


Figure 6.8:  $n(d_{3/2}) + n(s_{1/2})$  in  $^{28}\text{Si}$  as the  $d_{5/2}$  single-particle energy is lowered relative to the other single-particle energies. The solid line is the (exact) shell-model value, the dotted line the HF value, and the dashed line the RPA value.

ment over the HF value, relative to the exact result. On the other hand, the RPA values, while closer to the mark, are not in very good agreement with the exact shell-model values, and sometimes overcorrect to negative, nonphysical expectation values (this can happen because RPA does not respect the Pauli exclusion principle). In Chapter 7 we will examine more closely the expectation values for  $J^2$ , as they can provide information about the “restoration” of symmetries in RPA.

In Table 6.6 we consider the expectation value of the pairing interaction,  $P^\dagger P$  where  $P^\dagger = \sum_{j,m>0} a_{j,m}^\dagger a_{j,-m}^\dagger$ , and of  $Q^2$  [13]. We also show the ratio of correlation energies (6.3) which is a measure of how well the RPA binding energy tracks the exact binding energy. There appears to be no correspondence: a good RPA value for the binding energy does not correspond to a good RPA expectation value. In particular, note the single-species (oxygen) results, where the RPA binding energy is particularly bad; yet for these nuclides  $\langle P^\dagger P \rangle$  and  $\langle Q^2 \rangle$  are very good. Actually, the good results in the case of pairing interaction, which has no one-body contribution, have inspired one test: we removed the one-body contribution (linear combinations of number operators) from the two-body operators. We present the results for the modified Wildenthal Hamiltonian and modified total orbital and total angular momentum in Tables 6.7 and 6.8; we found that the pure two-body pieces performed neither better nor worse on the whole than the one-body pieces.

Again we look at the transition from deformed to spherical in  $^{28}\text{Si}$  for  $\langle Q^2 \rangle$  and  $\langle P^\dagger P \rangle$ , in Fig. 6.9, which clearly shows the RPA values are in better agreement in the spherical regime than in the deformed regime. (As it happens, of the nuclides we investigated  $^{28}\text{Si}$ , while convenient for comparing spherical vs. deformed regimes, is the only nuclide for which the RPA value of  $Q^2$  is worse than the HF value, using the original Wildenthal single-particle energies.) This is not universal behavior; as seen in Table 6.5, the RPA expectation value for some operators is better in the deformed regime [13].

Table 6.5: Ground-state averages of  $S^2$ ,  $L^2$ , and  $J^2$  for nuclei in  $sd$  and  $pf$  shells. For each observable we show the SM, HF and RPA estimates. The nuclides have been grouped into even-even, single-species, odd-odd, and odd-A.

Nucleus	$S^2$			$L^2$			$J^2$		
	HF	RPA	SM	HF	RPA	SM	HF	RPA	SM
$^{20}\text{Ne}$	0.35	0.33	0.26	15.90	-0.25	0.26	16.06	-0.45	0
$^{22}\text{Ne}$	1.48	0.48	0.88	16.76	0.31	0.88	17.17	-1.16	0
$^{24}\text{Mg}$	1.39	1.38	1.03	20.65	-1.17	1.03	20.13	-2.52	0
$^{26}\text{Mg}$	2.04	1.14	1.45	18.94	-0.34	1.45	18.61	-1.72	0
$^{28}\text{Si}$	1.62	1.28	1.45	21.50	-0.75	1.45	20.89	-1.99	0
$^{44}\text{Ti}$	1.03	0.75	0.64	30.34	-2.48	0.64	31.65	-3.10	0
$^{46}\text{Ti}$	2.24	1.20	1.36	29.72	-2.94	1.36	31.53	-5.00	0
$^{48}\text{Cr}$	3.12	0.99	1.70	29.77	5.38	1.70	29.37	4.72	0
$^{20}\text{O}$	1.50	0.45	0.75	6.80	0.92	0.75	6.07	1.76	0
$^{22}\text{O}$	2.40	-0.15	1.26	2.40	6.36	1.26	0.00	7.99	0
$^{24}\text{O}$	2.40	-0.27	1.29	2.39	6.06	1.29	0.00	7.38	0
$^{20}\text{F}$	2.00	1.44	1.74	14.21	8.09	3.55	18.46	12.41	6
$^{22}\text{Na}$	2.20	1.90	2.14	21.32	9.08	8.07	25.57	14.57	12
$^{26}\text{Al}$	3.14	1.96	1.45	29.56	20.14	1.45	35.98	27.92	0
$^{46}\text{V}$	2.51	1.50	1.36	35.39	16.33	1.36	39.56	20.00	0
$^{19}\text{F}$	1.09	0.80	0.87	12.61	4.39	0.22	15.12	5.52	0.75
$^{21}\text{F}$	2.11	0.76	1.52	13.31	5.60	6.41	15.51	9.47	8.75
$^{21}\text{Ne}$	1.11	0.44	1.00	17.55	10.11	3.22	19.05	12.68	3.75
$^{23}\text{Na}$	2.02	0.88	1.15	18.81	7.46	3.93	19.42	11.87	3.75
$^{25}\text{Mg}$	2.04	0.38	1.73	22.56	11.77	7.68	23.87	14.51	8.75

Table 6.6: Ground-state expectation values of  $P^\dagger P$  (pairing) and  $Q^2$ . The final column is the ratio of the RPA correlation energy to the shell-model correlation energy, and =1 when the RPA binding energy is equal to the exact binding energy.

Nucleus	Pairing			$Q^2$			$R$
	HF	RPA	SM	HF	RPA	SM	
$^{20}\text{Ne}$	2.99	5.47	6.81	715	825	793	0.75
$^{22}\text{Ne}$	3.99	7.25	9.31	876	1007	944	0.97
$^{24}\text{Mg}$	5.99	10.14	11.72	1167	1263	1268	0.92
$^{26}\text{Mg}$	6.99	11.51	14.56	1001	1104	1048	0.94
$^{28}\text{Si}$	8.99	12.73	15.16	1304	1389	1214	0.90
$^{20}\text{O}$	2.00	5.18	7.25	257	353	339	1.09
$^{22}\text{O}$	3.00	5.83	6.20	163	277	270	1.67
$^{24}\text{O}$	4.00	6.52	6.58	122	194	191	1.83

Table 6.7: The effect of removing the single-particle energies from the interaction: SM, HF and RPA estimates of the binding energy for four even-even *sd* shell nuclei.

Nucleus	HF	RPA	SM
<sup>20</sup> Ne	-26.58	-29.67	-31.32
<sup>22</sup> Ne	-37.86	-42.20	-43.18
<sup>24</sup> Mg	-65.01	-70.40	-72.24
<sup>28</sup> Si	-112.91	-117.80	-119.21

Table 6.8: The effect of removing one-body contributions from  $J^2$  and  $L^2$ : SM, HF and RPA estimates for the two-body part only.

Nucleus	$J^2$			$L^2$		
	HF	RPA	SM	HF	RPA	SM
<sup>20</sup> Ne	-7.64	-22.69	-23.97	-1.51	-16.23	-17.64
<sup>20</sup> Ne	-25.00	-42.53	-42.70	-13.52	-29.82	-30.20
<sup>24</sup> Mg	-36.18	-60.67	-56.61	-21.34	-44.01	-41.50
<sup>28</sup> Si	-58.57	-81.76	-84.59	-38.15	-59.99	-61.21
<sup>22</sup> Na	-16.54	-26.28	-30.21	-8.98	-21.75	-22.46
<sup>26</sup> Al	-36.64	-43.97	-73.70	-10.22	-33.81	-52.84
<sup>20</sup> O	-27.21	30.47	-31.43	-16.22	-22.21	-21.48
<sup>21</sup> O	-34.31	-27.68	-32.34	-20.99	-18.88	-21.37
<sup>22</sup> O	-52.50	-40.62	-48.96	-33.60	-28.64	-34.33
<sup>23</sup> O	-52.37	-35.25	-37.96	-33.54	-25.11	-24.33
<sup>24</sup> O	-54.00	-44.29	-53.11	-33.60	-30.37	-36.42

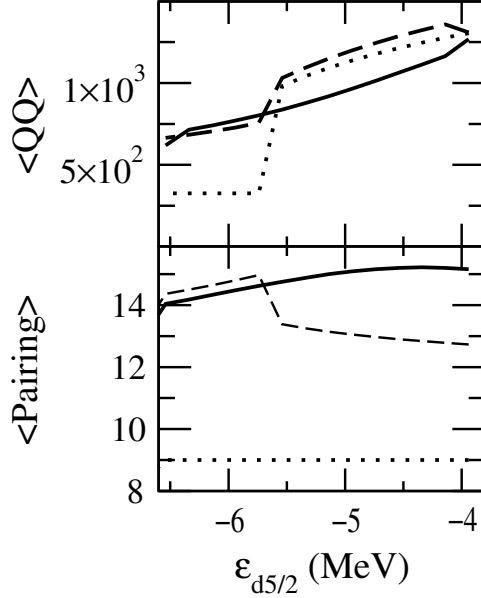


Figure 6.9:  $\langle Q^2 \rangle$ ,  $\langle P^\dagger P \rangle$  in  $^{28}\text{Si}$  as the  $d_{5/2}$  single-particle energy is lowered relative to the other single-particle energies. The solid line is the (exact) shell-model value, the dotted line the HF value, and the dashed line the RPA value.

An obvious step will be to try QRPA, which may improve performance in the deformed regime. On the other hand, we reran our calculations with all the explicit pairing matrix elements set to zero, and found no qualitative change in our results, much as was found for the RPA correlation energy in Table 6.2.

### 6.3 Transitions

In the previous sections we have investigated HF+RPA estimates for binding energies, ground-state expectation values of one- and two-body operators against the exact SM results. We found that RPA is not entirely reliable, although many times HF+RPA is close to the exact value. However, the review in Sec. 5.3 shows that the main applications of RPA are to transition strengths.

It is the general belief that RPA is reliable for describing transitions, as it is primarily a model for excited states. However, the main assumption in RPA is that the excited states are 1p-1h mixtures. Is this the case? That is, are the excited states *mainly* mixtures of 1p-1h correlations? The answer is no: one knows from SM calculations that, for example, the first excited state in  $^{16}\text{O}$  has a predominant 4p-4h character [133], outside the RPA model space. It is therefore no surprise that RPA fails in these situations. Despite this, as outlined in Sec. 5.3, RPA was the method of choice for description of negative parity states in closed shell nuclei [100, 101, 104–107] and in open shell nuclei [103, 111, 112]. RPA and QRPA calculations (sometimes including continuum states) using phenomenological interac-

tions have been successful in describing the experimental position of giant resonances [85], particularly  $E1$  [111, 112, 122] and  $M1$  [134] from electron or proton scattering, or Gamow-Teller resonances [124–129]. In general, however, the description of low-lying transitions is poor [108, 109, 124]. Other studies have used QRPA to compute transitions of interest for astrophysics but did not directly compare to experiment [97, 135].

Tests of transitions have been mainly against ‘toy’ models, as for the binding energies [136–138], although the QRPA has been tested against exact diagonalization in the full SM space for  $\beta^\pm$  or double  $\beta$  decays [139–142], with mixed success. Broader tests of RPA transitions strengths against an exact model, e.g., SM, have not been done. In the following, we test the RPA against full  $0\hbar\omega$  calculation for several nuclei in the  $sd$  and  $pf$  shells for electromagnetic transitions. Unlike previous tests however, we consider mean-field solutions which break the rotational symmetry.

In general, transitions are described by  $A$ -body multipole operators; nevertheless, for most applications they can be taken as *one-body* operators of the form [3, 11]

$$F_{JM;TT_z} = \tilde{e}_{JT} \sum_{\alpha\beta} \langle \alpha || F_{JT} || \beta \rangle [a_\alpha^\dagger \otimes a_\beta]_{JM}^{TT_z}, \quad (6.9)$$

the phenomenological charge  $\tilde{e}_{JT} = \tilde{e}_p - (-)^T \tilde{e}_n$  being a combination of phenomenological proton and neutron charges (see Appendix A for some details). As discussed in Chapter 3, phenomenological charges should be used to account for space restriction. However, the main contribution of effective charges is a rescaling of the strengths, not relevant for our investigation; therefore for simplicity we took the bare charges,  $\tilde{e}_p = 1$  and  $\tilde{e}_n = 0$ .

For testing purposes, we have considered  $F_{JT} = \tilde{e}_T r^J Y_J$ , with  $J = 2$ , that is isoscalar ( $T = 0$ ) and isovector ( $T = 1$ ) electric quadrupole ( $E2$ ). In addition, we tested transition distributions for spin flip (SF) and Gamow-Teller (GT) which are the isoscalar and isovector components of the spin operator  $\sigma$ . To avoid confusion, note that the actual GT operator we used is  $\sigma\tau_z$  so that  $T_z = Z - N$  was conserved.

A large fraction application of RPA calculations are to  $E1$  transitions. Because our shell model valence space does not include single-particle states of opposite parity, we could not investigate  $E1$  transitions here.

### 6.3.1 High-Lying Collectivity

In this section we show results for isovector  $E2$ , SF and GT transition operators. The main common feature is that their collective transitions lie relatively high in energy. We find that for such transitions the RPA is in reasonably good agreement with the SM results, especially for the total transition strength.

Figures 6.10–6.12 compare the RPA and SM transition strengths; we choose for exemplification  $^{20}\text{Ne}$  (even-even),  $^{21}\text{Ne}$  (even-odd) and  $^{22}\text{Na}$  (odd-odd), but the general trend is the same for all the nuclides investigated [19]. The excitation spectra are discrete, but to guide the eye we folded in a Gaussian of width 0.7 MeV. In addition, Tables 6.9–6.11 summarize

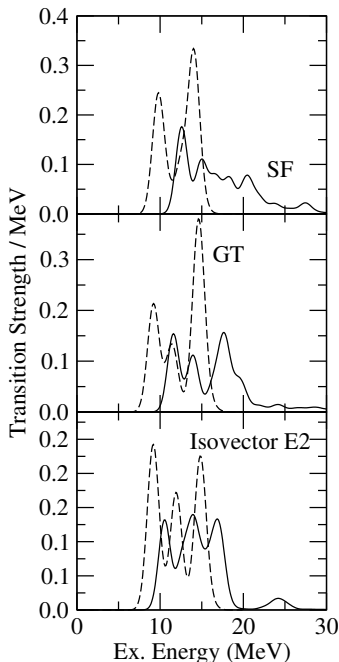


Figure 6.10: Isovector  $E2$ , SF and GT transition strengths for  $^{20}\text{Ne}$ . Both the exact SM (solid curve) and RPA (dashed curve) distributions have been smoothed with a Gaussian of width 0.7 MeV to facilitate comparison.

the results in both SM and RPA for several nuclei [19]; we present only the total strengths, the centroids and the widths of the distributions.

The figures show that the RPA calculations follow the general features of the SM transition strength distributions. Note however that by comparison to SM, the RPA distributions have smaller widths (see Tables 6.9–6.11). This is not surprising, as higher-order particle-hole correlations are expected to further fragment the distribution. The RPA centroids are generally shifted to lower energies than the SM. Although the centroids are related to the energy-weighted sum rule  $S_1$ , we remind the reader that we do not violate Eq. (3.14) because the HF state is only an approximation to the ground state. Furthermore, the shift in the centroid does not appear correlated with the correctness of the RPA estimations of the ground state energy [16] or other observables [13]. One might expect that the correct inclusion of the pairing interaction by means of HFB+QRPA would improve the results. This is reasonable and worth trying, but see discussion and caveats regarding pairing and QRPA in Secs. 6.1 and 6.2.

For computational simplicity, we restrict ourselves to real wave functions; this has no effect for even-even nuclei. But because the rotations about the  $x$  or  $z$  axis are complex, for odd-odd or odd- $A$  nuclei the RPA does not identify all the corresponding generators as exactly zero-frequency modes. Instead, we obtain a ‘soft’ mode at very low excitation energy. Transition strengths to the soft mode are in fact ground-state-to-ground-state strength normally not computed in RPA.

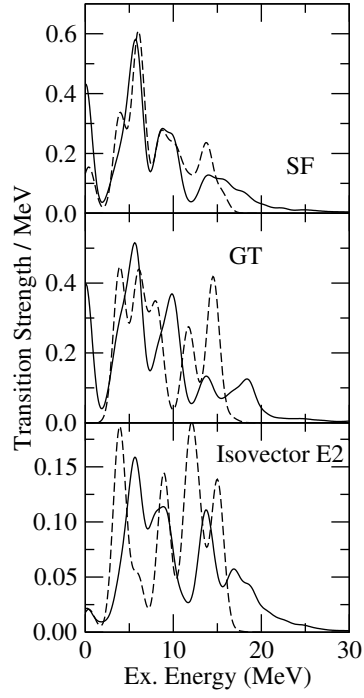


Figure 6.11: Same as in Fig. 6.10 for  $^{21}\text{Ne}$ .

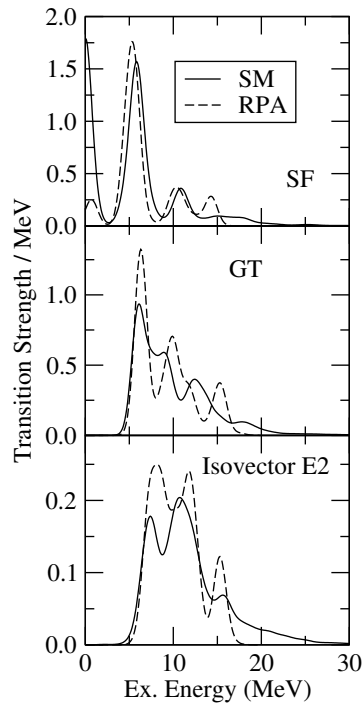


Figure 6.12: Same as in Fig. 6.10 for  $^{22}\text{Na}$ .

Table 6.9: Total strength, centroid, and width for isovector  $E2$  transition operator. The nuclei have been grouped into even-even, odd-odd and odd-A.

Nucleus	$S_0$		$\bar{S}$ (MeV)		$\Delta S$ (MeV)	
	SM	RPA	SM	RPA	SM	RPA
$^{20}\text{Ne}$	0.98	1.15	14.53	11.92	3.47	2.44
$^{22}\text{Ne}$	2.37	1.86	8.15	7.70	5.85	4.25
$^{24}\text{Mg}$	1.88	1.96	14.40	11.86	4.09	2.46
$^{28}\text{Si}$	2.28	1.96	14.35	13.41	4.29	1.93
$^{36}\text{Ar}$	1.38	1.34	12.49	11.01	4.24	3.56
$^{44}\text{Ti}$	2.15	1.90	8.23	6.68	2.86	1.98
$^{22}\text{Na}$	1.60	1.69	11.67	10.44	4.37	2.61
$^{24}\text{Na}$	2.07	2.09	9.82	8.21	6.26	4.14
$^{46}\text{V}$	2.32	3.00	7.96	6.62	4.17	1.97
$^{21}\text{Ne}$	1.39	1.43	10.52	9.41	5.66	4.27
$^{25}\text{Mg}$	2.28	2.20	11.48	9.47	6.21	4.41
$^{29}\text{Si}$	2.52	2.20	11.61	10.21	5.68	4.25

Table 6.10: Same as in Table 6.9 for SF transition operator.

Nucleus	$S_0$		$\bar{S}$ (MeV)		$\Delta S$ (MeV)	
	SM	RPA	SM	RPA	SM	RPA
$^{20}\text{Ne}$	1.05	1.23	17.10	12.26	4.38	1.95
$^{22}\text{Ne}$	3.53	4.44	11.40	8.82	4.32	2.37
$^{24}\text{Mg}$	4.15	4.78	13.22	10.17	4.48	1.97
$^{28}\text{Si}$	5.82	5.20	12.75	11.62	4.34	1.89
$^{36}\text{Ar}$	2.68	2.70	14.53	11.17	3.69	2.88
$^{44}\text{Ti}$	2.56	3.32	9.98	7.86	2.56	1.55
$^{22}\text{Na}$	8.57	5.78	5.01	6.67	5.22	3.49
$^{24}\text{Na}$	10.06	7.66	5.83	7.05	5.48	3.19
$^{46}\text{V}$	5.44	7.68	8.76	6.40	2.51	2.34
$^{21}\text{Ne}$	4.02	3.54	7.50	7.62	5.92	3.95
$^{25}\text{Mg}$	6.94	6.33	9.19	8.47	5.73	3.36
$^{29}\text{Si}$	8.42	8.47	9.38	7.86	5.07	4.45

Table 6.11: Same as in Table 6.9 for GT transition operator.

Nucleus	$S_0$		$S$ (MeV)		$\Delta S$ (MeV)	
	SM	RPA	SM	RPA	SM	RPA
$^{20}\text{Ne}$	1.05	1.33	16.32	12.53	4.35	2.42
$^{22}\text{Ne}$	3.87	4.85	12.00	9.37	4.48	3.16
$^{24}\text{Mg}$	4.26	4.85	14.46	11.74	4.24	2.42
$^{28}\text{Si}$	6.65	5.70	15.19	13.77	3.59	1.88
$^{36}\text{Ar}$	2.74	2.79	14.85	12.09	3.45	2.99
$^{44}\text{Ti}$	3.03	3.74	10.12	8.42	2.86	2.43
$^{22}\text{Na}$	5.51	5.47	9.96	9.28	4.35	3.18
$^{24}\text{Na}$	7.43	7.71	10.32	9.29	4.87	3.48
$^{46}\text{V}$	10.60	7.85	4.93	8.15	4.37	2.28
$^{21}\text{Ne}$	4.25	3.55	7.87	8.67	5.97	3.98
$^{25}\text{Mg}$	7.12	6.76	11.02	10.00	6.05	4.21
$^{29}\text{Si}$	9.42	8.63	12.28	10.39	5.41	4.99

To summarize the results in this section, we have compared the SM and RPA distribution strengths for isovector  $E2$ , SF and GT transition operators. We found in general good agreement for the total strength in several nuclei. While less satisfactory, the centroids and widths of the distributions are still close. As a general feature however, the RPA distributions are smaller in width and lower in energy than the SM results.

### 6.3.2 Low-Lying Collectivity

This section presents comparison between the SM and RPA distribution strength for the isoscalar quadrupole transition operator. The main difference with respect to the other transitions investigated here is that the collective strength lies very low in energy as predicted by the Brown-Bolsterli model (Sec. 5.2), for realistic Hamiltonians have a strong attractive isoscalar quadrupole-quadrupole component.

We considered again for comparison the same nuclides investigated previously, and we plot the SM and RPA distributions in figures 6.13–6.15 [19]. Characteristics of the distributions for several other nuclei are given in table 6.12. In contrast with the results in Sec. 6.3.1, we find a large discrepancy between the total strengths in RPA and SM, especially for even-even nuclei.

Figure 6.13 shows that, if one ignores the low energy transitions, one obtains again a reasonable agreement between the SM and RPA distributions. Similar features encountered for other transitions appear, that is a lower energy centroid and smaller width of the RPA distribution with respect to SM.

As for the relative good agreement for odd-odd and odd- $A$  nuclei, we have to point out that most of the RPA strength is concentrated in the lowest energy state which, as already noted, appears just as an artifact of our approach (restriction to real numbers). A

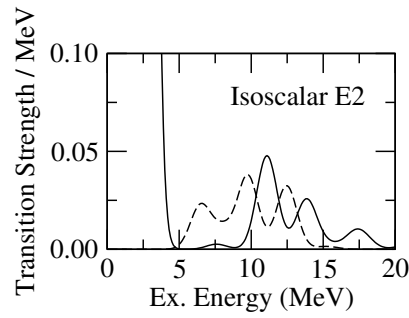


Figure 6.13: Isoscalar  $E2$  transition strengths for  $^{20}\text{Ne}$ . The SM (solid curve) and RPA (dashed curve) distributions have been smoothed with a Gaussian of width 0.7 MeV. The large collective peak at low but nonzero excitation energy for the SM is absent in the RPA; see text for discussion.

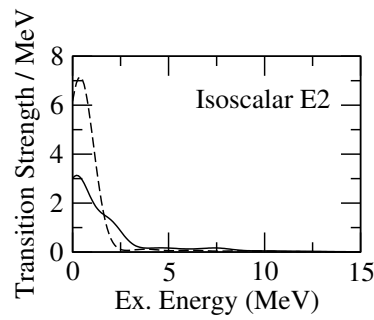


Figure 6.14: Same as Fig. 6.13 for  $^{21}\text{Ne}$ .

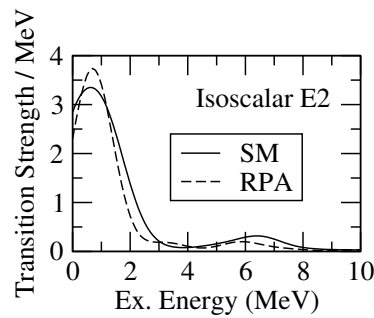


Figure 6.15: Same as Fig. 6.13 for  $^{22}\text{Na}$ .

Table 6.12: Same as in Table 6.9 for isoscalar  $E2$  transition operator.

Nucleus	$S_0$		$\bar{S}$ (MeV)		$\Delta S$ (MeV)	
	SM	RPA	SM	RPA	SM	RPA
$^{20}\text{Ne}$	7.86	0.19	2.12	9.81	1.92	2.30
$^{22}\text{Ne}$	9.36	0.89	2.01	5.52	2.19	2.79
$^{24}\text{Mg}$	12.57	0.51	2.13	7.99	2.09	2.75
$^{28}\text{Si}$	12.04	0.56	2.51	9.88	2.33	2.33
$^{36}\text{Ar}$	7.17	0.23	2.42	9.57	1.91	2.74
$^{44}\text{Ti}$	10.87	1.50	1.73	3.99	1.73	1.70
$^{22}\text{Na}$	9.53	7.49	1.47	1.27	2.63	1.82
$^{24}\text{Na}$	8.81	6.33	2.10	1.81	2.85	1.88
$^{46}\text{V}$	15.21	15.20	1.62	0.87	1.94	1.63
$^{21}\text{Ne}$	8.74	13.27	1.53	0.64	2.82	1.35
$^{25}\text{Mg}$	10.71	12.49	2.25	1.08	2.66	1.62
$^{29}\text{Si}$	9.70	1.38	2.72	4.66	2.62	4.25

full treatment of rotations by inclusion of complex numbers would shift these ‘soft-mode’ states to zero modes, that is, degenerate with respect to the ground-state, and we would expect the odd-odd and odd- $A$  cases to then resemble the even-even cases: missing the low-energy collective strength. (Note that qualitatively the results for  $^{29}\text{Si}$ , for which we obtain the correct number of zero RPA modes, are similar to the even-even nuclei.) Conversely, we can turn around these results into a hypothesis: that the missing low-lying collective strength in even-even nuclides are due to incomplete symmetry restoration, and that the missing strength resides in the RPA ground state. Alternately, one can make the reasonable, and perhaps simpler, interpretation that the RPA does not adequately model rotational motion, and that the missing strength resides in the ground-state rotational band; because the ground state band is projected out of the Hartree-Fock intrinsic state, this appears as a ‘ground-state to ground-state transition.’ The fact that the missing strength shows up in soft modes that arise as artifacts of our computational methods bolsters this hypothesis. In the next chapter we discuss in more detail the connection between missing strength from the low-lying collective transitions and the incomplete symmetry restoration.

# 7 RPA: Myths and Facts

A couple of concepts are always associated with RPA in the literature. First, it was long believed that the RPA linear energy-weighted sum rule (EWSR) takes a very simple form. In 1961, Thouless showed that the RPA linear EWSR can be written, similarly to Eq. (3.16), as the *mean-field* expectation value of a particular double commutator [18]. However, the result has been obtained assuming a HF state which does not break any symmetries [10,18]. We find that in the case symmetries are broken in the mean-field solution, Thouless theorem needs non-trivial corrections. Moreover, we found, surprisingly, contributions to EWSR  $S_1$  [see Eq. (3.14)] coming from zero modes, that is from broken symmetries.

Second, RPA is usually associated with a restoration of symmetries broken in mean field. In fact, RPA identifies the generators of broken symmetries in the HF solution as states lying at zero excitation energy. However, the results for the expectation values of scalar operators, in particular  $J^2$ , as well as the bad description of the low-lying collective transitions, suggest that the symmetries are only partly restored.

## 7.1 Energy-Weighted Sum Rules

As noted in Chapter 4, the RPA has the famous property [10,18]:

$$\sum_{\nu} \Omega_{\nu} |\langle \nu | F | \text{RPA} \rangle|^2 = \frac{1}{2} \langle \text{HF} | [F, [H, F]] | \text{HF} \rangle, \quad (7.1)$$

sometimes referred to as Thouless's energy-weighted sum rule theorem. Note that although  $|\text{HF}\rangle$  is *not* an exact eigenstate of the Hamiltonian, Eq. (7.1) is similar to Eq. (3.14), suggesting the interpretation that “the RPA conserves the energy-weighted sum rule” (see Ref. [12], p. 275). This is *not* an entirely true statement, as  $|\text{RPA}\rangle \approx |\text{HF}\rangle$  is only approximate, and never exact. Furthermore, in this section we revisit the derivation of Eq. (7.1) and find that it can be violated *if* an exact symmetry such as rotational invariance is broken. We confirm the violation numerically, and find the worse case to be where the bulk of the transition strength lies very low in energy, such as isoscalar  $E2$ . Because previous applications of RPA have usually assumed spherical symmetry they are not invalidated, but ambitious RPA calculations that allow for broken symmetries in the mean field [143] should be approached with caution. Of particular interest, which we have not yet explored, is the QRPA which breaks particle number conservation.

Table 7.1: Comparison of energy-weighted sum rule  $S_1$  as computed in the shell model (SM), taking the weighted sum of RPA strengths (RPA), and taking the HF expectation value of a double-commutator (HF); see text for more details. Notation on  $^{28}\text{Si}$ :  $\dagger$  indicates a modified  $d_{5/2}$  single-particle energy to obtain a spherical HF state.

Nucleus	Isovector $E2$			Isoscalar $E2$		
	SM	RPA	HF	SM	RPA	HF
$^{20}\text{Ne}$	14.27	13.74	13.74	16.63	1.82	7.43
$^{22}\text{Ne}$	19.28	14.34	14.40	18.84	4.92	10.51
$^{24}\text{Ne}$	21.89	14.89	15.06	20.87	8.42	11.99
$^{24}\text{Mg}$	27.09	23.28	23.28	26.71	4.08	14.87
$^{36}\text{Ar}$	17.24	14.72	14.72	17.32	2.21	8.64
$^{28}\text{Si}$	32.66	26.22	26.22	30.22	5.58	17.67
$^{28}\text{Si}^\dagger$	40.13	35.76	35.76	34.31	28.26	28.26
$^{22}\text{O}$	11.46	8.56	8.56	11.46	8.56	8.56
$^{24}\text{O}$	10.42	7.99	7.99	10.42	7.99	7.99

We begin by presenting in Table 7.1 the results for the EWSR  $S_1$  [19] computed in three different ways: in SM, RPA (using the RPA strengths and frequencies), and HF, that is the right hand side of Eq. (7.1). There are a couple of things to note. First, the large discrepancy between the SM and RPA EWSRs for isoscalar  $E2$  transitions. If our interpretation from Sec. 6.3.2 that the missing strength is due to a ground state to ground state transition, more precisely ground state to spurious mode transition, one would expect no consequence for the EWSR  $S_1$ , as those states lie at *zero* excitation energy. We will see later in the derivation why this assertion is not correct.

Second, we violate very badly Eq. (7.1); the only cases we do verify numerically the latter are systems with spherical symmetries, such as  $^{22,24}\text{O}$  and  $^{28}\text{Si}^\dagger$ , and for the operators having high collectivity, isovector  $E2$  as well as SF and GT not shown here. But Eq. (7.1) is a valuable numerical check for any RPA code, so one might suspect an error in the numerical implementation. To prove that this is not the case, we revisit the derivation of Eq. (7.1), paying special attention to the correct treatment of zero modes.

Suppose we have a broken symmetry, such as rotational invariance. The HF state is deformed and has a particular orientation, but the HF energy is independent of the orientation. This shows up in the RPA matrix equation (4.29) as a zero-frequency mode. We showed in Sec. 4.2 that for  $\Omega > 0$  one has the normalization  $\vec{X}^2 - \vec{Y}^2 = 1$  but this normalization is impossible for  $\Omega = 0$ . Instead we have introduced collective coordinates  $\vec{Q}_\nu$  and conjugate momenta  $\vec{P}_\nu$  [10,17], which satisfy Eqs. (4.50) and (4.51) supplemented by the normalization of condition (4.52) Note that if  $\mathbf{A}$  and  $\mathbf{B}$  are real, then  $X, Y$  are real, but of necessity  $P$  and  $Q$  are complex (one is real and the other imaginary). For the zero-mode frequencies one must supplement the quasi-boson operators  $\beta, \beta^\dagger$  in Eq. (4.20) with the generalized coordinate and momentum operators  $\hat{Q}, \hat{P}$ .

Because of the expansion (4.71) one can use the definitions (4.10), (4.11), and able to use  $A$  and  $B$  to write the right hand side of Eq. (7.1) for an angular momentum tensor operator of order  $K$  as

$$\frac{1}{2} \sum_M (-1)^M \langle \text{HF} | [F_{K,-M}, [F_{KM}, H]] | \text{HF} \rangle = \sum_M \sum_{mi,nj} (A_{mi,nj} f_{mi}^M f_{nj}^M - (-1)^M B_{mi,nj} f_{mi}^M f_{nj}^{-M})$$

The matrices  $\mathbf{A}$  and  $\mathbf{B}$  can be written in terms of particle hole amplitudes  $X$  and  $Y$ , and the canonical momentum operators associated with broken symmetries

$$\mathbf{A} = \mathbf{X}\Omega\mathbf{X}^\dagger + \mathbf{Y}^*\Omega\mathbf{Y}^T + \mathbf{P}\mathbf{M}^{-1}\mathbf{P}^\dagger, \quad (7.2)$$

$$-\mathbf{B} = \mathbf{X}\Omega\mathbf{Y}^\dagger + \mathbf{Y}^*\Omega\mathbf{X}^T - \mathbf{P}\mathbf{M}^{-1}\mathbf{P}^T. \quad (7.3)$$

Substitution and some algebra yields

$$\begin{aligned} \frac{1}{2} \sum_M (-1)^M \langle \text{HF} | [F_{K,-M}, [F_{KM}, H]] | \text{HF} \rangle = \\ \sum_M \sum_{\nu(\Omega_\nu \neq 0)} \Omega_\nu |\langle \text{RPA} | F_{KM} | \nu \rangle|^2 + \sum_M \sum_{\mu(\Omega_\mu = 0)} \frac{1}{2M_\mu} |f^M \cdot P_\mu - (-1)^M f^{-M} \cdot P_\mu^*|^2. \end{aligned} \quad (7.4)$$

Moreover, it is a simple exercise to rewrite the most right-hand side of the last equation as

$$\begin{aligned} \sum_M \sum_{\mu(\Omega_\mu = 0)} \frac{1}{2M_\mu} |f^M \cdot P_\mu - (-1)^M f^{-M} \cdot P_\mu^*|^2 = \\ \sum_M \sum_\mu (-1)^M \frac{1}{2M_\mu} [F_{K,-M}, \hat{P}_\mu] [F_{KM}, \hat{P}_\mu] = \frac{1}{2} \sum_M \sum_\mu (-1)^M \left[ F_{K,-M}, \left[ F_{KM}, \frac{\hat{P}_\mu}{2M_\mu} \right] \right]. \end{aligned} \quad (7.5)$$

At this point, there are a couple of comments we should make. First, note that in Eq. (7.5), we do not take an average on a state. That is because in RPA the commutators involved are simply numbers. Second, the elegant forms in both (7.4) and (7.5) cannot be obtained if the transition operators are not spherical tensors. Nonetheless, even for an arbitrary transition operator one can calculate corrections to Eq. (7.1) due to broken symmetries in the mean-field solution.

As further motivation, one can start from Eq. (4.72) and write the contribution from a single frequency to the RPA energy-weighted sum rule as [19]

$$S_1^{RPA}(\mu) = \Omega_\mu \sum_M |f^M \cdot X_\mu + (-1)^M f^{-M} \cdot Y_\mu|^2. \quad (7.6)$$

Even if  $\mu$  is not a zero mode, one is free to transform to collective coordinates and momenta [10],

$$X_\mu = \sqrt{\frac{M_\mu \Omega_\mu}{2}} Q_\mu - i \sqrt{\frac{1}{2M_\mu \Omega_\mu}} P_\mu \quad (7.7)$$

$$Y_\mu = -\sqrt{\frac{M_\mu \Omega_\mu}{2}} Q_\mu^* + i \sqrt{\frac{1}{2M_\mu \Omega_\mu}} P_\mu^*. \quad (7.8)$$

Inserting into (7.6) and letting  $\Omega_\mu \rightarrow 0$ , there is a finite remainder exactly equal to the rightmost term of (7.4).

It is of course surprising to find contribution to the energy-weighted sum rule from ‘zero excitation energy’. To illustrate this peculiar result in a simple example, let us consider the simple case of the quantum harmonic oscillator<sup>1</sup> (HO), described by the Hamiltonian (again,  $\hbar = 1$ )

$$H_{\text{HO}} = -\frac{1}{2m} \frac{d^2}{dx^2} + \frac{1}{2} m\omega x^2, \quad (7.9)$$

satisfying the well-known eigenvalue equation

$$H_{\text{HO}}|n\rangle = \omega \left( n + \frac{1}{2} \right) |n\rangle, \quad (7.10)$$

with  $n$  an integer. If we consider now  $x$  as transition operator, it connects the ground state only with the first excited state, that is

$$\langle 0|x|n\rangle = \frac{1}{\sqrt{2m\omega}} \delta_{n,1}. \quad (7.11)$$

The EWSR for this operator is therefore

$$S_1 = \sum_n n\omega |\langle 0|x|n\rangle|^2 = \frac{1}{2m}, \quad (7.12)$$

so that even in the limit  $\omega \rightarrow 0$ , the contribution to the sum rule is still finite, as the transition strength in Eq. (7.11) goes to infinity. (Note the similarity with the TRK sum rule for the dipole operator, where also one obtains a constant value for  $S_1$ .) That is exactly what is happening in RPA, for as noted in Chapter 4, RPA describes small oscillations about the mean-field solution, treating the energy surface around the HF minimum as a harmonic oscillator.

Rowe (in section 14.5 of [12]) points out that when applying RPA to deformed nuclei one “necessarily makes a distinction between excitations which are *intrinsic* and those which are *rotational*.” (Italics in original.) The missing RPA strength is almost certainly associated with a  $0^+ \rightarrow 2^+$  transition in the ground-state rotational band and not described by the RPA vibrations. Instead, the rotational wave functions should be described by Wigner  $D$ -functions, as in geometric collective models [10, 12, 144, 145]. It would be illuminating to express the remainder of Eq. (7.4) in terms of rotational transitions, but it appears complicated in the RPA framework and we leave it for future work.

With this in mind, we can reconsider the results in Table 7.1. For nuclei with spherical HF states, that is, no zero modes, the RPA  $S_1$  and the HF value are identical; this is the usual theorem regarding the energy-weighted sum rule. For nuclei with deformed HF states, and thus with zero modes, the RPA and HF values differ, a small amount for isovector  $E2$  and

---

<sup>1</sup>The author thanks B. K. Jennings (TRIUMF–Vancouver, Canada) for suggesting this example.

dramatically for isoscalar  $E2$ . Interestingly enough, there is no discrepancy for transitions with a  $\Delta J = 1$  character, such as SF or GT. This bolsters the picture of the missing strength residing in the ground state rotational band, which has only  $J = 0, 2, 4, \dots$  states. Overall these results are consistent with our hypothesis that low-lying strength is subsumed into the RPA ground state (which retains the intrinsic-state nature of the HF state); the difference is larger for isoscalar  $E2$  because of the large strength at low energy.

We find numerically that the discrepancy in Table 7.1 is given exactly by the last term in Eq. (7.4). Our *interpretation* of Table 7.1 and Eq. (7.4) is missing strength that goes into ground-state to ground-state transitions, due to incomplete symmetry restoration. We bring more arguments to support this hypothesis in the next sections.

## 7.2 Symmetry Restoration

The random phase approximation respects broken symmetries by exactly separating out spurious motion as zero modes. This is sometimes interpreted as an “approximate restoration of the symmetry” [10]. The restoration cannot be exact, because the RPA wave function is valid only in the vicinity of the HF state [17] and cannot be extrapolated to, for example, large rotation angles. In this section we investigate in detail the results for the total angular momentum ground-state expectation value and for low-lying collectivity, bringing evidence that they can be interpreted as incomplete symmetry restoration in the ground state.

### 7.2.1 Observables

Equation (4.68) provides a tool to further explore symmetry restoration, by computing Casimir operators of symmetry groups. Specifically, we consider  $\langle J^2 \rangle$ . Ideally, if the RPA restores a broken symmetry, one might imagine that one either regains the exact ground state value of  $\langle J^2 \rangle$  or gets very close to it.

We presented our results in Table 6.5. The pattern is the same as with other operators:  $\langle J^2 \rangle$  is generally better in RPA than in HF but not always very close to the exact shell-model value. Even worse are the cases with a closed shell in HF, such as  $^{22,24}\text{O}$ : the HF value is correct, while the RPA value is terrible!

To examine this issue more closely, in Fig. 7.1 we again plot, for  $^{28}\text{Si}$ ,  $\langle J^2 \rangle$  versus the  $d_{5/2}$  single-particle energy through the transition from deformed to spherical HF state. The results are better for the deformed HF state, although we obtain slightly negative, and thus nonphysical, values of  $\langle J^2 \rangle$ .

Calculation of  $\langle J^2 \rangle$  is not necessarily the only test of restoration of symmetry. One would also expect, for nuclides with  $J = 0$  ground states, that  $\langle J_i \rangle = 0, i = x, y, z$ . This will be an important test of the restoration of symmetry, but as  $J_i$  is a non-scalar observable it is beyond the scope of the present paper. Note, however, that for even-even nuclides,  $\langle J_i \rangle = 0$  for the HF state due to time-reversal invariance. The question then becomes whether or not for deformed states the RPA corrections to  $\langle J_i \rangle$  are also zero. In the near future we will

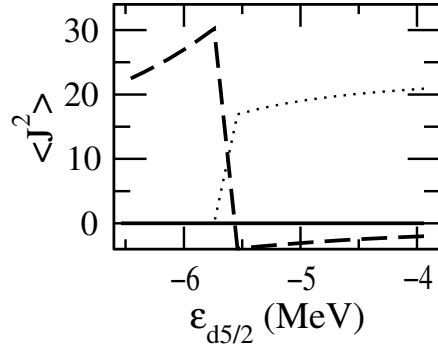


Figure 7.1:  $\langle J^2 \rangle$  in  $^{28}\text{Si}$  as the  $d_{5/2}$  single-particle energy is lowered relative to the other single-particle energies. The solid line is the (exact) shell-model value, the dotted line the HF value, and the dashed line the RPA value.

perform these calculations as evidence for or against the restoration of rotational symmetry in the RPA.

An additional test of symmetry restoration would be computation of the expectation value of other non-scalar observables, such as the magnetic dipole moment or electric quadrupole moment, for a deformed nucleus with a  $J = 0$  shell-model ground state. Marshalek and Weneser [17] discuss expectation values for electric quadrupole and magnetic moments, but their approach is not very transparent for general implementation; moreover, they specialize their discussion to a tensor operator, which restricts applicability to breaking of rotational symmetry. Most discussions of the RPA do not give a well-defined procedure to calculate ground-state to ground-state transitions, in part because they vanish when the Hartree-Fock state has spherical symmetry.

## 7.2.2 Transitions

Another means for investigating the symmetry restoration is the ability of RPA to describe transitions. If RPA does not fully restore broken symmetries, a significant contribution to the total strength could be absorbed into otherwise forbidden g.s. to g.s. transitions. We presented the results for low-lying collectivity in Sec. 6.3.2, and indeed we found that significant strength to excited states can be missing for even-even nuclides. Here we provide further evidence supporting our hypothesis that the low-lying collective strength is missing due to incomplete symmetry restoration in the RPA, and a significant fraction of the RPA strength gets absorbed in a ground state to ground state transition.

Our first test of incomplete symmetry restoration is the comparison of the transition strength for spherical and deformed HF solutions. While the proton-neutron interaction induces deformation in the HF Slater determinant for  $^{28}\text{Si}$ , we saw previously that it is possible to force a transition to a spherical HF state (both protons and neutrons filling the  $d_{5/2}$  orbits) by increasing the gap between the  $d_{5/2}$  single particle energy and the other single-particle states. The calculations reported in Chapter 6 for  $^{28}\text{Si}$  use the USD value of

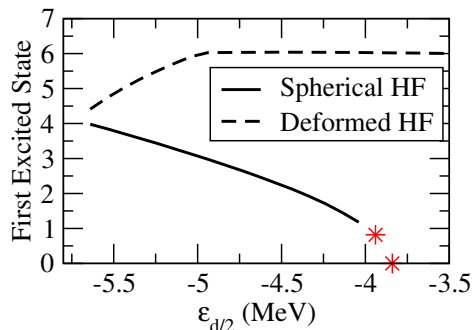


Figure 7.2:  $^{28}\text{Si}$ : first RPA excited states for both deformed and spherical HF solutions. The left red star is for the Wildenthal value  $\epsilon_{d_{5/2}} = -3.94$  MeV, while the right one is for a collapsing spherical solution.

$\epsilon(d_{5/2}) = -3.94$  MeV, which yields a deformed HF state. In addition we computed  $^{28}\text{Si}$  at  $\epsilon(d_{5/2}) = -5.64$  MeV and  $-5.74$  MeV. At  $-5.64$  MeV the HF state is still deformed while at  $-5.74$  MeV the HF state is spherical. Actually, for these values of  $\epsilon(d_{5/2})$  there exist both spherical and deformed locally stable HF solutions, but at  $-5.64$  MeV the deformed state has a slightly lower HF energy while at  $-5.74$  MeV the spherical state has the lowest HF energy. Thus this is a first order ‘phase transition’ as described in section 4 of [18]. We illustrate this in Fig. 7.2, where we plot the first RPA excited state for the deformed and spherical mean field. (in the case of the axially deformed HF, this is actually the third RPA frequency, as the first two modes are zero, identifying the generators of broken symmetries). The so-called collapse or breakdown of RPA, readily seen in toy models such as the Lipkin model [10], only occurs when one has a second order ‘phase transition,’ when one has only one stable HF solution. In other words, our RPA calculations do not collapse at the transition point.

Figure 7.3 shows small difference in the SM strength distribution in contrast with a dramatic change for RPA [19]. The difference between the  $d_{5/2}$  single-particle energies in the two cases is small and one can follow a smooth change for all observables in the SM; we have therefore no reason to suspect any fundamental difference in the structure of the states. Note however that, when the HF state is spherical, the low lying states are correctly described in the RPA, the reason why the RPA was successful in describing low lying collectivity in closed shell nuclei; but note also that the high-lying part of the strength is not correctly described. In contrast, when the HF state is deformed, the RPA strength distribution changes dramatically, even though the SM strength distribution does not: the low-lying strength vanishes, but the high-lying strength is approximately correct.

As a second test, we compare the total strength  $S_0$  computed in different ways. Table 7.2 presents the total strength  $S_0$  for a transition operator  $F$ , where  $F$  is either the spin-flip operator or isoscalar  $E2$  operator. The columns labeled ‘SM’ are the exact shell model results, for which  $S_0 = \langle 0|F^\dagger F|0\rangle = \sum_\nu |\langle \nu|F|0\rangle|^2$  [19]. Of course, for the shell model both methods yield the same result. The columns RPA-X and RPA- $\Sigma$  correspond to equivalent methods for the RPA. RPA-X is the expectation value  $\langle \text{RPA}|F^\dagger F|\text{RPA}\rangle$  as laid out in Sec. 6.2, where

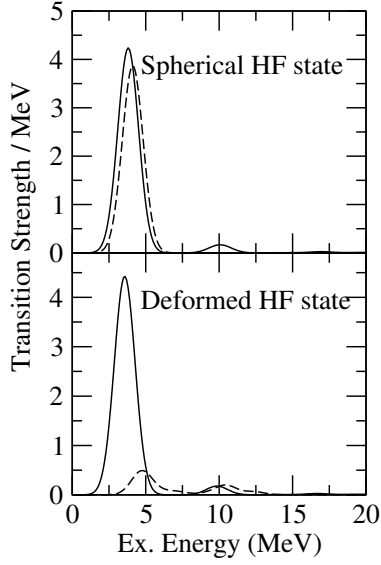


Figure 7.3:  $^{28}\text{Si}$ : Isoscalar  $E2$  for deformed and spherical HF state.

Table 7.2: Comparison of the total strength  $S_0$  as computed in the shell model (SM), by taking the expectation value of an observable (RPA-X), and by summing the RPA strengths directly (RPA- $\Sigma$ ); see text for more details. The horizontal lines separate even-even deformed nuclei, even-even spherical nuclei, odd-odd and odd-A. Notation on  $^{28}\text{Si}$ :  $\dagger$  indicates  $\varepsilon_{d5/2} = -5.74$  MeV and a spherical HF state.

Nucleus	SF			Isoscalar $E2$		
	SM	RPA-X	RPA- $\Sigma$	SM	RPA-X	RPA- $\Sigma$
$^{20}\text{Ne}$	1.05	1.34	1.23	7.86	8.17	0.19
$^{22}\text{Ne}$	3.52	1.94	4.44	9.36	9.98	0.89
$^{24}\text{Mg}$	4.15	5.53	4.78	12.57	12.52	0.51
$^{36}\text{Ar}$	2.68	2.90	2.70	7.17	7.66	0.23
$^{28}\text{Si}$	5.82	5.13	5.20	12.04	13.77	0.56
$^{28}\text{Si}^\dagger$	9.07	-5.22	12.53	7.95	7.50	6.86
$^{22}\text{O}$	5.04	-0.60	6.31	2.71	2.75	2.36
$^{24}\text{O}$	5.17	-1.07	6.24	1.88	1.92	1.57
$^{22}\text{Na}$	8.57	7.64	5.78	9.53	9.92	7.49
$^{24}\text{Na}$	10.06	6.97	7.66	8.81	9.61	6.33
$^{21}\text{Ne}$	4.02	1.77	3.54	8.74	8.69	13.27
$^{25}\text{Mg}$	6.94	1.52	6.33	10.71	12.34	12.49
$^{29}\text{Si}$	8.42	5.77	8.47	9.70	11.67	1.38

we showed that the RPA expectation value was often a reasonable approximation to the shell model result, though not always as seen for some of the spin-flip cases.  $\text{RPA-}\Sigma$  is the sum  $\sum_{\nu} |\langle \nu | F | \text{RPA} \rangle|^2$ , where the sum is only to excited states as g.s.-to-g.s. transitions are difficult to define in RPA.

The horizontal lines in Table 7.2 segregate even-even nuclei with deformed HF states, even-even spherical nuclei, odd-odd nuclei, and odd-A nuclei. Keep in mind that for the latter two groups we do not get all the true zero modes (because we restricted the Slater determinant to real single-particle wave functions), but at least one zero mode is replaced by a soft mode, except for the case of  $^{29}\text{Si}$  which does have all the expected zero modes.

What do we learn from Table 7.2? We draw the reader's attention to the isoscalar  $E2$  strength in deformed even-even-nuclides, and in  $^{29}\text{Si}$ , all of which have the expected number of exact zero modes. Here the summed RPA strength ( $\text{RPA-}\Sigma$ ) is dramatically and consistently smaller than either the exact SM result, or the expectation value  $\text{RPA-X}$ . By way of contrast, the nuclides with spherical HF states and thus no zero modes, or those who have soft modes rather than zero modes, have summed RPA strength in reasonable accord with the SM total strength. Furthermore the RPA expectation value of  $Q \cdot Q$  also agrees with the SM total strength, which suggests to us that some of the missing RPA strength is in g.s. to g.s. transitions. This line of reasoning is weakened by the poor reliability of the RPA expectation value, as discussed in Sec. 6.2 and as seen in the spin-flip values, which take on unphysical negative values for spherical nuclei.

## 8 Conclusions

We have investigated the accuracy of HF+RPA for computing the nuclear binding energies, ground-state expectation values, and transition strengths, by comparing against the exact results obtained through full  $0\hbar\omega$  diagonalization. Although we made these calculations for stable, light-to-medium nuclides, we are ultimately interested in the applicability to heavy and far-from-stability nuclides.

In simpler models [14, 15, 146], the RPA binding energy is generally, but not always [147], satisfactory. We found this also to be true with our significantly more complicated shell-model Hamiltonians. Moreover, we investigated a couple of basic assumptions in RPA, but found no correlation between their accuracy and RPA's ability to estimate the exact correlation energy. Because of this, we cannot point to a faulty approximation whose correction would improve significantly the results.

As outlined in the introduction, the binding energies are not the only quantities a global microscopic theory should predict. Therefore, we derived an expression, i.e., Eq. (4.68), for the ground-state expectation value of observables in the matrix formulation of RPA, using the quasi-boson approximation, and tested it against exact shell-model calculations for selected scalar operators. The RPA value was in general an improvement over the Hartree-Fock value, but failed to be a consistent and reliable estimate of the exact expectation value.

In particular we considered the expectation value of  $J^2$ . If one starts with a deformed Hartree-Fock state, which breaks rotational invariance, the RPA approximately restores rotational symmetry, as evinced by better values of  $\langle J^2 \rangle$ . The results are not wholly satisfactory, however, as  $\langle J^2 \rangle$  can take on unphysical (negative) values; furthermore, if one starts from a Hartree-Fock state with good symmetry, the HF value of  $\langle J^2 \rangle$  is correct while the RPA value is large and positive, a disappointing result. Thus, while the RPA *respects* or identifies broken symmetries exactly, one can only characterize the *restoration* of symmetry in the RPA as approximate and somewhat unreliable.

The comparison between RPA and SM for transition strengths showed two different results, depending upon the nature of transitions. Thus, we found that when the strong collectivity lies at high energies, such as isovector  $E2$ , SF and GT transitions, the RPA and SM are in reasonable agreement. When the transitions lie at low energies however, the agreement is poor.

We presented further evidence that the problem arises from an incomplete restoration of the symmetries broken by the mean-field; for low-lying transitions we propose that significant part of the transition strength is subsumed into the RPA ground state, and should

be interpreted as transitions within the ground-state rotational band. Future work should directly investigate ground-state to ground-state transitions in the RPA. (These are also needed for ground state moments, such as magnetic dipole or electric quadrupole, of odd- $A$  nuclides.) Undoubtedly more work remains, but we hope our results act to inspire further careful investigation. For example, for some transition operators there is no or very small contribution from the zero modes even for nuclides with deformed HF states; this seems to be associated with transitions with high-lying giant resonances, again consistent with our interpretation of incomplete restoration of symmetries and *low-lying* strength being subsumed into the RPA ground state.

It was long believed [10, 18] that RPA “preserves” exactly the energy weighted sum rule, that is Eq. (7.1). We have revisited the derivation and found out that, if symmetries are broken in the HF solution, the energy weighted sum rule is violated. We calculated correction terms which arise from zero modes, associated with the generators of broken symmetries. And since we can show explicitly that the ‘zero excitation energies’ contribute to the energy weighted sum rule, identifying real transitions in the rotational band, we consider this as further evidence that the symmetries are not restored in RPA.

In this work we have considered only broken rotational symmetry. One should however further investigate consequences of other broken symmetries, such as translational or particle number conservation. In such cases, non zero contributions to the energy-weighted sum rule could be hardly identified as special transitions as noted for rotations, and would be further evidence for RPA’s inability to restore symmetries. Allowing for translational symmetry violation is a very difficult task for SM calculations, as spurious center of mass excitations, which would appear in these cases, mix with the physical ones.

As an overall conclusion, the results presented in this work indicate that the mean-field corrected through the random phase approximation cannot be used as a microscopic theory for global accurate predictions of the nuclear properties. So, how could one make RPA more reliable? There are two obvious steps. The first is to attempt to build pairing directly into the mean-field state through Hartree-Fock-Bogoliubov and then computing the QRPA correlations energy. Removing explicit pairing matrix elements does not improve the performance of HF+RPA, however, and because we found no relation between the accurate calculation of the expectation value of the pairing Hamiltonian and the accurate calculation of the total binding energy, we are far from confident that HFB+QRPA will yield significant gains.

The other possibility is to correct RPA for its violation of the Pauli principle as well as using the RPA ground state wave function function in computing  $\mathbf{A}$  and  $\mathbf{B}$  matrices in equations (4.10) and (4.11). The literature documents numerous proposals along these lines: self-consistent renormalization of the mean-field single-particle energies and the residual interaction [81, 148]; treating the particle-hole amplitudes as variational parameters [149]; rederivation of the RPA equations via the “number-operator method” to account for ground state correlations [150]; and dressing the RPA phonons to account for ground state correlations [151]. None of these methods have become widely accepted, and they overlap each other to a large degree, although the literature does not clarify similarities and differences;

the second RPA, which has been shown to differ significantly from the standard RPA in its description of  $E2$  giant resonances of  $^{16}\text{O}$  [152]. As in the case of unadorned RPA, most of these proposals for improving RPA have only been tested against toys such as the Lipkin model [84]. Perhaps by implementing these various proposals for full-scale shell model calculations one could compare their efficacy and practicality.

# Bibliography

- [1] Donald D. Clayton, *Principles of Stellar Evolution and Nucleosynthesis* (The University of Chicago Press, Chicago 1983).
- [2] S. E. Woosley, A. Heger, and T. A. Weaver, *Rev. Mod. Phys.* **74**, 1015 (2002).
- [3] K. Langanke and G. Martínez-Pinedo, *Rev. Mod. Phys.* **75**, 819 (2003).
- [4] I. Hamamoto and X. Z. Zhang, *Phys. Rev. C* **52**, R2326 (1995).
- [5] J. Dobaczewski, W. Nazarewicz, and T. R. Werner, *Z. Phys. A* **354**, 27 (1996).
- [6] G. A. Lalazissis et. al., *Nucl. Phys.* **A632**, 363 (1998).
- [7] H. Sagawa, *Phys. Lett. B* **286**, 7 (1992).
- [8] S. Takahara, N. Onishi, and N. Tajima, *Phys. Lett. B* **331**, 261 (1994).
- [9] P. G. et. al., *Annu. Rev. Nucl. Part. Sci.* **45**, 591 (1995).
- [10] P. Ring and P. Shuck, *The Nuclear Many-Body Problem*, 1st ed. (Springer-Verlag, New York 1980).
- [11] Kris L. G. Heyde, *The nuclear shell model* (Springer-Verlag, Berlin, 1990).
- [12] D. J. Rowe, *Nuclear Collective Motion* (Methuen and Co. Ltd., London 1970).
- [13] C. W. Johnson and I. Stetcu, *Phys. Rev. C* **66**, 064304 (2002).
- [14] K. Hagino and G. F. Bertsch, *Phys. Rev. C* **61**, 024307 (2000).
- [15] K. Hagino and G. F. Bertsch, *Nucl. Phys.* **A679** 163 (2000).
- [16] I. Stetcu and C. W. Johnson, *Phys. Rev. C* **66**, 034301 (2002).
- [17] E. R. Marshalek and J. Weneser, *Ann. Phys. (N.Y.)* **53**, 569 (1969).
- [18] D. J. Thouless, *Nucl. Phys.* **22**, 78 (1961).
- [19] I. Stetcu and C. W. Johnson, *Phys. Rev. C* **67**, 044315 (2003).

- [20] W. C. Haxton, *Nuclear Problems in Astrophysics*, arXiv:nucl-th/0301005 (2003).
- [21] R. G. Couch, A. B. Schmiedekamp, and W. D. Arnett, *Astrophys. J.* **190**, 95 (1974); F. Käapler *et. al.*, *Astrophys. J.* **437**, 396 (1994).
- [22] E. Baron, J. Cooperstein, and S. Kahana, *Phys. Rev. Lett.* **55**, 126 (1985).
- [23] E. Baron H. A. Bethe, G. E. Brown, J. Cooperstein, and S. Kahana, *Phys. Rev. Lett.* **59**, 736 (1987).
- [24] S. W. Bruenn, *Astrophys. J.* **340**, 955 (1989); *ibid.* **341**, 385 (1989).
- [25] E. S. Myra and S. A. Buldman, *Astrophys. J.* **340**, 384 (1989).
- [26] E. Baron and J. Cooperstein, *Astrophys. J.* **353**, 597 (1990).
- [27] S. A. Colgate and R. H. White, *Astrophys. J.* **143**, 626 (1966).
- [28] H. A. Bethe and J. R. Wilson *Astrophys. J.* **295**, 14 (1985); H. A. Bethe, *Rev. Mod. Phys.* **62**, 801 (1990).
- [29] D. D. Clayton and M. E. Rassbach, *Astrophys. J.* **148**, 69 (1967).
- [30] C. Doll *et. al.*, *Phys. Rev. C* **59**, 492 (1999).
- [31] J. J. Conwan, F.-K. Thielemann, and J.W. Truran, *Phys. Rep.* **208**, 261 (1991).
- [32] J. Lattimer and D. N. Schramm, *Astrophys. J. , Lett. Ed.* **192**, 145 (1974); *ibidem* *Astrophys. J.* **210**, 549 (1976).
- [33] W. Hillebrandt and F.-K. Thielemann, *Mitt. Astron. Ges.* **43**, 234 (1978); J. Truran, J. J. Cowan, and A. G. W. Cameron, *Astrophys. J. , Lett. Ed.* **222**, L63 (1978).
- [34] S. E. Woosley *et. al.*, *Astrophys. J.* **433**, 229 (1994).
- [35] K. Langanke and G. Martínez-Pinedo, *Nucl. Phys.* **A704** 154c (2002).
- [36] T. Kajino, S. Wanajo, and G.J. Mathews, *Nucl. Phys.* **A704**, 165c (2002).
- [37] C. Sneden *et. al.*, *Astrophys. J.* **467**, 819 (1996); R. Cayrel *et. al.*, *Nature* **409** 691 (2001).
- [38] H. Schatz *et. al.*, *Phys. Rep.* **294**, 167 (1998).
- [39] T. D. Lee and C. N. Yang, *Phys. Rev.* **104**, 822 (1956).
- [40] C. S. Wu *et. al.*, *Phys. Rev.* **105**, 1413 (1957).
- [41] C. J. Horowitz *et. al.*, *Phys. Rev. C* **63**, 025501 (2001).

- [42] S. J. Pollock, E. N. Fortston, and L. Wilets, *Phys. Rev. C* **46**, 2587 (1992).
- [43] B. Q. Chen and P. Vogel, *Phys. Rev. C* **48**, 1392 (1993).
- [44] C. F. von Weizsäcker, *Z. Phys.* **96**, 431 (1935); H. A. Bethe and R. F. Cacher, *Rev. Mod. Phys.* **8**, 82 (1936).
- [45] C. Samanta and S. Adhikari, *Phys. Rev. C* **65**, 037301 (2002).
- [46] P. Möller, J. R. Nix, W. D. Myers and W. J. Swiatecki, *At. Data Nucl. Data Tables* **59**, 185 (1995).
- [47] P. Möller, J. R. Nix, and K.-L. Kratz, *At. Data Nucl. Data Tables* **66**, 131 (1997).
- [48] Z. Patyk et. al., *Phys. Rev. C* **59**, 704 (1999).
- [49] W. D. Myers and W. J. Swiatecki, *Nucl. Phys.* **A601**, 141 (1996).
- [50] Y. Aboussir, J. M. Pearson, A. K. Dutta, and F. Tondeur, *Nucl. Phys.* **A549**, 155 (1992); *At. Data Nucl. Data Tables* **61**, 127 (1995).
- [51] H. de Vries, C. W. de Jager, and C. de Vries, *At. Data Nucl. Data Tables*, **36**, 495 (1987).
- [52] T.H. Skyrme, *Philos. Mag.* **1**, 1043 (1965).
- [53] D. M. Brink and E. Boeker, *Nucl. Phys. A* **91**, 1 (1967).
- [54] D. Gogny, *Proceedings of the International Conference on Nuclear Physics*, edited by J. de Boer, and H. J. Mang (North Holland, Amsterdam, 1973), p. 48.
- [55] O. Bohigas and P. Leboeuf, *Phys. Rev. Lett.* **88**, 092502 (2002).
- [56] G. A. Lalazissis, D. Vretenar, and P. Ring, *Phys. Rev. C* **60**, 051302 (2002).
- [57] J. Dufflo and A. P. Zuker, *Phys. Rev. C* **52**, R23 (1995).
- [58] L. Pauling and E. B. Wilson Jr., *Introduction to quantum mechanics: with applications to chemistry* (McGraw-Hill, London, 1935).
- [59] O. Haxtel, J. H. D. Jensen, and H. E. Suess, *Phys. Rev.* **75**, 1766 (1949).
- [60] M. G. Mayer, *Phys. Rev.* **75**, 1969 (1949).
- [61] R. R. Whitehead, A. Watt, B. J. Cole, and I. Morrison, *Adv. Nucl. Phys.* **9**, 123 (1977).
- [62] E. Caurier, computer code ANTOINE, CRN, Strasbourg, 1989 (unpublished); E. Caurier, A. P. Zuker, and A. Poves, in *Nuclear Structure of Light Nuclei Far from Stability*, Proceedings of the Obernai Workshop, 1989, edited by G. Koltz (CRN, Strasbourg, 1989).

- [63] W. E. Ormand (private communication).
- [64] A. Etchegoyen et al., MSU-NSCL Report No. 524, 1985.
- [65] J. P. Elliott, Proc. Roy. Soc. A **245**, 128 (1958).
- [66] B. A. Brown, W. A. Richter, R. E. Julies and B. H. Wildenthal, Ann. Phys. (N.Y.) **182**, 191 (1988).
- [67] A. R. Edmonds, *Angular Momentum in Quantum Mechanics* (Princeton University Press, Princeton, New Jersey, 1960).
- [68] R. R. Whitehead, in *Moment Methods in Many Fermion Systems*, edited by B. J. Dalton, S. M. Grimes, J. D. Vary, and S. A. Williams (Plenum, New York, 1980), p. 235.
- [69] E. Caurier, A. Poves, and A. P. Zuker, Phys. Lett. **B252**, 13 (1990); Phys. Rev. Lett **74**, 1517 (1995).
- [70] H. Feshbach, Ann. Phys. (N.Y.) **19**, 287 (1962).
- [71] T. T. S. Kuo, Ann. Rev. Nucl. Sci. **24**, 101 (1974).
- [72] B. H. Wildenthal, Prog. Part. Nucl. Phys. **11**, 5 (1984).
- [73] T. T. S. Kuo and G. E. Brown, Nucl. Phys. **A114**, 235 (1968); A. Poves and A. P. Zuker, Phys. Rep. **70**, 235 (1981).
- [74] P. Navrátil and B. R. Barrett, Phys. Rev. C **57**, 562 (1998); *ibidem* Phys. Rev. C **59**, 1906 (1999).
- [75] P. Navrátil, G. P. Kamuntacičius, and B. R. Barrett, Phys. Rev. C **61**, 044001 (2000).
- [76] P. Navrátil and W. E. Ormand, Phys. Rev. Lett. **87**, 172502 (2001).
- [77] S. C. Pieper, K. Varga, and R. B. Wiringa, Phys. Rev. C **66**, 044310 (2002).
- [78] A.C. Hayes, P. Navrátil, and J. P. Vary, *Neutrino-<sup>12</sup>C scattering in the ab initio shell model calculations with a realistic three-body interaction*, arXiv:nucl-th/0305072 (2003).
- [79] D. J. Thouless, Nucl. Phys. **21**, 225 (1960).
- [80] W. H. Press, S. A. Teukolsky, W. T. Vetterling, and B. P. Flannery, *Numerical Recipes in FORTRAN; The Art of Scientific Computing*, 2nd ed. (Cambridge University Press, Cambridge 1986).
- [81] D. J. Rowe, Rev. Mod. Phys. **40**, 153 (1968).
- [82] Y. R. Shimizu, P. Donnati and R. A. Brogna, Phys. Rev. Lett. **85**, 2260 (2000).

- [83] G. E. Brown and M. Bosterli, Phys. Rev. Lett. **3**, 427 (1959).
- [84] H. J. Lipkin, N. Meshkov, and A. J. Glick, Nucl. Phys. **62**, 188 (1965).
- [85] K. Goeke and J. Speth, Annu. Rev. Nucl. Part. Sci. **32**, 65 (1982).
- [86] D. Gogny (private communication).
- [87] P. Quentin and H. Flocard, Annu. Rev. Nucl. Part. Sci. **28**, 523 (1978).
- [88] A. B. Migdal, *Theory of Finite Fermi Systems* (Wiley, New York 1967).
- [89] K. F. Liu and G. E. Brown, Nucl. Phys. **A265**, 385 (1976).
- [90] J. Friedrich and P.-G. Reinhard, Phys. Rev. C **33**, 335 (1986).
- [91] I. M. Green and S. A. Moszkowski, Phys. Rev. **139**, B790 (1965).
- [92] L. S. Kisslinger and R. A. Sorensen, Rev. Mod. Phys. **35**, 853 (1963).
- [93] A. Faessler and A. Plastino, Nucl. Phys. **A94**, 580 (1967).
- [94] V. O. Nesterenko, W. Kleinig, V. V. Gudkov, and J. Kvasil, Phys. Rev. C **53**, 1632 (1996).
- [95] J. Terasaki, J. Engel, W. Nazarewicz, and M. Stoitsov, Phys. Rev. C **66**, 054313 (2002).
- [96] D. Almeded, F. Donau, and R. G. Nazmitdinov, Phys. At. Nucl. **64**, 1080 (2002).
- [97] J.U. Nabi and H.V. Klapdor-Kleingrothaus, Acta Phys. Polonica **B 30**, 825 (1999);  
Atom. Data Nucl. Data **71**, 149 (1999).
- [98] H. Homma, E. Bender, M. Hirsch, K. Muto, H. V. Klapdor-Kleingrothaus, T. Oda,  
Phys. Rev. C **54**, 2972 (1996).
- [99] C. W. Johnson, B. F. Bertsch, D. J. Dean and I. Talmi, Phys. Rev. C **61**, 014311  
(2000); I. Stetcu, *Investigation of effective interaction in the sd shell*, Louisiana State  
University, Department of Physics and Astronomy, final report for course PHYS 7996  
(unpublished).
- [100] A. Kallio and K. Kolltveit, Nucl. Phys. **53**, 87 (1964).
- [101] V. Gillet and N. Vin Mau, Nucl. Phys. **54**, 321 (1964).
- [102] V. Gillet, A. M. Green, and E. A. Sanderson, Nucl. Phys. **88**, 321 (1964).
- [103] J. P. Blaizot and D. Gogny, Nucl. Phys. **A284**, 429 (1977).
- [104] T. T. S. Kuo, J. Blomqvist, and G. E. Brown, Phys. Lett. **31B**, 93 (1970).

- [105] N. Ullah and D. J. Rowe, Phys. Rev. **188**, 1640 (1969).
- [106] J. Blomqvist and T. T. Kuo, Phys. Lett. **29B**, 544 (1969).
- [107] W. W. True, C. W. Ma, and W. T. Pinkston, Phys. Rev. C **3**, 2421 (1971).
- [108] G. F. Bertsch and S. F. Tsai, Phys. Rep. **18**, 125 (1975).
- [109] J. E. Wise et. al, Phys. Rev. C **31**, 1699 (1985).
- [110] K. F. Liu and N. van Giai, Phys. Lett **65B**, 23 (1976).
- [111] D. J. Rowe and S. S. M. Wong, Phys. Lett. **30B**, 147 (1969).
- [112] D. J. Rowe and S. S. M. Wong, Nucl. Phys. **A153**, 561 (1970).
- [113] G. Coló, P. F. Bortignon, N. Van Giai, A. Bracco, and R. A. Broglia, Phys. Lett. **B276**, 279 (1992).
- [114] M. L. Gorelik, S. Shlomo, and M. H. Urin, Phys. Rev. C **62**, 044301 (2000).
- [115] S. Stringari, Phys. Rev. C **29**, 1482 (1984).
- [116] V. A. Rodin and M. H. Rodin, Phys. Rev. C **62**, 067601 (2000).
- [117] M. L. Gorelik and U. H. Urin, Phys. Rev. C **64**, 047301 (2001).
- [118] S. Shlomo and A. I. Sanzhur, Phys. Rev. C **65**, 044310 (2002).
- [119] G. Colò, N. Van Giai, P. F. Bortignon, and M. R. Quaglia, Phys. Lett. **B485**, 362 (2000).
- [120] V. Gillet and M. A. Melkanoff, Phys. Rev. **133**, B1190 (1964).
- [121] S. G. Nilsson, J. Sawicki, and N. K. Glendemming, Nucl. Phys. **33**, 239 (1960).
- [122] A. M. Oros, K. Heyde, C. De Coster, and B. Decroix, Phys. Rev. C **57**, 990 (1988).
- [123] S. P. Kamedzhiev, R. J. Liotta, and V. I. Tselyaev, Phys. Rev. C **63**, 034304 (2001)
- [124] S.M. Grimes et. al, Phys. Rev. C **53**, 2709 (1996).
- [125] M. C. Etterli et. al., Phys. Rev. C **45**, 997 (1995).
- [126] M. K. Cheoun, A. Faessler, F. Simkovic, G. Teneva, and A. Bobik, Nucl. Phys. **A587**, 301 (1995).
- [127] K. Junker, V. A. Kuzmín, and T. V. Tetereva, Eur. Phys. J. A **5**, 37 (1999).
- [128] A. Krasznahorkay et. al., Phys. Rev. C **64**, 067302 (2001).

- [129] P. Sarriguren, E. M. de Guerra, and R. Alvarez-Rodriguez, Nucl. Phys. **A716**, 230 (2003).
- [130] W. E. Ormand, D. J. Dean, C. W. Johnson, G. H. Lang, and S. E. Koonin, Phys. Rev. C **49**, 1422 (1994).
- [131] D. J. Rowe, Phys. Rev. **175**, 1283 (1968).
- [132] J. K. Parikh, Phys. Rev. C **8**, 1433 (1973); E. Tinková and M. Gmitro, Phys. Rev. C **14**, 1213 (1976).
- [133] G. E. Brown and A. M. Green, Nucl. Phys. **75**, 401 (1966); W.C. Haxton and C. W. Johnson, Phys. Rev. Lett. **65**, 1325 (1990); E. K. Warburton, B. A. Brown, and D. J. Millener, Phys. Lett. **B293**, 7 (1992).
- [134] V.G. Soloviev, A.V. Sushkov, N.Yu. Shirikova, and N.Lo Iudice, J. Phys. G **25**, 1023 (1999); N. Lo Iudice, A.V. Sushkov, and N. Y. Shirikova, Phys. Rev. C **64**, 054301 (2001).
- [135] I. Hamamoto, H. Sagawa, and X.Z. Zhang, Phys. Rev. C **55**, 2361 (1997); Phys. Rev. C **56**, 3121 (1997); P. Urkedal, X.Z. Zhang, and I. Hamamoto, Phys. Rev. C **64**, 054304 (2001).
- [136] O. Civitarese and M. Reboiro, Phys. Rev. C **57**, 3062 (1998).
- [137] S. Stoica, I. Mihut, and J. Suhonen, Phys. Rev. C **64**, 017303 (2001).
- [138] J. Engel, S. Pittel, M. Stoitsov, P. Vogel, and J. Dukelsky, Phys. Rev. C **55**, 1781 (1997).
- [139] B. Lauritzen, Nucl. Phys. **A489**, 237 (1998).
- [140] O. Civitarese, H. Müller, L. D. Skouras, and A. Faessler, J. Phys. G. **17**, 1363 (1991).
- [141] L. Zhao and B. A. Brown, Phys. Rev. C **47**, 2641 (1993).
- [142] N. Auerbach, G. F. Bertsch, B. A. Brown, and L. Zhao, Nucl. Phys. **A556**, 190 (1993).
- [143] G.F. Bertsch and K. Hagino, Phys. Atom. Nucl. **64**,588 (2001) [arXiv:nucl-th/0006032]
- [144] A. Bohr and B. Mottelson, *Nuclear Structure, Vol. II: Nuclear Deformations* (W.A. Benjamin, New York, 1969).
- [145] J. M. Eisenberg and W. Greiner, *Nuclear Models: Collective and Single-Particle Phenomena* (North-Holland, Amsterdam, 1975).
- [146] J.C. Parikh and D.J. Rowe, Phys. Rev. **175**, 1293 (1968).

- [147] N. Ullah and D.J. Rowe, Phys. Rev. **188**, 1640 (1969).
- [148] P. Schuck and S. Ethofer, Nucl. Phys. **A212**, 269 (1973).
- [149] R. M. Dreizler, A. Klein, F.R. Krejs and G.J. Dreiss, Nucl. Phys. **A166**, 624 (1971).
- [150] A. Klein, N. R. Walet and G. Do Dang, Nucl. Phys. **A535**, 1 (1991).
- [151] N. Dinh Dang and V. Zelevinsky, Phys. Rev. C **64**, 064319 (2001).
- [152] M. Tohyama, Phys. Rev. C **58**, 2603 (1998).

# Appendix A: Transition Operators

In this Appendix, we review the theory relevant to transition operators. The general form of a single-particle transition operator is [10, 11]

$$\begin{aligned} F(JM, TT_z) &= \sum_{\alpha\beta} \langle \alpha | F(JM, TT_z) | \beta \rangle a_\alpha^\dagger a_\beta \\ &= \frac{1}{\sqrt{(2J+1)(2T+1)}} \sum_{\alpha,\beta} \langle \alpha j_\alpha t_\alpha ||| F_{JT} ||| \beta j_\beta t_\beta \rangle [a_\alpha^\dagger \otimes \tilde{a}_\beta]_{JJ_z; TT_z}, \end{aligned} \quad (\text{A.1})$$

where  $a_\alpha^\dagger(a_\beta)$  is the fermion creation (annihilation) operator for *single-particle*  $\alpha(\beta)$ , and  $\tilde{a}_{\alpha(j_\alpha, m_\alpha; t_\alpha, t_\alpha^z)}$  is the time reversed annihilation operator,

$$\tilde{a}_{\alpha(j_\alpha, m_\alpha; t_\alpha, t_\alpha^z)} = (-1)^{j_\alpha - m_\alpha} (-1)^{t_\alpha - t_\alpha^z} a_{\alpha(j_\alpha, -m_\alpha; t_\alpha, -t_\alpha^z)}.$$

The eigenstates of a general nuclear Hamiltonian are also eigenstates for total angular momentum  $J$  and total isospin, which allows removing the angular dependence from calculations by means of the Wigner-Echart theorem,

$$\begin{aligned} \langle i; J_i M_i, T_i T_i^z | F(J J_z; T T_z) | f; J_f M_f, T_f T_f^z \rangle &= \\ (-1)^{J_i - M_i} \begin{pmatrix} J_i & J & J_f \\ M_i & -M & M_f \end{pmatrix} (-1)^{T_i - T_i^z} \begin{pmatrix} T_i & T & T_f \\ T_i^z & -T_z & T_f^z \end{pmatrix} \\ \times \langle i; J_i T_i ||| F(J J_z; T T_z) ||| f; J_f T_f \rangle. \end{aligned} \quad (\text{A.2})$$

Using Eq. (A.1), the double reduced matrix element in the last equation becomes

$$\langle i; J_i T_i ||| F_{JT} ||| f; J_f T_f \rangle = \sum_{\alpha,\beta} \rho_{\beta\alpha}(JT) \langle \alpha; j_\alpha t_\alpha ||| F_{JT} ||| \beta; j_\beta t_\beta \rangle, \quad (\text{A.3})$$

with  $\rho_{\beta\alpha}(JT)$  the reduced one-body density given by

$$\rho_{\beta\alpha}(JT) = \frac{\langle i; J_i T_i ||| [a_\alpha^\dagger \otimes \tilde{a}_\beta]_{JT} ||| f; J_f T_f \rangle}{\sqrt{(2J+1)(2T+1)}}. \quad (\text{A.4})$$

Eq. (A.3) allows computation of the transition strengths between any two states for any tensor operator of order  $J$ , the three- $j$  symbols in (A.2) imposing the selection rules. The

only ingredients that have to be calculated using the initial and final eigenstates, i.e., shell model wave functions, are the reduced single-particle densities in Eq. (A.4).

Before ending this brief appendix, we define the isoscalar and isovector components of transition operators, as most textbooks elude a clear discussion. We start from an equivalent definition of the multipole operator, which segregates explicitly the contributions from protons and neutrons:

$$F(JM) = \sum_{\alpha\beta} \langle \alpha | F_p(JM) | \beta \rangle \pi_\alpha^\dagger \pi_\beta + \sum_{\alpha\beta} \langle \alpha | F_n(JM) | \beta \rangle \nu_\alpha^\dagger \nu_\beta. \quad (\text{A.5})$$

In the single-particle spaces used in this work, the protons and neutrons have identical orbits, so that the only difference between the matrix elements of the transition operators are the (effective) charges,

$$\frac{1}{\tilde{e}_p} \langle \alpha | F_p(JM) | \beta \rangle = \frac{1}{\tilde{e}_n} \langle \alpha | F_n(JM) | \beta \rangle = \langle \alpha | F(JM) | \beta \rangle,$$

so that Eq. (A.5) becomes, taking into account also the third axis projection for isospin,  $t_p = 1/2$  for protons and  $t_n = -1/2$  for neutrons

$$\begin{aligned} F(JM) &= \\ & \left( \frac{1}{2} + t_p \right) \tilde{e}_p \sum_{\alpha\beta} \langle \alpha | F(JM) | \beta \rangle \pi_\alpha^\dagger \pi_\beta + \left( \frac{1}{2} - t_n \right) \tilde{e}_n \sum_{\alpha\beta} \langle \alpha | F(JM) | \beta \rangle \nu_\alpha^\dagger \nu_\beta \\ &= \frac{1}{2} (\tilde{e}_p + \tilde{e}_n) \sum_{\alpha\beta} \langle \alpha | F(JM) | \beta \rangle (\pi_\alpha^\dagger \pi_\beta + \nu_\alpha^\dagger \nu_\beta) \\ &+ \frac{1}{2} (\tilde{e}_p - \tilde{e}_n) \sum_{\alpha\beta} \langle \alpha | F(JM) | \beta \rangle (\pi_\alpha^\dagger \pi_\beta - \nu_\alpha^\dagger \nu_\beta) \\ &= \tilde{e}_1 \sum_{\alpha\beta} \langle \alpha | F_J | \beta \rangle [a_\alpha^\dagger \otimes \tilde{a}_\beta]_{JM}^{T=1, T_z} + \tilde{e}_0 \sum_{\alpha\beta} \langle \alpha | F_J | \beta \rangle [a_\alpha^\dagger \otimes \tilde{a}_\beta]_{JM}^{T=0, T_z=0} \end{aligned} \quad (\text{A.6})$$

where  $\tilde{e}_T = \tilde{e}_p - (-1)^T \tilde{e}_n$  are the isovector ( $T = 1$ ) and isoscalar ( $T = 0$ ) effective charges. Thus, we have shown analytically that a multipole operator can be written as sum of isovector and isoscalar components, and because of the isospin selection rules in Eq. (A.2), we can calculate their responses separately.

# Appendix B: Special Eigenvalue Problems

The diagonal and off-diagonal RPA matrices for the Lipkin Hamiltonian have a special form, i.e.,

$$A_{ij} = a + \Delta\delta_{ij} \quad (\text{B.1})$$

(and similar for  $\mathbf{B}$ ). One can easily verify that

$$X_c = \frac{1}{\sqrt{N}} \begin{pmatrix} 1 \\ 1 \\ \vdots \\ 1 \end{pmatrix} \quad (\text{B.2})$$

is an eigenvector for the matrix  $\mathbf{A}$ , corresponding to the eigenvalue

$$\alpha_c = Na + \Delta. \quad (\text{B.3})$$

Because the eigenvalue  $\alpha_c$  is proportional to  $N$  and hence one can imagine all the components adding coherently, we call this *collective* eigenvalue, corresponding to the collective eigenvector (B.2). In addition, there is one more *non-collective* eigenvalue  $(N - 1)$  fold degenerate

$$\alpha_{nc} = \Delta. \quad (\text{B.4})$$

We can solve now the non-symmetric eigenvalue problem (4.29) in the particular case of the RPA matrices for the Lipkin model. The two matrices  $\mathbf{A}$  and  $\mathbf{B}$  admit simultaneously the same collective and non-collective eigenvectors, the only difference being their eigenvalues [we will use  $\alpha$  for  $\mathbf{A}$  and  $\beta$  for  $\mathbf{B}$ , the collective and non collective eigenvalues being given by (B.3) and (B.4) respectively]. We rewrite first Eq. (4.29) as

$$\mathbf{A}X + \mathbf{B}Y = \Omega X \quad (\text{B.5})$$

$$\mathbf{B}X + \mathbf{A}Y = -\Omega Y. \quad (\text{B.6})$$

Since the collective and non-collective eigenvectors provide a complete basis for the space of vectors with  $N$  components, we use them to expand  $X$  and  $Y$  in the last two equations, that is

$$X = C^X X_c + \sum_{j=1}^{N-1} D_j^X X_{nc}^{(j)}, \quad (\text{B.7})$$

$$Y = C^Y X_c + \sum_{j=1}^{N-1} D_j^Y X_{nc}^{(j)}. \quad (\text{B.8})$$

Eqs. (B.5) and (B.6) transform now into  $N$  eigenvalue problems which determine the RPA eigenvalues  $\Omega$  and the coefficients  $C$  and  $D$ . Thus, we obtain one new eigenvalue equation for the collective excitation

$$\begin{pmatrix} \alpha_c & \beta_c \\ -\beta_c & -\alpha_c \end{pmatrix} \begin{pmatrix} C^X \\ C^Y \end{pmatrix} = \Omega_c \begin{pmatrix} C^X \\ C^Y \end{pmatrix}, \quad (\text{B.9})$$

and  $N - 1$  for the non-collective excitations

$$\begin{pmatrix} \alpha_{nc} & \beta_{nc} \\ -\beta_{nc} & -\alpha_{nc} \end{pmatrix} \begin{pmatrix} D_j^X \\ D_j^Y \end{pmatrix} = \Omega_{nc} \begin{pmatrix} D_j^X \\ D_j^Y \end{pmatrix}. \quad (\text{B.10})$$

Although the last equations involve non-hermitian matrices, it is nevertheless trivial to calculate the solutions (each matrix is 2 by 2). We obtain indeed for collective and non-collective eigenvalues the results given in (5.22) and (5.23). Simple algebra provides also the coefficients  $C$  and  $D$  which in turn can be used in order to calculate corrections to other observables, e.g.  $K_0$ . Note that each equation will provide one positive and one negative eigenvalue, as pointed out in Sec. 4.2.

# Appendix C: Letter of Permission

Figure 2.1 is a reproduction from Nuclear Physics A. Attached is the permission letter from Elsevier.



30 April 2003

Our ref: HW/LJR/may03/J004

Dr Ionel Stetcu  
Louisiana State University  
Department of Physics and Astronomy  
202 Nicolson Hall  
Baton Rouge, LA 70803-4001  
USA

Dear Dr Stetcu

*NUCLEAR PHYSICS A, Vol 704, No 1, 2002, pp 154c-164c, Langanke & Martinez-Pinedo: "Applications of the shell model in ...", figure 2 only*

As per your letter dated 18 April 2003, we hereby grant you permission to reprint the aforementioned material at no charge **in your thesis, in print and on the Louisiana State University web site** subject to the following conditions:

1. If any part of the material to be used (for example, figures) has appeared in our publication with credit or acknowledgement to another source, permission must also be sought from that source. If such permission is not obtained then that material may not be included in your publication/copies.
2. Suitable acknowledgment to the source must be made, either as a footnote or in a reference list at the end of your publication, as follows:  
  
"Reprinted from Publication title, Vol number, Author(s), Title of article, Pages No., Copyright (Year), with permission from Elsevier".
3. Reproduction of this material is confined to the purpose for which permission is hereby given.
4. This permission is granted for non-exclusive world **English** rights only. For other languages please reapply separately for each one required. Permission excludes use in an electronic form other than as specified above.
5. This includes permission for UMI to supply single copies, on demand, of the complete thesis. Should your thesis be published commercially, please reapply for permission.

Yours sincerely

Helen Wilson  
Rights Manager

**Your future requests will be handled more quickly if you complete the online form at**  
[www.elsevier.com/locate/permissions](http://www.elsevier.com/locate/permissions)

# Vita

Ionel Stetcu was born March 24, 1972, in Corabia, Romania. He was fortunate to meet a passionate high-school professor who influenced strongly years later his decision to study physics. After finishing high school in his natal town, he was admitted in 1991 in the Physics Department at the University of Bucharest, from where he graduated five years later with a Bachelor's Degree in Physics. In 1996 he started the Master program at the same school, and at the same time he become Research Assistant at the National Institute for Physics and Nuclear Engineering, Bucharest, Romania. One year and a half after he got his Master's Degree, he moved to Baton Rouge, where he joined the Ph. D. program in the Department of Physics and Astronomy at Louisiana State University. After graduation in August 2003, he will join the nuclear theory group at the University of Arizona as a postdoc.